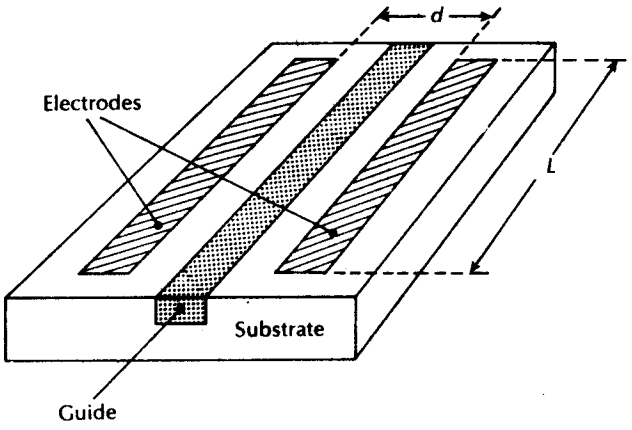

Figure 10.21 A simple strip waveguide phase modulator.

A simple phase modulator may therefore be realized on a strip waveguide in which the ratio L/d is large as shown in Figure 10.21. These devices when, for example, fabricated by diffusion of Nb into $LiTaO_3$ provide a phase change of π radians with an applied voltage in the range 5 to 10 V.

Example 10.3

A lithium niobate strip waveguide phase modulator designed for operation at a wavelength of 1.3 μm is 2 cm long with a distance between the electrodes of 25 μm. Determine the voltage required to provide a phase change of π radians given that the electro-optic coefficient for lithium niobate is $30.8 \times 10^{-12}\,\mathrm{mV}^{-1}$ and its refractive index is 2.1 at 1.3 μm.

Solution: When the phase change is π radians, using Eq. (10.28) we can write:

$$\delta\phi = \pi = \frac{\pi}{\lambda} n_1^3 r \frac{V_\pi L}{d}$$

Hence the voltage required to provide a π radian phase change is:

$$V_\pi = \frac{\lambda}{n_1^3 r} \frac{d}{L}$$

$$= \frac{1.3 \times 10^{-6} \times 25 \times 10^{-6}}{(2.1)^3 \times 30.8 \times 10^{-12} \times 2 \times 10^{-2}}$$

$$= 5.7 \text{ V}$$

The result obtained in Example 10.3 has assumed the spatially uniform electric field of an ideal parallel plate capacitor. However, because the electro-optic

refractive index change is small this is rarely the case and its effect on the optical phase velocity is dependent on the overlap integral of the electrical and optical fields. The consequence of these nonuniform fields can be incorporated into an overlap integral α, having a value between 0 and 1 which gives a measure of the overlap between the electrical and optical fields [Refs. 42, 45]. The electro-optic refractive index change of Eq. (10.24) therefore becomes:

$$\delta n = \frac{\pm \alpha n_1^3 r}{2} \frac{V}{d} \tag{10.29}$$

where the factor α represents the efficiency of the electro-optic interaction relative to an idealized parallel plate capacitor with the same distance between the electrodes.

As mentioned previously the electro-optic property can be employed in an interferometric intensity modulator. Such a Mach–Zehnder type interferometer is shown in Figure 10.22. The device comprises two Y-junctions which give an equal division of the input optical power. With no potential applied to the electrodes, the input optical power is split into the two arms at the first Y-junction and arrives at the second Y-junction in phase giving an intensity maximum at the waveguide output. This condition corresponds to the 'on' state. Alternatively when a potential is applied to the electrodes, which operate in a push-pull mode on the two arms of the interferometer, a differential phase change is created between the signals in the two arms. The subsequent recombination of the signals gives rise to constructive or destructive interference in the output waveguide. Hence the process has the effect of converting the phase modulation into intensity modulation. A phase shift of π between the two arms gives the 'off' state for the device.

High speed interferometric modulators have been demonstrated with titanium doped lithium niobate waveguides. A 1.1 GHz modulation bandwidth has been reported [Ref. 61] for a 6 mm interferometer employing a 3.8 V on/off voltage across a 0.9 μm gap. Similar devices incorporating electrodes on one arm only

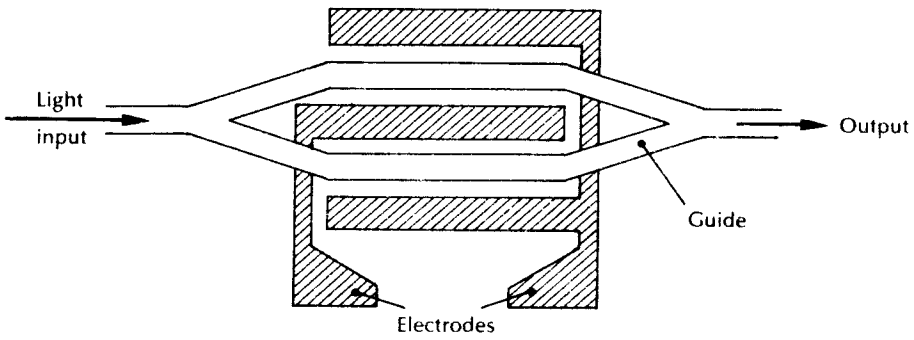

Figure 10.22 A Y-junction interferometric modulator based on the Mach–Zehnder interferometer.

may be utilized as switches and are generally referred to as balanced bridge interferometric switches [Ref. 59].

Useful modulators may also be obtained employing the acousto-optic effect. These devices which deflect a light beam are based on the diffraction of light produced by an acoustic wave travelling through a transparent medium. The acoustic wave produces a periodic variation in density (i.e. mechanical strain) along its path which, in turn, gives rise to corresponding changes in refractive index within the medium due to the photoelastic effect. Therefore, a moving optical phase-diffraction grating is produced in the medium. Any light beam passing through the medium and crossing the path of the acoustic wave is diffracted by this phase grating from the zero order into higher order modes.

Two regimes of operation are of interest: the Bragg regime and the Raman–Nath regime. The interaction, however, is of greatest magnitude in the Bragg regime where the zero order mode is partially deflected into only one higher order (i.e. first order) mode, rather than the multiplicity of higher order modes obtained in the Raman–Nath regime. Hence most acousto-optic modulators operate in the Bragg regime providing the highest modulation depth for a given acoustic power.

The Bragg regime is obtained by effecting a suitably long interaction length for the device so that it performs as a 'thick' diffraction grating. An IO acousto-optic Bragg deflection modulator is shown in Figure 10.23. It consists of a piezoelectric substrate (e.g. lithium niobate) on to the surface of which a thin film optical waveguide is formed by, for example, titanium indiffusion or lithium outdiffusion. An acoustic wave is launched parallel to the surface of the waveguide forming a surface acoustic wave (SAW) in which most of the wave energy is concentrated within a depth of one acoustic wavelength. The wave is generated from an interdigital electrode system comprising parallel electrodes deposited on the substrate.

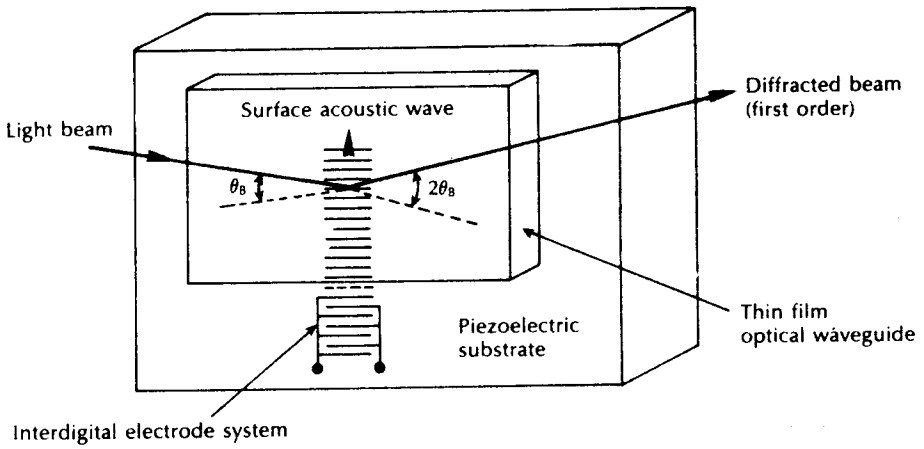

Figure 10.23 An acousto-optic waveguide modulator. The device gives deflection of a light beam due to Bragg diffraction by surface acoustic waves.

A light beam guided by the thin film waveguide interacts with the SAW giving beam deflection since both the light and the acoustic energy are confined to the same surface layer. The conditions for Bragg diffraction between the zero and first order mode are met when [Ref. 41]:

$$\sin \theta_B = \frac{\lambda_1}{2\Lambda} \tag{10.30}$$

where θ_B is the angle between the light beam and the acoustic beam wavefronts, λ_1 is the wavelength of light in the thin film waveguide and Λ is the acoustic wavelength. In this case the light is deflected by $2\theta_B$ from its original path as illustrated in Figure 10.23.

The fraction of the light beam deflected depends upon the generation efficiency and the width of the SAW, the latter also defining the interaction length for the device. Although diffraction efficiencies are usually low (no more than 20%), the diffracted on/off ratio can be very high. Hence these devices provide effective switches as well as amplitude or frequency modulators.

10.6.3 Periodic structures for filters and injection lasers

Periodic structures may be incorporated into planar waveguides to form integrated optical filters and resonators. Light is scattered in such a guide in a similar manner to light scattered by a diffraction grating. A common example of a periodic waveguide structure is the corrugated slab waveguide shown in Figure 10.24. When light propagating in the guide impinges on the corrugation, some of the energy will be diffracted out of the guide into either the cover or the substrate. The device, however, acts as a one-dimensional Bragg diffraction grating, and light which satisfies the Bragg condition is reflected back along the guide at 180° to the original direction of propagation (Figure 10.24).

The Bragg condition for the case of 180° reflection can be obtained from Eq. (10.30) if we let the corrugation period D (Figure 10.24) equal the acoustic

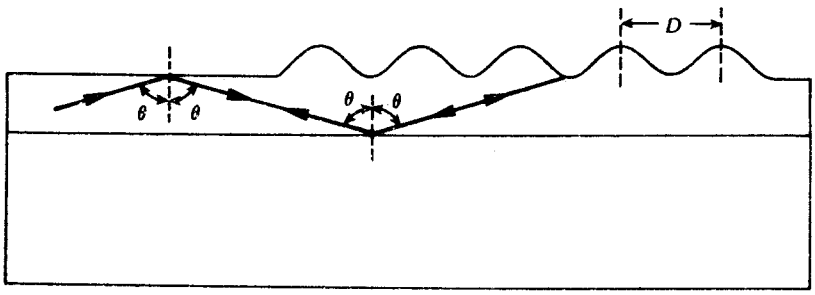

Figure 10.24 A slab waveguide with surface corrugation giving reflection back along the guide when the Bragg condition is met. Hence the structure performs as a one dimensional Bragg diffraction grating.

wavelength Λ and let λ_1 equal λ_B/n_e, where λ_B (the Bragg wavelength) is the optical wavelength in a vacuum and n_e is the effective refractive index of the guide. If we also assume that λ_B is equal to 90°, then Eq. (10.30) becomes

$$D = \frac{l\lambda_B}{2n_e} \tag{10.31}$$

where $l = 1, 2, 3, \ldots, m$ is the order of the grating which was unity in Eq. (10.30) because diffraction took place between the zero and first order mode. The vacuum wavelength of light that will be reflected through 180° by such a grating is therefore:

$$\lambda_B = \frac{2n_eD}{l} \tag{10.32}$$

When the reflected light is incident at an angle (Figure 10.24) then [Ref. 39]:

$$n_e = n_1 \sin 2\theta \tag{10.33}$$

where n_1 is the refractive index of the guide. Hence depending on the corrugation period of the structure all the incident power at a particular wavelength will be reflected. Devices of this type therefore behave as frequency selective rejection filters or mirrors. An example of such a reflection filter is shown in Figure 10.25. It comprises a InGaAsP/InP grating waveguide device in which the surface corrugation is typically written as a photoresist mask using two interfering ultraviolet beams before chemical or physical etching. The filter bandwidth can be quite small (6Å) with modest interaction lengths using this technique [Ref. 62]. Moreover in glass waveguides filter bandwidths as narrow as 0.1 Å have been obtained with a 1 cm long grating filter [Ref. 63]. The low substrate–waveguide refractive index difference using lithium niobate devices, however, combined with the inherent etching difficulties have limited the development of Ti:$LiNbO_3$ waveguide reflection filters.

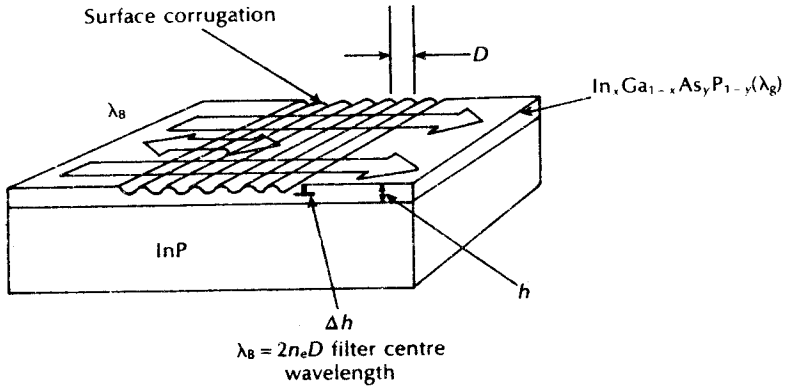

Figure 10.25 An InGaAsP/InP waveguide grating filter.

For a waveguide grating filter which exhibits a large change in effective refractive index with a fine grating period, the 3 dB fractional bandwidth is given approximately by [Ref. 45]:

$$\frac{\delta\lambda}{\lambda} \simeq \frac{D}{L} \tag{10.34}$$

where L is the grating length. Hence Eq. (10.34) allows estimates of the filter 3 dB bandwidth, $\delta\lambda$, to be obtained.

Example 10.4

A 1 cm long InGaAsP/InP first order grating filter is designed to operate at a centre wavelength of 1.52 μm. The reflected light is incident at an angle of 1° and the refractive index of InGaAsP is 3.1. Determine the corrugation period and estimate the filter 3 dB bandwidth. A large change in effective refractive index may be assumed.

Solution: The effective refractive index of the waveguide is given by Eq. (10.33) as·

$$\begin{aligned} n_e &= n_1 \sin 2\theta = 3.1 \sin 2^\circ \\ &= 0.11 \end{aligned}$$

The corrugation period for the first order grating may be obtained from Eq. (10.31) as:

$$D = \frac{\lambda_B}{2n_e} = \frac{1.52 \times 10^{-6}}{2 \times 0.11} = 6.9\ \mu\text{m}$$

Finally, the filter 3 dB bandwidth can be estimated from Eq. (10.34) where

$$\begin{aligned} \delta\lambda \simeq \frac{D\lambda}{L} &= \frac{6.9 \times 10^{-6} \times 1.52 \times 10^{-6}}{10^{-2}} \\ &= 10.5\ \text{Å}\ (\simeq 1\ \text{nm}) \end{aligned}$$

It may be observed that a relatively narrow filter bandwidth is obtained in Example 10.4. Such devices could find use for wavelength demultiplexing of a larger number of channels. Alternatively, wide bandwidth filters may be realized by forming gratings which exhibit a gradual change in the corrugation period. Such grating devices are said to have a chirped structure [Ref. 64].

Finally, it should be noted that the corrugated gratings discussed above are also incorporated into advanced single-mode injection laser structures; namely, the distributed feedback and the distributed Bragg reflector lasers (see Section 6.6.2).

10.6.4 Polarization transformers and frequency translators

The electro-optic effect typically in lithium niobate waveguide devices can be used to facilitate TE–TM mode conversion. However, to allow the transformation of an arbitrary input polarization, not just TE or TM, it is necessary to control the relative phase between the TE and TM components. Such polarization transformers which operate as TE–TM mode converters can be employed as elements within intensity modulators (when combined with a polarizer), optical filters or polarization controllers. A basic example of the latter device is shown in Figure 10.26 [Ref. 65]. It comprises two phase modulators and a single TE–TM mode converter on X-cut* lithium niobate.

The first phase modulator is required to adjust the phase difference between the incoming TE and TM modes to be $\pi/2$ so that the polarization controller can operate with all incoming polarization states. When this condition is satisfied the central phase matched mode converter is operated as a linear polarization rotator. Although a linear output polarization of either TE or TM is sufficient in some applications, for full polarization control a second phase shifter is required to adjust the output phase to a desired value of elliptical output polarization.

A number of electro-optic waveguide devices can be used to provide frequency translation of an optical signal [Refs. 42, 66]. A common technique is to employ a phase modulator in a serrodyne configuration to alter the optical frequency by a linearly increasing voltage applied to the device electrodes [Ref. 67]. In practice a continuously increasing ramp signal voltage cannot readily be produced and hence a sawtooth voltage waveform is used. However, sawtooth waveforms with instantaneous fall-times can be generated and hence additional frequency components

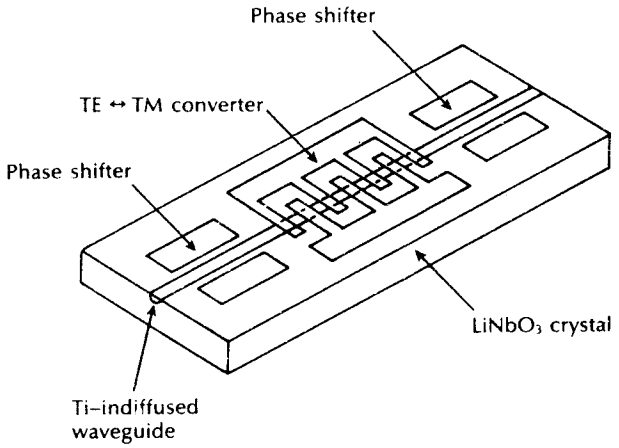

Figure 10.26 An IO polarization controller.

* Conventional Y-cut lithium niobate is not normally used as the electro-optic coefficient is smaller, necessitating higher operating voltages.

tend to be produced. This factor, combined with the need to vary the rate of change of the applied voltage to alter the extent of the frequency shift, limits the use of this device to applications where a small constant frequency shift is required. In applications where large frequency translations are necessary and where the device is used as a control element in a feedback loop (e.g. coherent optical receivers), alternative frequency translators are utilized [Ref. 42].

Devices based on TE–TM mode conversion are also capable of generating frequency translated optical signals [Ref. 68]. When the region where the mode conversion takes place is made to move relative to the direction of the optical wave, then the source of the converted signal appears to be moving to a stationary observer and the light is therefore Doppler shifted. To generate the effect of a moving coupling grating in practice, a mode converter is divided into several sections and each is driven with a correctly phase shifted sinusoidal signal which has a frequency equal to the desired up or down frequency translation. In principle, this technique should be highly efficient and generate no unwanted optical signals. However, significant unwanted sidebands have been observed with such devices which appear to arise from parasitic electrical fields [Ref. 42]. Careful device design is therefore necessary to maintain these signals at an acceptable level.

Mach–Zehnder interferometric Y-junction modulators (see Figure 10.22) can also be used to generate double sideband frequency translated optical signals when they are modulated with a sinusoidal voltage waveform. In this case the optical frequency shift is proportional to the frequency of the electrical modulating signal

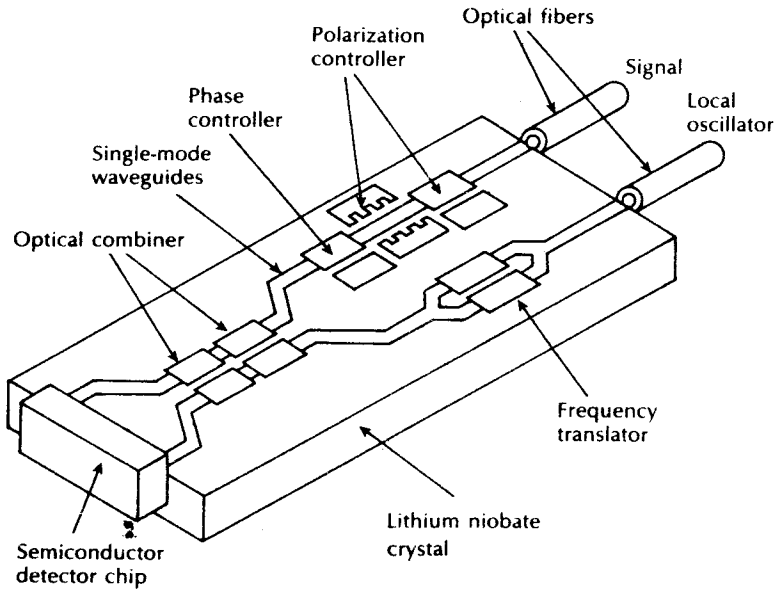

Figure 10.27 Coherent optical receiver device.

[Ref. 69]. However, in simple device structures the charging of the electrode capacitance limits the maximum modulation frequency and thus the magnitude of the frequency translation that can be obtained. To overcome this problem Mach–Zehnder interferometers with travelling wave electrode structures have been designed which provide multigigahertz bandwidths. Frequency translations of 3 GHz and 6.5 GHz at wavelengths of 0.85 and 1.52 μm, respectively, have been reported [Refs. 70, 71] using devices of this type.

Integration of the aforementioned electro-optic devices into a single lithium niobate substrate, particularly for use in coherent optical fiber communications systems (see Chapter 12) has become an increasing area of interest both to reduce losses between individual devices as well as system cost. For example, the configuration of a potential coherent optical receiver device is illustrated in Figure 10.27 [Refs. 42, 73]. It was fabricated on Z-cut lithium niobate and comprises a polarization controller with output phase controller, and a frequency translator together with a directional coupler for mixing the two optical signals. Successful operation of this integrated device was demonstrated and a similar X-cut lithium niobate device requiring a lower operating voltage has been proposed [Ref. 73].

10.7 Optoelectronic integration

The integration of interconnected optical and electronic devices is an important area of investigation for applications within optical fiber systems [Ref. 73]. Monolithic optoelectronic integrated circuits (OEICs) incorporating both optical sources and detectors have been successfully realized for a number of years. Monolithic integration for optical sources has been generally confined to the use of group III–V semiconductor compounds. These materials prove useful as they possess both optical and electronic properties which can be exploited to produce high performance devices. Circuits are often fabricated from GaAs/AlGaAs for operation in the shorter wavelength region between 0.8 and 0.9 μm. Such a circuit is shown in Figure 10.28(a) where an injection laser is fabricated on a GaAs substrate with a MESFET (metal-Schottky FET, see Section 9.5.1) which is used to bias and modulate the laser. Alternatively, Figure 10.28(b) demonstrates the integration of a longer wavelength (1.1 to 1.6 μm) injection laser fabricated from InGaAsP/InP together with a MISFET (metal integrated-semiconductor FET) where the conventional n type substrate is replaced by a semi-insulating InP substrate.

The realization of OEICs has, however, lagged behind other developments in IO using dielectric materials such as lithium niobate. This situation has been caused by the inherent difficulties in the fabrication of OEICs even when III–V compound semiconductors are employed [Ref. 74]. Compositional and structural differences between photonic devices and electronic circuits create problems in epitaxial crystal growth, planarization for lithography, electrical interconnections, thermal and chemical stability of materials, electrical matching between photonic and electrical

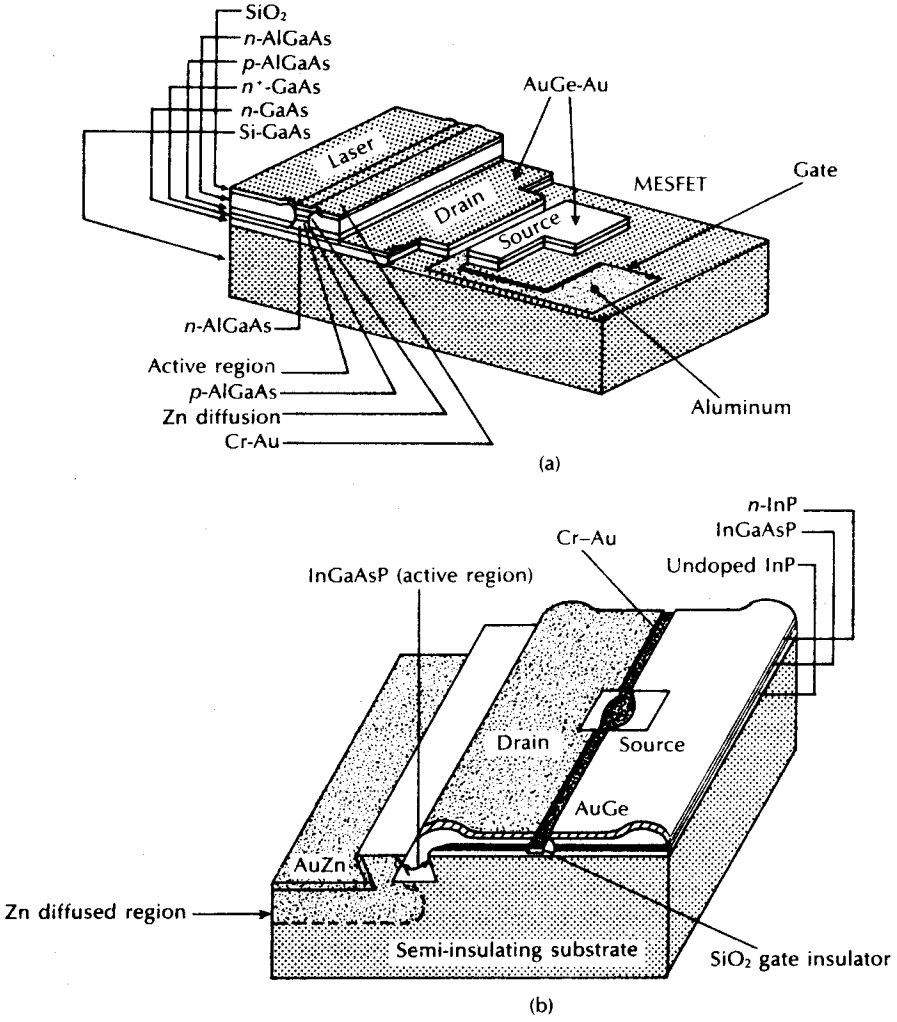

Figure 10.28 Monolithic integrated transmitter circuits: (a) GaAs/AlGaAs injection laser fabricated with a MESFET on a GaAs substrate; (b) InGaAsP/InP injection laser fabricated with a MISFET on a semi-insulating InP substrate.

devices together with heat dissipation. Nevertheless, the maturing of gallium arsenide technology for integrated circuits (as opposed to OEICs) [Ref. 75] has helped stimulate the more recent research activities into high speed OEICs. For example, a 2 Gbit s^{-1} optical transmitter incorporating five active devices was reported in 1986 [Ref. 76]. Moreover, the structure of a monolithically integrated DFB laser with an optical intensity modulator is shown in Figure 10.29 [Ref. 77].

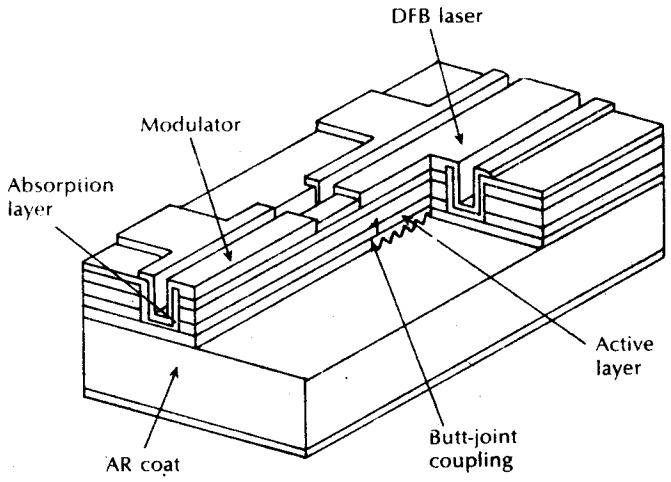

Figure 10.29 Device structure for an optical intensity modulator monolithically integrated with a DFB laser [Ref. 77].

This InGaAsP/InP device, which was designed to avoid the large chirp associated with directly modulated semiconductor lasers, displayed good dynamic characteristics at a modulation rate of 5 Gbit s^{-1} when operating at a wavelength of 1.55 μm. Hence OEIC transmitters for operation in both the short wavelength [Ref. 78] and longer wavelength regions [Refs. 79, 80] have received significant attention in recent years.

The monolithic integration of optical detectors with other active components has also been achieved using the group III–V semiconductor alloys. The structure of an OEIC photoreceiver fabricated for operation in the 0.8 to 0.85 μm wavelength range is illustrated in Figure 10.30 [Ref. 81]. This device incorporates a Schottky

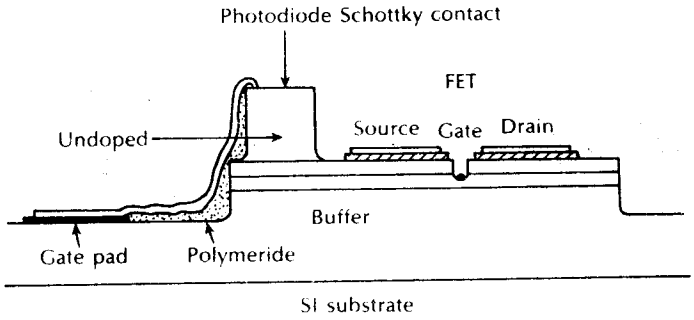

Figure 10.30 A planar monolithic integrated photoreceiver incorporating a Schottky photodiode and field effect transistor [Ref. 81].

photodiode and an FET on a GaAs semi-insulating substrate. It displayed a sensitivity of -30 dBm at a transmission rate of 250 Mbit s^{-1} for a bit error rate of 10^{-9}.

Receiver OEICs for the longer wavelength region have also been given attention. A design incorporating a *p–i–n* photodiode with three junction FETs forming a preamplifier was fabricated in InGaAsP on a semi-insulating InP substrate [Ref. 82]. Photoreceiver sensitivies of -25.5 dBm at 565 Mbit s^{-1} and -14.2 dBm at 1.2 Gbit s^{-1} were obtained for a bit error rate of 10^{-9} with this device. Furthermore, an improved process for fabricating the junction FETs has enabled a longer wavelength receiver OEIC to be fabricated which demonstrates higher receiver sensitivity of -22.8 dBm at a transmission rate of 1.2 Gbit s^{-1} [Ref. 80]. Nevertheless, this improved receiver sensitivity value is stili around 10 dB lower than those achieved with a well designed PIN–FET hybrid receiver (see Section 9.5.2).

Optoelectronic integrated transmitter and receiver arrays have also been fabricated for applications such as wavelength division multiplexing and optical interconnection. For the latter application a four channel OEIC transmitter array comprising single quantum-well lasers integrated with FET drive circuits, as well as monitor photodiodes, has been demonstrated [Ref. 83]. This device which was fabricated using the GaAs/AlGaAs material system operated at a wavelength of 0.83 μm with a transmission rate in excess of 1.5 Gbit s^{-1}. GaAs-based photoreceiver arrays have also been fabricated. An example, also a four channel device, integrated a metal-semiconductor–metal photodiode with six MESFETs for each channel [Ref. 85]. A single element sensitivity for the receiver circuit of -26 dBm at 1 Gbit s^{-1} was obtained with low crosstalk up to transmission rates of 1.5 Gbit s^{-1}.

More complex optoelectronic integration is shown in Figure 10.31 [Ref. 87] where two possible designs of monolithic integrated circuits which serve as receive terminals in a wavelength division multiplex system are illustrated. These wavelength demultiplexers utilized micrograting filters (either transmission or reflection

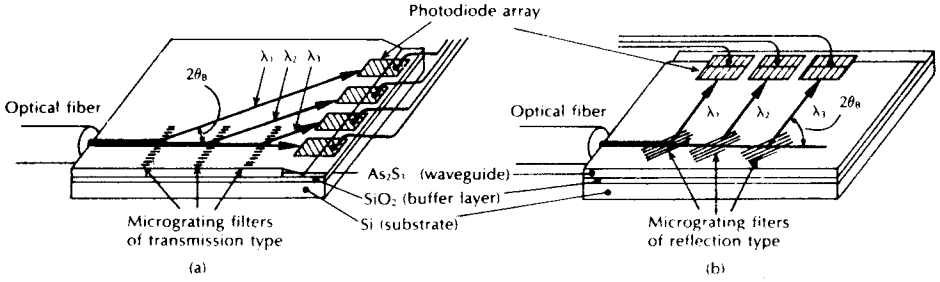

Figure 10.31 Monolithic integrated optical wavelength demultiplexers fabricated with micrograting filters and a Schottky barrier photodiode array on a silicon substrate: (a) using transmission gratings; (b) using reflection gratings [Ref. 87].

type) together with an array of Schottky barrier photodiodes fabricated on a silicon substrate. In each case the filters picked out individual transmission wavelengths directing them to the appropriate photodiode for detection.

A more recent monolithic integrated wavelength demultiplexer device is displayed in Figure 10.32 [Ref. 88]. This structure utilized a novel single-mode optical waveguide which is fabricated on a semiconductor substrate. The antiresonant reflecting optical waveguide (ARROW) shown in Figure 10.32(a) comprised an interference cladding inserted between the core and the substrate which consisted of two different films having a large refractive index difference. Therefore, the first cladding layer had a high refractive index whilst the second cladding layer exhibited a low refractive index. Using this mechanism the waveguide maintained single-mode propagation through loss discrimination of the higher order modes. Furthermore, the propagation loss of the fundamental mode displayed a wavelength dependence resulting from any changes in the resonant condition inside the interference cladding.

The structure of the ARROW-type wavelength demultiplexer and photodetector device is illustrated in Figure 10.32(b). It may be observed that the wavelength division multiplexed optical signal propagates through the low loss silicon dioxide

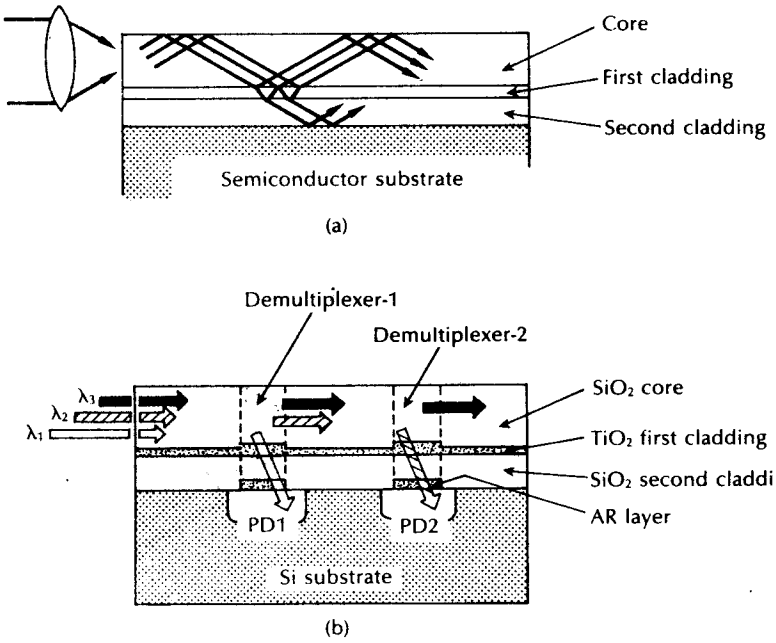

Figure 10.32 Wavelength demultiplexing using the antiresonant reflecting optical waveguide (ARROW): (a) structure of the ARROW; (b) an ARROW-type wavelength demultiplexer and photodetector integrated device [Ref. 88].

core layer. Wavelength demultiplexing was obtained in a region where the thickness of the first cladding layer had been adjusted to the resonant condition for which a particular wavelength band was radiated to a photodetector fabricated in the substrate. An antireflection (AR) layer was provided adjacent to the photodetector in order to enhance the coupling efficiency for the demultiplexed optical wavelength band. However, the remaining optical signal, being at other wavelengths, passed through the demultiplexing region with low loss. This device has been successfully demonstrated for demultiplexing of two wavelengths at 0.78 and 0.88 μm with a crosstalk isolation of -21.6 dB [Ref. 88]. It is therefore likely that IO circuits based on the above types will find application within WDM systems in the near future.

The monolithic integration of both sources and detectors on the same substrate has been achieved using group III–V semiconductor compounds. For example, a rudimentary AlGaAs OEIC optical repeater was implemented in 1984 [Ref. 89]. This monolithic integrated device, which is illustrated in Figure 10.33, incorporated a BH laser, *p–i–n* photodiode and a MESFET together to provide amplification on a semi-insulating GaAs substrate. Moreover, a longer wavelength OEIC repeater has also been demonstrated [Ref. 90]. The device fabricated on a semi-insulating InP substrate also incorporated a BH with a *p–i–n* photodiode and two FETs. In this case an overall repeater gain of 5.5 dB was obtained.

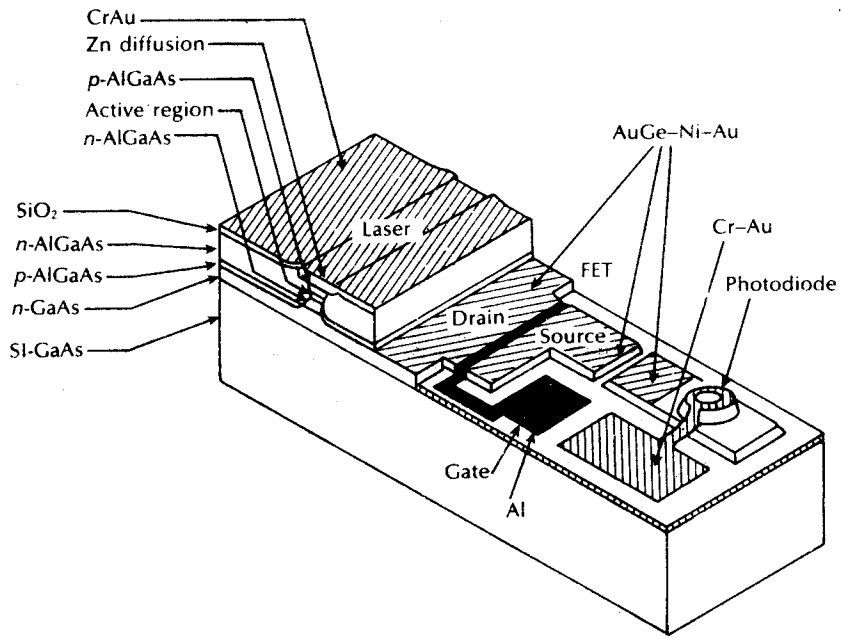

Figure 10.33 Monolithic integrated optoelectronic repeater chip [Ref. 89].

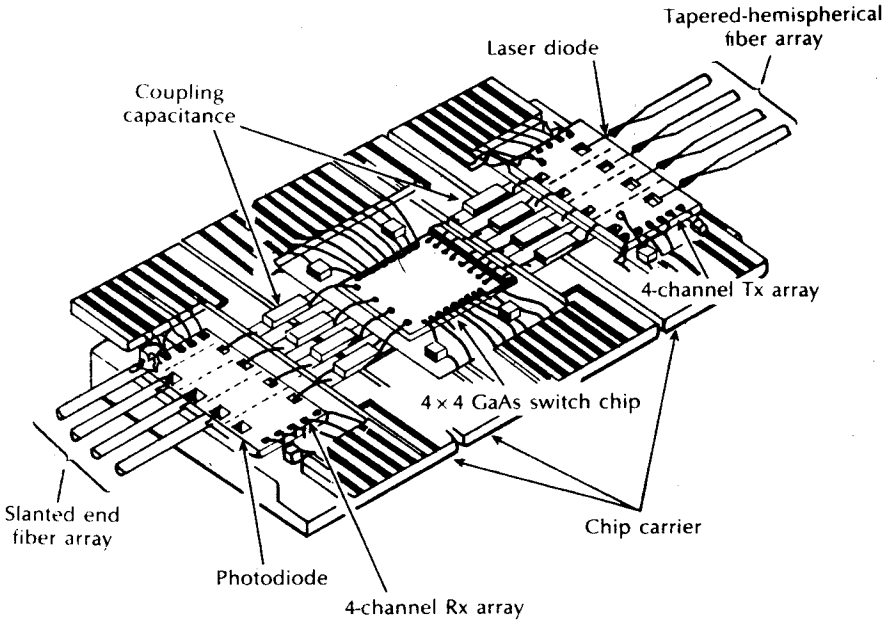

Figure 10.34 A 4 x 4 hybrid crossbar switch fabricated using gallium arsenide-based OEIC technology [Ref. 92].

There is also significant interest in the use of OEICs to provide optical switching matrices within future optical communication networks [Ref. 91]. Such optoelectronic switches form a hybrid optical switching technology which can facilitate space, time, and frequency division switching. An example of a 4×4 space division crossbar switch module is shown in Figure 10.34 [Ref. 92]. This hybrid device, which was fabricated using GaAs OEIC technology, comprises a laser array and the receiver array outlined above combined with a GaAs switch circuit. The all-GaAs device has been successfully operated at transmission rates up to 560 Mbit s^{-1}.

Although the present state of the art for OEICs centres on high speed transmitters, receivers and optoelectronic switching matrices for optical communications, it is perceived that OEICs will in the future perform a variety of functions. These include intrachip optical connection and parallel processing as well as interchip optical connection.

10.8 Optical bistability and digital optics

Bistable optical devices have been under investigation for a number of years to provide a series of optical processing functions. These include optical logic and memory elements, power limiters and pulse shapers, differential amplifiers, and

A–D converters. Moreover, the bistable optical device (BOD) in providing for digital optical logic – namely, a family of logic gates whose response to light is nonlinear – gives the basis for optical computation.

In its simplest form the BOD comprises a Fabry–Perot cavity containing a material in which variations in refractive index with optical intensity are nonlinear (nonlinear optical absorption also gives rise to bistability), as shown in Figure 10.35(a). In a similar manner to the laser such a cavity exhibits a sharp resonance to optical power passing into and through it when the optical path length in the nonlinear medium is an integer number of half wavelengths. By contrast with the laser the value of refractive index within the cavity controls the optical transmission giving high optical output on resonance and low optical output off resonance. The transfer characteristic for the device exhibits two-state hysteresis which results from tuning into and out of resonance, as illustrated in Figure 10.35(b). BODs are therefore able to latch between two distinct optical states (0 or 1) in response to an external signal to act as a memory or flip flop. Furthermore, by careful adjustments of the device bias and input levels, the BOD can act as an AND-gate, an OR-gate, or a NOT-gate, hence providing logic functions [Ref. 94].

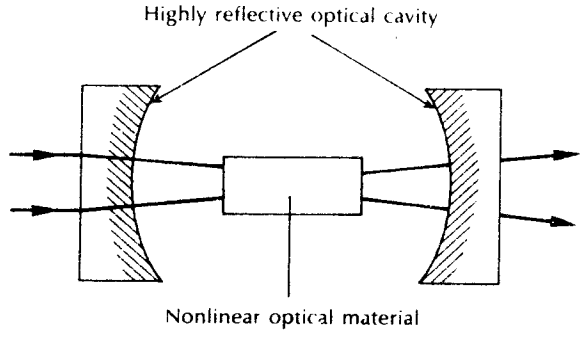

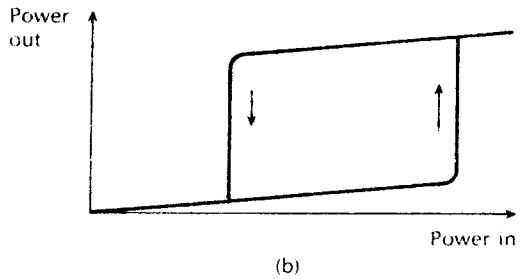

Figure 10.35 A generalized bistable optical device: (a) schematic structure; (b) typical transfer characteristic.

Although the switching speed of BODs is dependent on drive power, they offer the potential for very fast switching at low power levels. Investigations are therefore directed towards the possibility of picosecond switching using only picojoules of energy. A BOD exhibiting these properties would prove far superior to an electronic device which performs the same function. However, suitable nonlinear materials and device structures to give this performance are still under investigation. BODs may be separated into two basic classes: all-optical or intrinsic devices which utilize a nonlinear optical medium between a pair of partially reflecting mirrors forming a nonlinear etalon in which the feedback is provided optically; and hybrid devices where the feedback is provided electrically.

In some cases hybrid devices employ an artificial nonlinearity such as an electro-optic medium within the cavity to produce variations in refractive index via the electro-optic effect. In materials such as lithium niobate and gallium arsenide this produces strong artificial nonlinearity which can be combined with an electronic feedback loop. Such hybrid BODs have been fabricated in integrated optical form. A typical device is shown in Figure 10.36. [Ref. 95]. It consists of a titanium diffused optical waveguide on a lithium niobate substrate with cleaved and silvered end faces to form the resonant optical cavity. The light emitted from the cavity is detected and amplified by an avalanche photodiode (APD). The electrical signal thus obtained is then fed back to the electrodes deposited on either side of the cavity in order to produce refractive index variations. Such a device therefore exhibits hysteresis and bistability. Although these hybrid BODs provide flexibility for experimental study their switching speeds are ultimately limited by the use of electrical feedback. Nevertheless, it is possible that several such devices could be interconnected to provide a more complex logic circuit.

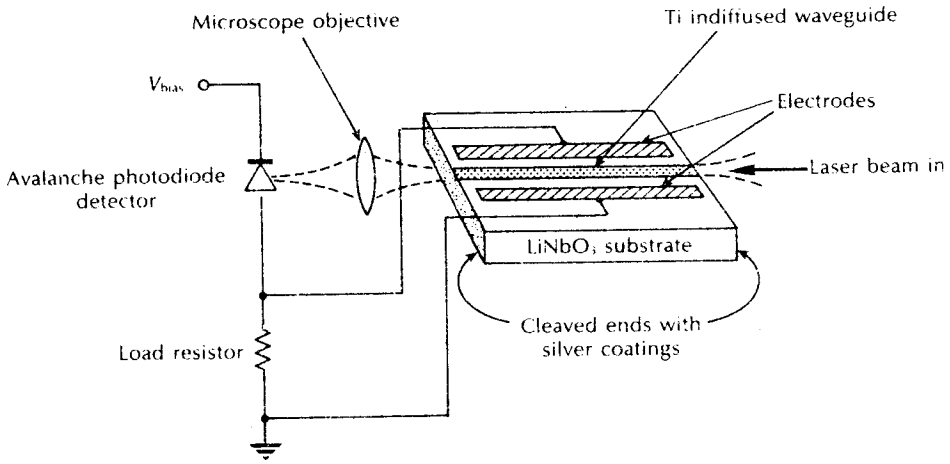

Figure 10.36 A hybrid integrated bistable optical device [Ref. 95].

An alternative hybrid approach based on the use of inorganic superlattices has been pursued at AT & T Bell Laboratories [Ref. 96], and elsewhere [Ref. 97]. These materials are constructed by alternating thin films of two different semiconductor materials which exhibit nonlinear properties. Combinations used include gallium arsenide and gallium aluminium arsenide, mercury telluride and cadmium telluride, silicon, and indium phosphide. This work has resulted in the development of the, so-called, self-electro-optic effect device (SEED) which exhibits hysteresis and bistate transmission. The device, a schematic of which is shown in Figure 10.37(a), comprises a single chip of alternating layers. Although the device is activated by light an electric field is required to 'prime' the material for switching. The switching results from wavelength sensitive absorption within the superlattice structure which causes current flow, thus decreasing the bias voltage which in turn

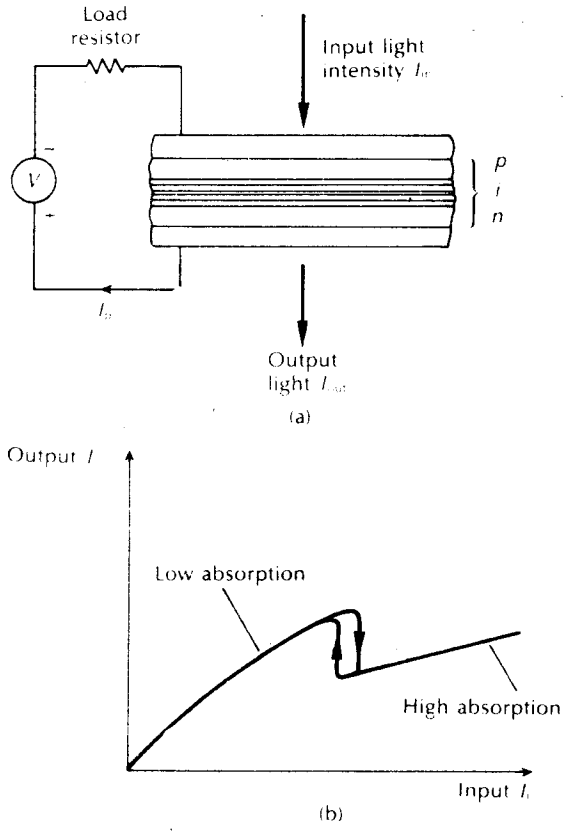

Figure 10.37 The self-electro-optic effect device (SEED): (a) schematic structure; (b) input/output response characteristic.

increases the absorption. Eventually a point is reached at which switching occurs and the device switches to high absorption as indicated in Figure 10.37(b).

Alternatively, all-optical or intrinsic BODs may employ an appropriate nonlinear optical medium. Investigations at present are centred around materials such as indium antimonide, zinc selenide, cadmium sulphide, gallium arsenide, indium arsenide, gallium aluminium arsenide and indium gallium arsenide phosphide in which optical absorption gives a change in refractive index. Unfortunately, these effects are generally weak and often require low temperatures to display themselves adequately. However, the possibility of low power, low energy, fast switching integratable devices for use in real time optical processing and digital optical computing is a proposition which has encouraged a concentrated activity in this area. Studies have involved the use of indium antimonide (InSb) in the near-infrared [Ref. 98] and more recently in the visible region, although operation is only achieved at low temperature (77 K). A more recent success, however, is the observation of bistability at room temperatures using thermal nonlinearities in zinc selenide (ZnSe) interference filter configurations [Refs. 99, 100]. This work was undertaken with visible light which provides the advantage that the switching and hysteresis effects can actually be seen.

Intrinsic optical bistability may also be obtained from large resonant nonlinearities available near the bandgaps of other semiconductor materials [Ref. 13]. Such bistability can be further distinguished as an active system which incorporates its own optical source, or a passive system which does not. The input to a passive bistable device is always optical while the input to an active device depends upon the method by which the source is to be excited. For example, in the former case room temperature bistability in bulk gallium arsenide at switching speeds of 30 ps has been observed [Ref. 101]. In addition, nonlinear channel waveguide structures in GaAs/GaAlAs multiple quantum-well material have shown optical bistability at relatively low power levels, but with slow switching speeds [Ref. 102].

The source of excitation for active bistability in semiconductors is normally provided by an injection current giving the configuration of a bistable laser diode [Ref. 103]. Semiconductor lasers exhibit optical bistability due to nonlinearities in absorption, gain, dispersion, waveguiding and the selection of the output polarization. One approach to laser diode bistability through nonlinear absorption is illustrated in Figure 10.38(a) [Ref. 104]. In this case the device is fabricated with a tandem electrode which provides two gain sections, with a loss region between them. The loss region acts as a saturable absorber creating the hysteresis characteristic displayed in Figure 10.38(b). Such devices fabricated in GaAs/GaAlAs and InP/InGaAsP have demonstrated nanosecond switching times with milliwatt power levels at room temperature [Ref. 13].

The above BODs have been discussed primarily in relation to the provision of optical logic and memory elements. However, investigations of optical bistability have also included the other functions mentioned previously. Optical pulse shaping can be achieved using a BOD with a very narrow bistable loop. Such a device can

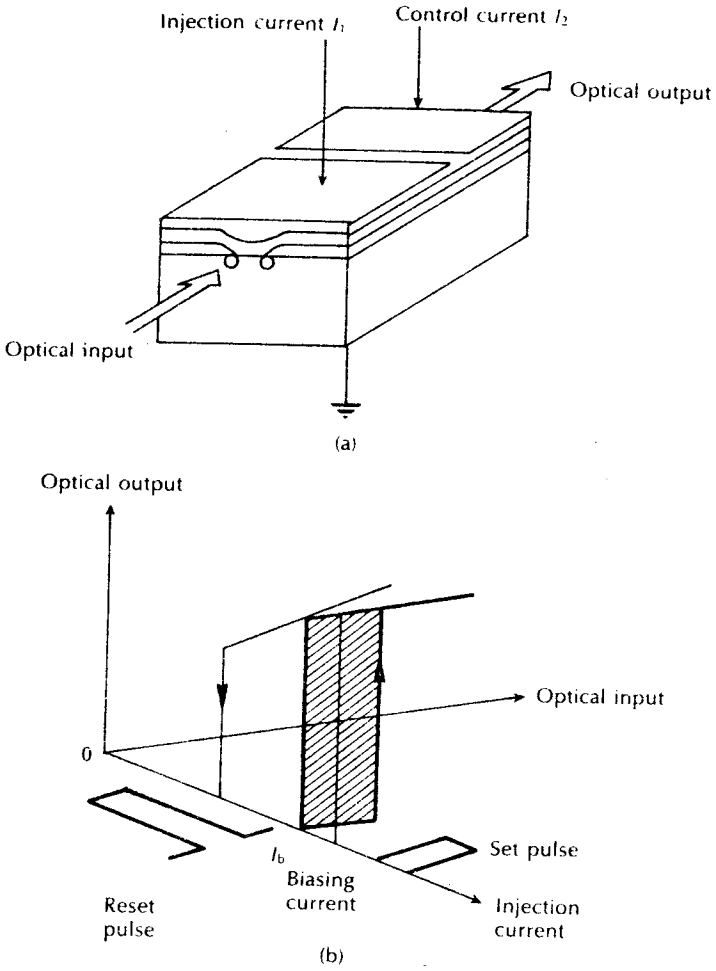

Figure 10.38 Bistable laser diode: (a) structure; (b) response characteristic.

be used to shape, clean-up and amplify a noisy input pulse, as illustrated in Figure 10.39(a).

Nonlinear optical amplification can also be obtained with certain BODs. In particular, the Fabry–Perot semiconductor laser amplifier can display dispersive bistability [Ref. 103] which, unlike its linear counterpart (see Section 10.3), provides a nonlinear gain characteristic, as shown in **Figure 10.39(b)**. The optical amplification mechanism in this case can involve the interaction of at least two optical fields through the field dependent dielectric constant of the nonlinear material. The operation of such a BOD differential amplifier is also illustrated in Figure 10.39(b). The introduction of a weak second beam into the nonlinear optical

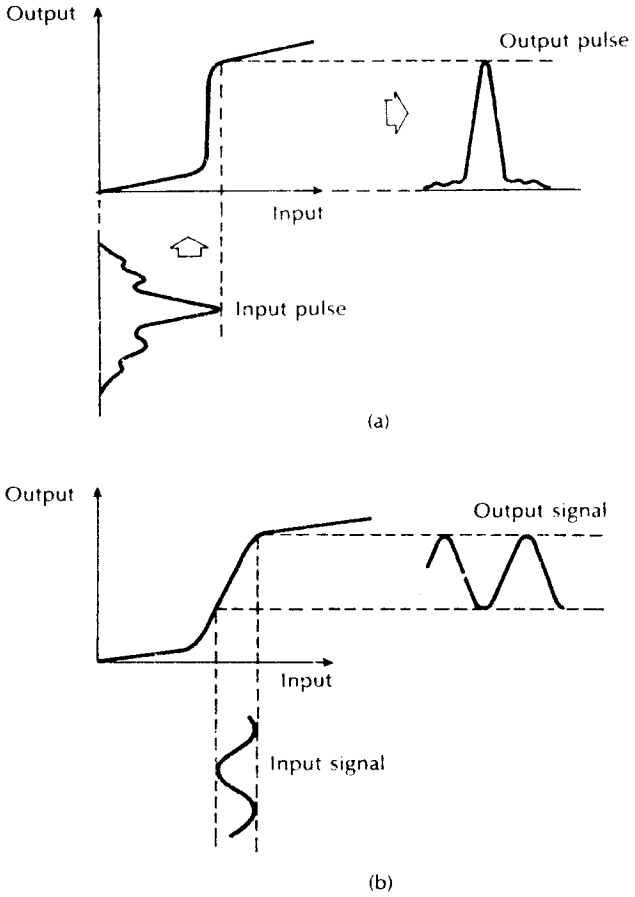

Figure 10.39 Illustration of two functions provided by the nonlinear characteristic of BODs: (a) optical pulse shaping; (b) optical amplification.

cavity is used to control the resonance and transmission of the main beam through the additive effects of its own stored energy. Hence differential optical gain is provided by the device. With this configuration a weak beam can control an intense main beam producing the optical, equivalent* of the electronic transistor.

Linear optical amplifiers exhibit the drawback of amplifying low level noise signals together with the desired signal. Bistable amplifiers, however, are useful because of their signal regeneration capability [Ref. 105]. In the ideal case no amplification is provided for signals below a particular intensity level. Once an intensity threshold has been surpassed, the large gain can be determined by the

* This two beam optical transistor has been dubbed 'the transphasor' by the authors of Ref. 98.

slope of the curve in Figure 10.39(b). Moreover, a saturated or maximum value of output intensity is also provided, displaying the power limiter function of the device.

10.9 Optical computation

Although the maximum potential switching speeds of individual IO logic devices have as yet to be accomplished, the use of parallel processing with optical signals mentioned in Section 10.5 can provide a net benefit over a similar serial electronic system, even at much slower optical device speeds. Conventional digital computers suffer from a bottleneck resulting from the limited number of interconnections which can be practically supported by an electronic-based communications technology. This restriction led to the classical von Neumann architecture for computing systems shown in Figure 10.40(a) in which the memory is addressed sequentially from the central processing unit (CPU). The CPU accesses the memory through a binary addressing unit and the memory contents are returned to the CPU via a small number of lines. This serial addressing of memory reduces the communications requirements and minimizes the number of lines, but this is achieved at the expense of overall computing speed. The problem, which is referred to as the von Neumann bottleneck, eventually limits the speed of the computer system.

With optical systems the situation is changed as they are capable of communicating many high bandwidth channels in parallel without interference. Thus parallel communication can easily be provided within an optical computer system at relatively low cost. In theory this lends itself to the use of non-von Neumann architecture (see Figure 10.40(b)) in which all memory elements are accessible in parallel, thus removing the speed limitation caused by the bottleneck. The potential

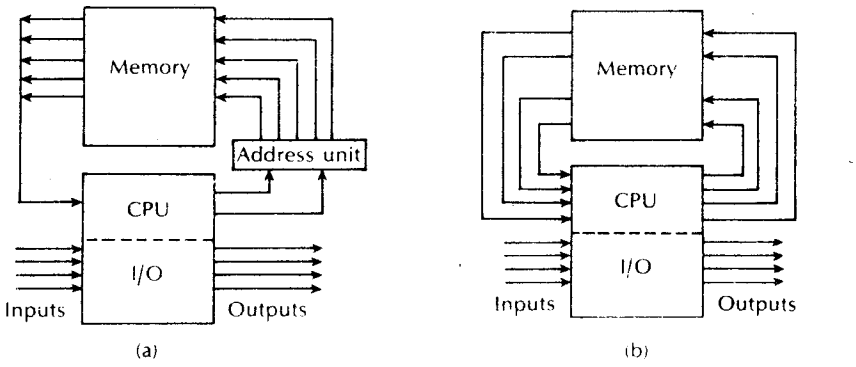

Figure 10.40 Computer architecture: (a) von Neuman; (b) non-von Neuman.

advantages offered by the digital optical computer are not therefore solely dependent upon the realization of subpicosecond optical switching devices.

For some time work in optical computation [Ref. 100] has been directed towards particular requirements which are necessary to provide a practical optical computing system. These include:

(a) High contrast. Logic devices must exhibit a large change between logic 0 and logic 1 levels.

(b) Steady state bias. To provide various different logic gates it is necessary that optical bias levels may be altered. For a BOD this implies that the device can be held indefinitely at any point on the characteristic with a CW laser beam. However, this holding beam necessitates a degree of thermal stability. Such stability has been demonstrated with devices based on InSb at 77 K and on ZnSe at 300 K (Ref. 99).

(c) External addressing. The function of external addressing is to provide for separate external optical signals which can be combined with the holding beam to switch the device, thus giving logic functions. The switching energy can be derived from the holding beam which is then switched and propagates in transmission or reflection as the output beam to further devices in the optical circuit.

(d) Cascadability. The output from a particular device must be sufficient to switch at least one following device. This condition may be fulfilled by setting a holding beam near the switch point since the extra increment is then small in comparison with the change in output.

(e) Fan-out and fan-in. The advantage of parallel processing requires that a particular device has the ability to drive a large number of following devices. This could be achieved using free space propagation for addressing purposes. Furthermore, the summed effect of several elements could be focused onto one device to achieve fan-in.

(f) Gain. In order to maintain (d) and (e) above, there is a requirement for differential gain. This could possibly be achieved by the use of optical amplifier devices.

(g) Arrays. The easy construction of two dimensional (2-D) arrays within the technology must ideally be available.

(h) Speed and power. For 1-D circuits, subnanosecond or picosecond switching times are desirable, although this may be relaxed to microseconds for parallel arrays. Speed and power tend to be interchangeable but a low power device is a necessity. The power requirements for a device should be in the milliwatt region or less.

Certain, although not all, of the above requirements are met by specific nonlinear devices described in Section 10.8. For example, it is suggested [Ref. 100] that the ZnSe interference devices, used as separate elements activated by external addresses, exhibit the possibilities of projection and display. Proposals for logic subsystems of this type are shown in Figure 10.41. In addition, Refs. 100 and 106 indicate the possible arrangements for more complex optical logic subsystems,

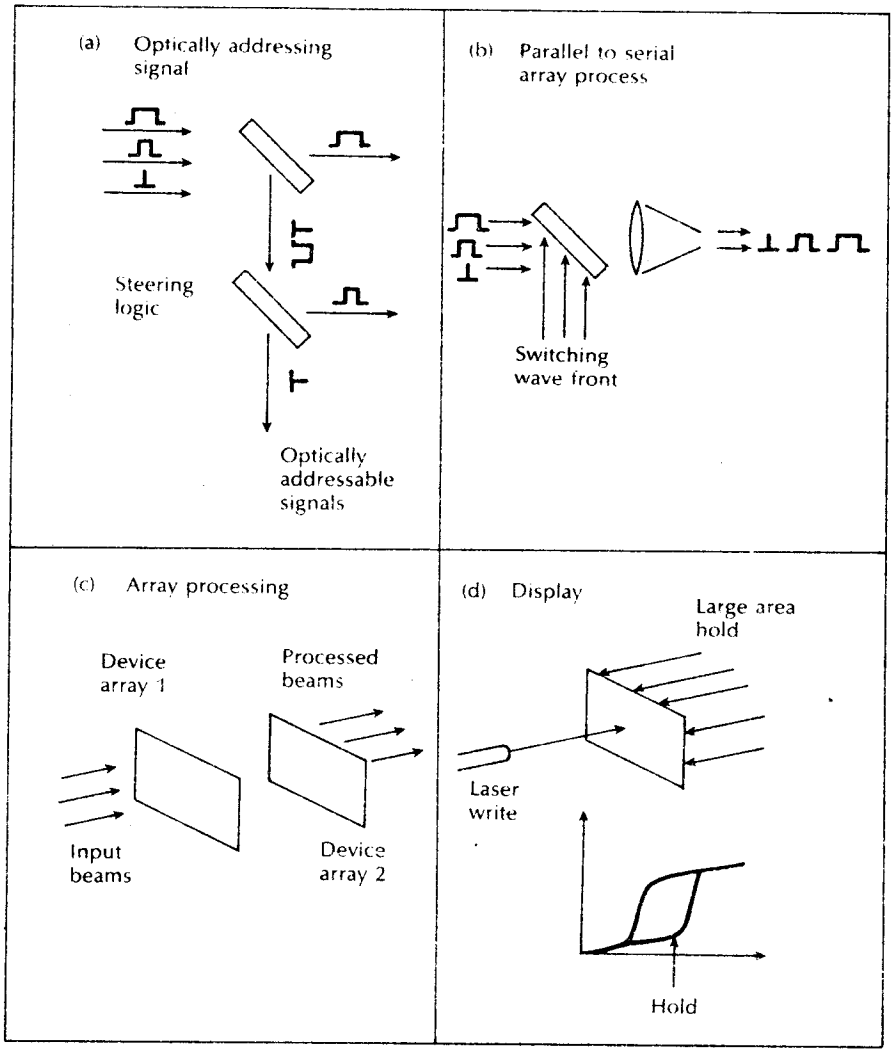

Figure 10.41 Proposals for logic subsystems based on the zinc selenide interference device, or similar [Ref. 100].

including a simple parallel processor, a serial to parallel convertor, a shift register and a packet switch. At present such proposals necessitate a solution which involves bulk optic, discrete elements together with possible monolithic IO devices. Moreover, a hybrid approach for the implementation of high speed switching matrices has been suggested [Ref. 107] which incorporates electronic logic elements with optical interconnections in order to exploit the best features of each technology.

In order to implement more complex optical logic subsystems, alternative nonlinear materials are already under investigation including inorganic insulators and organic nonlinear compounds [Refs. 108, 109]. Apart from lithium niobate, the three leading inorganic insulator materials are strontium barium niobate, bismuth silicon oxide and barium titanate. Unfortunately, these materials exhibit drawbacks in relation to poor thermal and mechanical properties, as well as slow response times (milliseconds). However, the organic nonlinear materials listed in Table 10.1 have displayed the potential for greater degrees of nonlinearity and much shorter response times. At present the major disadvantage with these materials is their relative environmental instability compared to inorganic materials (e.g. oxidation). However, work is still at a preliminary stage and more favourable results may be anticipated in the future.

Success with such materials, together with further developments of the other optical devices mentioned in Section 10.8, could lead to the implementation of an all-optical computer. However, it is more likely that initially hybrid optical/electronic computational machines will evolve. For example, a multiprocessing system under development, called the Connection Machine [Ref. 110], comprises a large array of printed circuit boards, each containing 512 processing elements divided equally between 32 electronic chips. This particular concept is illustrated in Figure 10.42 where, for simplicity, only four chips per level are shown. It may be observed that each electronic board contains a frequency selective filter (hologram) in addition to optoelectronic chips. These OEICs contain semiconductor lasers and

Table 10.1 Some organic nonlinear materials

Substituted and disubstituted acetylenes and diacetylenes
Anthracines and derivatives
Dyes
Macrocyclics
Polybenzimidazole
Polybenzimidazole and polybenzobisoxazole
Polyester and polyesteramids
Polyetherketone
Polyquinoxalines
Porphyrins and metal-porphyrin complexes
Metal complexes of TCNQ or TNAP
Urea

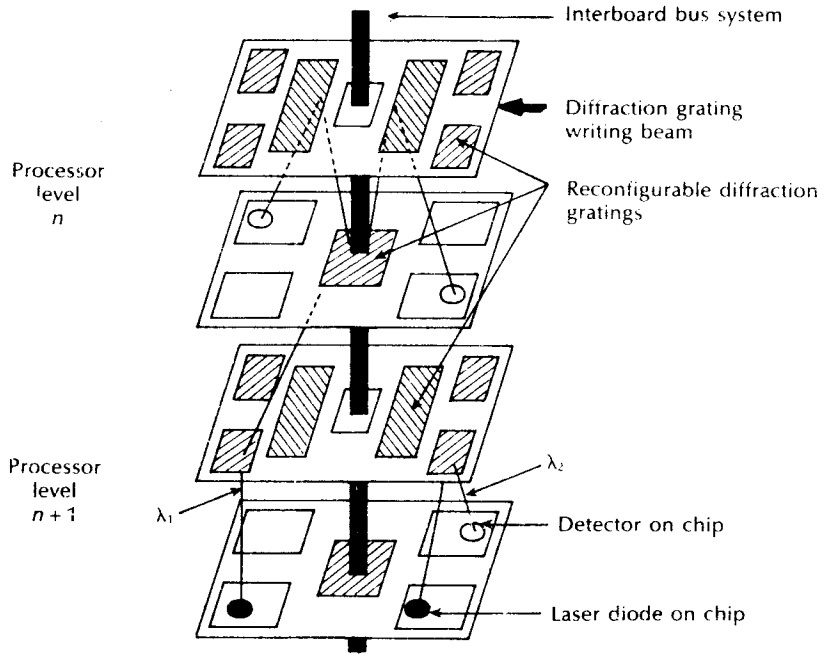

Figure 10.42 A hybrid optical/electronic multiprocessor architecture.

photodiodes which enable communications to be established between the chips. The switching operations for the interconnection process are performed by a planar array of reconfigurable diffraction gratings located on each board. Moreover, the architecture employs WDM to direct bit streams to the appropriate board as illustrated by λ_1 and λ_2 in Figure 10.42.

A possible all-optical digital multiprocessor architecture is shown in Figure 10.43 [Refs. 109, 111]. The input to the machine is via either an array of independently addressable semiconductor lasers, or alternatively via a 2-D spatial light modulator (SLM). A laser array is capable of higher modulation speeds but necessitates more complex circuitry, especially when uniformity is required over the complete array. The gate array illustrated in Figure 10.43 comprises either another 2-D SLM with a nonlinear response or an array of BODs. In theory the BODs would provide much greater switching speed but currently exhibit the drawbacks mentioned in Section 10.8. The beam controller employs reconfigurable diffraction gratings in order to provide switching and interconnection. However, as a result of the large number of channels required in the all-optical computer it is likely that multiple planes of real time hologram arrays would be utilized.

It may be observed in Figure 10.43 that all three computer interconnect systems (CPU–CPU, CPU–memory and CPU–I/O) are combined in the beam controller, although they could be implemented by three different components. Nevertheless,

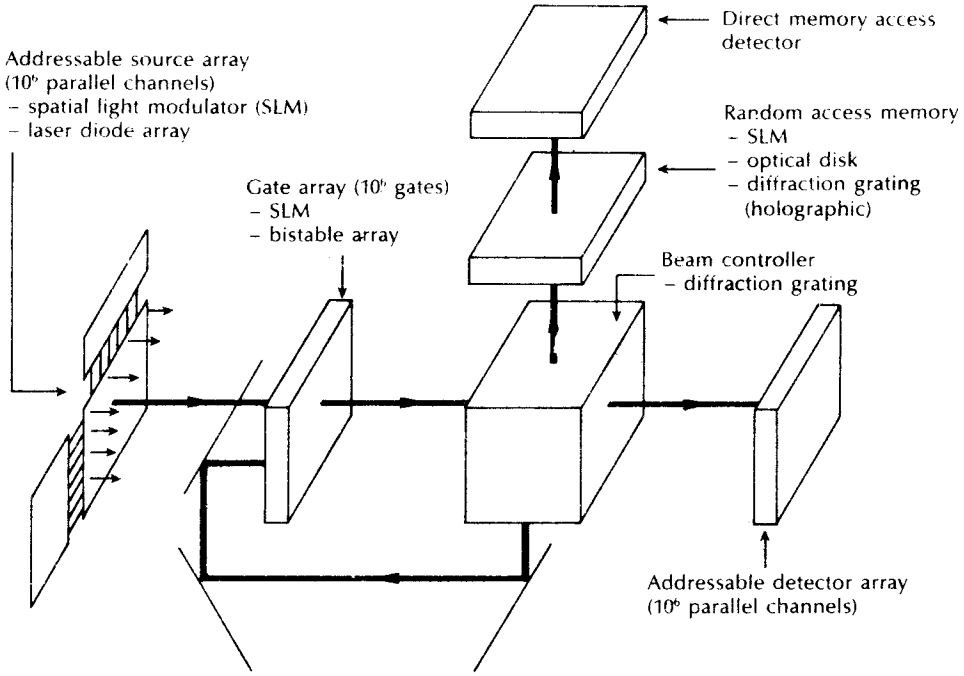

Figure 10.43 A possible all-optical multiprocessor architecture.

the ideal solution involves the beam controller directing any beam emerging from the gate array to any particular location on either the detector array, the memory, or the input of the gate array. Moreover, several logic elements can be interconnected via the beam controller to form a processing element. An example of a possible structure for a processing element, or node, in which individual elements in the gate array are designated to typical functions such as logic unit, clock, cache memory, etc., is illustrated in Figure 10.44. The example shown depicts a 5×5 rectangular array of logic elements, or gates, which gives 25 per processor. A practical multiprocessor might require 4×10^4 nodes giving 10^6 switching elements in the gate array.

A variant on the above architecture has been developed by AT & T Laboratories who recently announced the first demonstration of a digital optical processor [Ref. 112]. This processor, which operates at 10^6 cycles per second, is shown in schematic in Figure 10.45. The hybrid bistable switching element is a GaAs/AlGaAs symmetric self-electro-optic effect device (S-SEED) which is claimed to offer a potential of 10^9 operations per second with a switching energy of 1 pJ (see Section 10.8). The S-SEEDs which are 5 μm square and contain two mirrors with controllable reflectivity are formed into thirty-two device arrays. Each array also

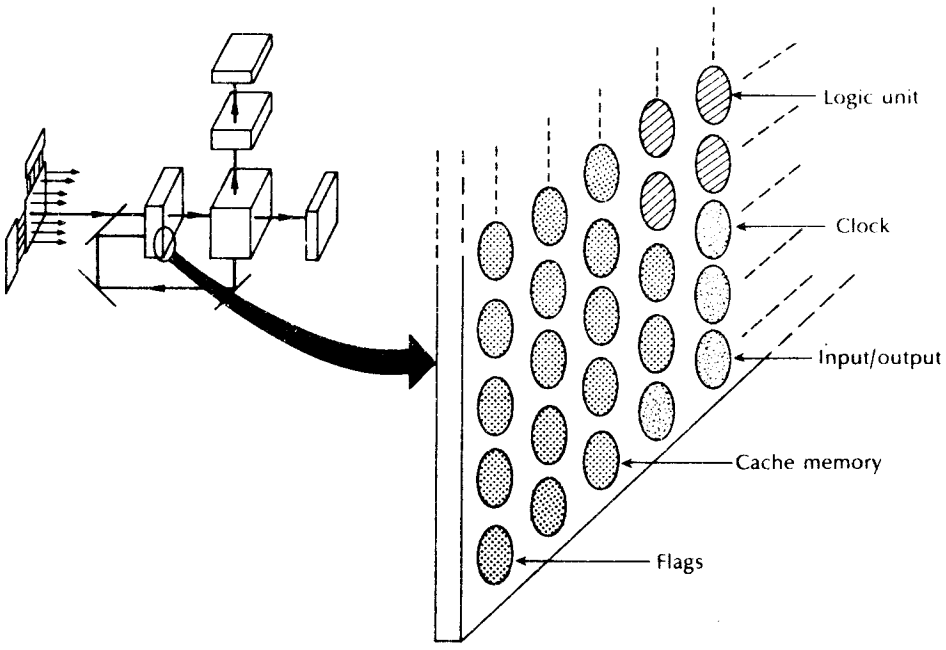

Figure 10.44 A processing element within the all-optical multiprocessor of Figure 10.43.

contains two 10 mW modulated injection laser diodes emitting at a wavelength of 0.85 μm as illustrated in Figure 10.45(a).

In the demonstration four S-SEED arrays were located within the processor, as may be observed in Figure 10.45(b). The injection lasers emitted many separate beams to provide communication between the arrays whilst each S-SEED drove two inputs. Interconnection between the four arrays was controlled by the lenses and masks, also shown in Figure 10.45. The masks comprised glass slides with patterns of transparent and opaque spots that allowed or impeded the transmission of light. Hence these patterns defined the connectivity within the processor.

The processor logic was accomplished by each S-SEED operating as a NOR-gate. Thus the output from each device array served as an input for the next array where the logic state of the S-SEEDs in the second array were determined by the state of the devices in the first array. Changing the on–off status of the switches in successive arrays allowed calculations to be performed. The memory resided in each S-SEED which did not change its state until the information represented by that state (i.e. a 0 or 1) was processed. In this way extensive pipelining of information was utilized within the processor (i.e. the output from one part of the machine served as the input for another part). Finally, the I/O was accomplished using both optical fibers and laser beams transmitted through free space.

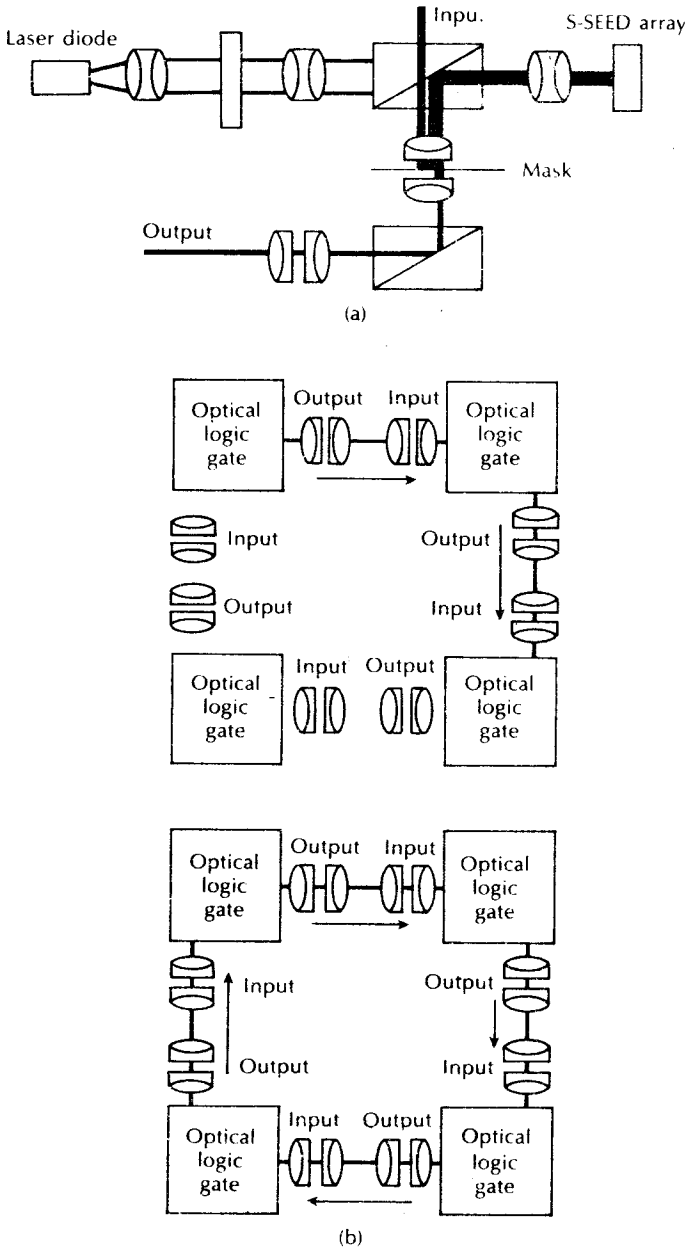

Figure 10.45 The A T & T digital optical processor: (a) structure of the processor S-SEED array module; (b) demonstration system using four array modules.

It is suggested that larger device arrays operating at faster switching speeds combined with the interconnection of greater numbers of modules will be demonstrated in the near future [Ref. 112]. Hence it would appear that the optical computer dimension to the future telecommunication network is firmly on the agenda.

Problems

10.1 Give the major reasons which have led to the development of optical amplifiers, outlining the attributes and application areas for these devices.

Describe the two main SLA types and indicate their distinguishing features.

10.2 A Fabry–Perot SLA has facet reflectivities of 23% and a single pass gain of 6 dB. The device has an active region with a refractive index of 3.6, a peak gain wavelength of 1.55 μm with a spectral bandwidth of 5 GHz. Determine the length of the active region for the FPA and also its mode spacing.

10.3 The following parameter values apply to a semiconductor TWA operating at a wavelength of 1.3 μm:

material gain coefficient	1000 cm^{-1}
effective loss coefficient	22 cm^{-1}
active region length	200 μm
facet reflectivities	0.1%
optical confinement factor	0.3

Calculate in decibels both the minimum and the maximum optical gain that could be obtained from the device.

10.4 Determine the peak–trough ratio of the passband ripple for the TWA of Problem 10.3. Compare this value with that obtained using a device with the same specification as Problem 10.3 excepting that the facet reflectivities are reduced to 0.03%.

Estimate the cavity gain for the latter semiconductor TWA.

10.5 Describe the phenomenon of backward gain in a semiconductor TWA and suggest a way in which it might be limited in systems that employ cascaded amplifiers.

A semiconductor TWA has a maximum cavity gain of 17 dB with a peak–trough ratio of 3 dB. Estimate the backward gain exhibited by the device under maximum gain operation.

10.6 (a) Sketch the major elements of a fiber amplifier and describe the operation of the device. Indicate the benefits of fiber amplifier technology in comparison with that associated with SLAs.

(b) Using an energy band diagram, briefly discuss the mechanism for the provision of stimulated emission in the erbium doped silica fiber amplifier. Name and describe a phenomenon occurring in this material system which creates a limitation to the optical gain that may be obtained from the device.

10.7 Explain the gain process in a Raman fiber amplifier and comment upon the flexibility associated with the pumping process in this fiber amplifier type.

The Raman gain coefficient for a 10 μm core diameter silica based fiber at a pump wavelength of 1.2 μm is 6.3×10^{-14} m W^{-1}. Determine the Raman gain obtained in a

25 km length of the fiber when it is pumped at this wavelength with an input power of 1.4 W and when the transmission loss is 0.8 dB km^{-1}. It may be assumed that the effective core radius is 1.15 times as large as the actual core radius and that complete polarization scrambling occurs.

10.8 Briefly describe the waveguide structures employed for IO.

The normalized effective thickness H for an asymmetric slab guide is given by Eq. (10.19), obtain an expression for the minimum effective thickness in order to provide optical confinement.

Determine the minimum effective thickness for a lithium niobate IO waveguide structure which has film and substrate refractive indices of 2.1 and 2.0, respectively, when it is operated at a wavelength of 1.3 μm.

10.9 Calculate the minimum effective thickness to provide optical confinement in a III–V semiconductor compound IO waveguide operating at a wavelength of 1.3 μm which has film and substrate refractive indices of 3.5 and 2.7, respectively, at this wavelength.

Comment on the value obtained in comparison to that determined in Problem 10.8.

10.10 Outline the techniques that can be employed to provide directional coupling between waveguides with IO.

Commencing with Eq. (10.25), show that the power coupled from one waveguide to another when their propagation constants are equal is proportional to the factor $\sin^2(Cz)$. The boundary conditions $A(z = 0) = A(0)$ and $B(z = 0) = 0$ may be assumed.

10.11 Compare the voltages required to operate lithium niobate and III–V semiconductor compound strip waveguide phase modulators in order to produce a phase change of π radians when using 3 cm long devices with a distance between the electrodes of 30 μm. The electro-optic coefficients for lithium niobate and the III–V semiconductor compound may be taken as 30.8×10^{-12} m V^{-1} and 1.3×10^{-12} m V^{-1}, respectively, whilst the refractive indices are 2.1 and 3.1, respectively, at the operating wavelength of 1.3 μm.

Comment on the values for the voltages obtained.

10.12 Assuming that the waveguide size for the III–V semiconductor waveguide modulator of problem 10.11 can be reduced by a factor of five, determine the reduced voltage needed to obtain a phase shift of π radians.

Comment on the value calculated in comparison with that obtained for the lithium niobate phase modulator of Problem 10.11.

10.13 A lithium niobate phase modulator has $V_\pi L$ of 45 V mm. Determine the interaction length required so that an applied voltage of 10 V will produce a phase shift of 2π radians.

10.14 A first order InGaAsP/InP waveguide grating filter is required for operation at a wavelength of 1.56 μm. The reflected light is expected to be incident over an angle of 3°. Estimate the filter length required to provide a 3 dB bandwidth of 2.5 Å for the device.

10.15 Discuss the function and operation of polarization transformers and frequency translators with specific reference to coherent optical transmission.

10.16 Outline the importance of optoelectronic integration in relation to the future developments in optical fiber communications. Illustrate your answer with descriptions of OEICs which have been fabricated to provide optical transmitter, receiver and multiplexing functions.

10.17 Describe the generalized bistable optical device and mention the applications in which

it is finding use. Indicate the primary reasons for the evolution of optical computational devices and discuss recent developments in this process which augur well for their future implementation.

Answers to numerical problems

10.2 234 μm, 1.43 nm
10.3 22.1 dB, 26.8 dB
10.4 4.6 dB, 0.7 dB
29.2 dB
10.5 12.1 dB
10.7 31.8 dB
10.8 1.42 μm
10.9 0.41 μm
10.11 4.6 V, 33.6 V
10.12 6.7 V
10.13 9.0 mm
10.14 1.5 cm

References

[1] M. J. O'Mahony, 'Semiconductor laser optical amplifiers for use in future fiber systems', *J. of Lightwave Technol.*, **6**(4), pp. 531–544, 1988.
[2] P. Cockrane, 'Future directions in long haul fibre optic systems', *Br. Telecom Technol. J.*, **8**(2), pp. 5–17, 1990.
[3] J. M. Senior and S. D. Cusworth, 'Devices for wavelength multiplexing and demultiplexing', *IEE Proc., Pt. J.*, **136**(3), pp.183–202, 1989.
[4] M. J. O'Mahony, 'Optical amplification techniques using semiconductors and fibres', *Proc. SPIE Int. Soc. Opt. Eng. USA, Fibre Optics'89*, **1120**, pp. 43–44, 1989.
[5] R. Baker, 'Optical amplification', *Physics World*, pp. 41–44, March 1990.
[6] J. Buus and R. Plastow, 'Theoretical and experimental investigations of 1.3 μm Fabry–Perot amplifiers, *IEEE J. Quantum Electron.*, **QE-21**(6), pp. 614–618, 1985.
[7] G. Eisenstein, B. L. Johnson and G. Raybon, 'Travelling-wave optical amplifier at 1.3 μm', *Electron. Lett.*, **23**(19), pp. 1020–1022, 1987.
[8] G. N. Brown, 'A study of the static locking properties of injection locked laser amplifiers', *Br. Telecom. Technol. J.*, **4**(1), pp. 71–80, 1986.
[9] T. Saitoh and T. Mukai, 'Recent progress in semiconductor laser amplifiers', *J. of Lightwave Technol.*, **6**(11), pp. 1656–1664, 1988.
[10] M. J. O'Mahony, I. W. Marshall and H. J. Westlake, 'Semiconductor laser amplifiers for optical communication systems', *Br. Telecom Technol J.*, **5**(3), pp. 9–18, 1987.
[11] T. Saitoh, T. Mukai and O. Mikami, 'Theoretical analysis of antireflection coatings on laser diode facets', *J. of Lightwave Technol.*, **LT-3**(2), pp. 288–293, 1985.
[12] G. Eisentein and R. M. Jopson, 'Measurements of the gain spectrum of near-travelling-wave and Fabry–Perot semiconductor optical amplifiers at 1.5 μm', *Int. J. Electron.*, **60**(1), pp. 113–121, 1986.
[13] M. J. Adams, H. J. Westlake, M. J. O'Mahony and I. D. Henning, 'A comparison of active and passive bistability in semiconductors', *IEEE J. Quantum Electron.*, **QE-21**(9), pp. 1498–1504, 1985.
[14] I.D. Henning, M. J. Adams and J. V. Collins, 'Performance predictions from a new optical amplifier model', *IEEE J. Quantum Electron.*, **QE-21**, pp. 609–613, 1985.

[15] T. Mukai, Y. Yamamoto and T. Kimwa, 'Optical amplification by semiconductor lasers', in *Semiconductor and Semimetals*, **22-E**, R. K. Willardson and A. C. Beer (Eds.), Academic Press, pp. 265–319, 1985.

[16] N. A. Olsson, 'Lightwave systems with optical amplifiers', *J. Lightwave Technol.*, **7**(7), pp. 1071–1082, 1989.

[17] P. Urquhart, 'Review of rare earth doped fibre lasers and amplifiers', *IEE Proc., Pt. J.*, **135**(6), pp. 385–407, 1988.

[18] Y. Aoki, 'Properties of fiber Raman amplifiers and their applicability to digital optical communication systems', *J. of Lightwave Technol.*, **6**(7), pp. 1225–1239, 1988.

[19] G. N. Brown and D. M. Spirit, 'Gain saturation and laser linewidth effects in a Brillouin fibre amplifier', *15th European Conf. on Opt. Commun.* (*ECOC-89*), Gottenburg, pp. 70–73, September 1989.

[20] R. J. Mears, L. Reekie, I. M. Jauncey and D. N. Payne, 'Low-noise erbium-doped fibre amplifier at 1.54 μm', *Electron Lett.*, **23**, pp. 1026–1028, 1987.

[21] E. Desurvire, J. R. Simpson and P. C. Parker, 'High-gain erbium-doped travelling-wave fibre amplifier', *Opt. Lett.*, **12**, pp. 888–890, 1987.

[22] D. N. Payne and L. Reekie, 'Rare-earth-doped fibre lasers and amplifiers', *14th European Conf. on Opt. Commun.* (*ECOC'88*), pp. 49–53, September 1988.

[23] C. A. Millar, M. C. Brierley and P.W. France, 'Optical amplification in an erbium-doped fluorozirconate fibre between 1480 nm and 1600 nm', *IEE Conf. Publ.*, **292**, *Pt. 1.*, pp. 66–69, 1988.

[24] Y. Aoki, S. Kishida, H. Honomon, K. Washio and M. Sugimoto, 'Efficient backward and forward pumping CW Raman amplification for InGaAsP laser light in silica fibres', *Electron. Lett.*, **19**, pp 620–622, 1983.

[25] Y. Durteste, M. Monerie and P. Lamouler, 'Raman amplification in fluoride glass fibres', *Electron. Lett.*, **21**, p. 723, 1985.

[26] N. Edegawa, K. Mochizuki and Y. Imamoto, 'Simultaneous amplification of wavelength division multiplexed signals by highly efficient amplifier pumped by higher power semiconductor lasers', *Electron. Lett.*, **23**, pp. 556–557, 1987.

[27] M. L. Dakss and P. Melman, 'Amplified stimulated Raman scattering and gain in fiber Raman amplifiers', *J. Lightwave Technol.*, **LT-3**, pp. 806–813, 1985.

[28] R. J. Stolen, 'Polarization effects in fiber Raman and Brillouin lasers', *IEEE J. Quantum Electron.*, **QE-15**, pp. 1157–1160, 1979.

[29] C. G. Atkins, D. Cotter, D. W. Smith and R. Wyatt, 'Application of Brillouin amplification in coherent optical transmission', *Electron. Lett.*, **22**, pp. 556–557, 1986.

[30] A. R. Charplyvy and R. W. Tkach, 'Narrow-band tunable optical filter for channel selection in densely packed WDM systems', *Electron. Lett.*, **22**, pp. 1084–1085, 1986.

[31] R. G. Waarts and R. P. Braun, 'Crosstalk due to stimulated Brillouin scattering in monomode fiber', *Electron. Lett.*, **21**, p. 1114, 1985.

[32] E. J. Bachus, R. P. Braun, W. Eutin, E. Grossman, H. Foisel, K. Heims and B. Strebel, 'Coherent optical fibre subscriber line', *Electron. Lett.*, **21**, p. 1203, 1985.

[33] D. B. Anderson, *Optical and Electrooptical Information Processing*, pp. 221–234, MII Press, 1965.

[34] S. E. Miller, 'Integrated optics: an introduction', *Bell Syst. Tech. J.*, **48**(7), pp. 2059–2069, 1969.

[35] L. Levi, *Applied Optics*, Vol. 2, Chapter 13, John Wiley, 1980.

[36] H. Kogelnik and V. Ramaswamy, 'Scaling rules for thin-film optical waveguides', *Appl. Opt.*, **13**(8), pp. 1857–1862, 1974.
[37] A. Reisinger, 'Attenuation properties of optical waveguides with a metal boundary', *Appl. Phys. Lett.*, **23**(5), pp. 237–239, 1973.
[38] H. Kogelnik, 'Limits in integrated optics', *Proc. IEEE*, **69**(2), 232–238, 1981.
[39] T. Tamir (Ed.), *Integrated Optics* (2nd edn), Springer-Verlag, New York, 1979.
[40] J. Wilson and J. F. B. Hawkes, *Optoelectronics: An introduction* (2nd edn), Chapter 3, Prentice Hall, 1989.
[41] P. J. R. Laybourne and J. Lamb, 'Integrated optics: a tutorial review', *Radio Electron. Eng. (IERE J.)*, **51**(7/8), pp. 397–413, 1981.
[42] B. K. Nayar and R. C. Booth, 'An introduction to integrated optics', *Br. Telecom Technol. J.*, **4**(4), pp. 5–15, 1986.
[43] R. Th. Kersten, 'Integrated optics for sensors', in J. Dakin and B. Culshaw (Eds.), *Optical Fiber Sensors: Principles and components*, Artech House, 1988.
[44] J. J. Veselka and S. K. Korotky, 'Optimization of Ti : $LiNbO_3$ optical waveguides and directional coupler switches for 1.5 μm wavelength, *IEEE J. Quantum Electron.*, **QE-22**, pp. 933–938, 1986.
[45] S. K. Korotky and R. C. Alferness, 'Waveguide electrooptic devices for optical fiber communication', in S. E. Miller and I. P. Kaminow (Eds.), *Optical Fiber Telecommunications II*, Academic Press, pp. 421–465, 1988.
[46] E. Kapron and R. Bhat, 'Low-loss GaAs/AlGaAs ridge waveguides grown by organmetallic vapour-phase epitaxy', *Tech. Dig. of Conf. on Lasers and Electrooptics*, Baltimore, USA, paper WQ3, 1987.
[47] H. Sasaki and I. Anderson, 'Theoretical and experimental studies on active Y-junctions in optical waveguides', *IEEE J. Quantum Electron*, **QE-14**, pp. 883–892, 1978.
[48] D. Marcuse, 'The coupling of degenerate modes in two parallel dielectric waveguides', *Bell Syst. Tech. J.*, **50**(6), pp. 1791–1816, 1971.
[49] A. Yariv, 'Coupled mode theory for guided wave optics', *IEEE J. Quantum Electron.*, **QE-9**, pp. 919–933, 1973.
[50] M. Papuchon, Y. Combemale, X. Mathieu, D. B. Ostrowsky, L. Reiber, A. M. Roy, B. Sejourne and M. Werner, 'Electrically switched optical directional coupler: COBRA', *Appl. Phys. Lett.*, **27**(5), pp. 289–291, 1975.
[51] S. F. Su, L. Jou and J. Lenart, 'A review on classification of optical switching systems', *IEEE Commun. Mag.*, **24**(5), pp. 50–55, 1986.
[52] S. D. Personick, 'Photonic switching: technology and applications', *IEEE Commun. Mag.*, **25**(5), pp. 5–8, 1987.
[53] T. Yasui and H. Goto, 'Overview of optical switching technologies in Japan', *IEEE Commun. Mag.*, pp. 10–15, 1987.
[54] M. Sakaguchi and K. Kaede, 'Optical switching device technologies', *IEEE Commun. Mag.*, **25**(5), pp. 27–32, 1987.
[55] W. A. Payne and H. S. Hinton, 'Design of lithium niobate based photonic switching systems', *IEEE Commun. Mag.*, pp. 37–41, 1987.
[56] S. D. Personick and W. O. Fleckenstein, 'Communications switching – from operators to photonics', *Proc. IEEE*, **75**(10), pp. 1380–1403, 1987.
[57] H. Goto, K. Nagashima, S. Suzuki, M. Kondo and Y. Ohta, 'Optical time-division digital switching: an experiment', *Topical Meeting on Opt. Fiber Commun.* (USA), MJ6, pp. 22–23, 1983.

[58] Y. Shimazu and S. Nishi, 'Wavelength-division optical switch using acousto-optic device', *Record of National Convention of IECEJ*, **510**, p. 2563, 1986.

[59] R. C. Alferness, 'Guided-wave devices for optical communication', *IEEE J. Quantum Electron.*, **QE-17**(6), pp. 946–959, 1981.

[60] D. B. Ostrowsky, 'Optical waveguide components' in M. J. Howes and D. V. Morgan (Eds.), *Optical Fibre Communications*, pp. 165–188, John Wiley, 1980.

[61] F. Auracher and R. Keil, 'Method for measuring the rf modulation characteristics of Mach-Zehnder-type modulators', *Appl. Phys. Lett.*, **36**, pp. 626–628, 1980.

[62] R. C. Alferness, C. H. Joyner, M. D. Divino and L. L. Buhl, 'InGaAsP/InP, waveguide grating filters for $\lambda = 1.5\ \mu$m', *Appl. Phys. Lett.*, **45**, pp. 1278–1280, 1984.

[63] R. V. Schmidt, D. C. Flanders, C. V. Shank and R. D. Standby, 'Narrow-band grating filters for thin-film optical waveguides', *Appl. Phys. Lett.*, **25**, pp. 651–652, 1974.

[64] A. Katzir, A. C. Livanos, J. B. Shellan and A. Yariv, 'Chirped gratings in integrated optics', *IEEE J. Quantum Electron.*, **QE-13**(4), pp. 296–304, 1977.

[65] R. V. Alferness and L. L. Buhl, 'Waveguide electro-optic polarization transformer', *Appl. Phys. Lett.*, **38**(9), pp. 655–657, 1981.

[66] W. A. Stallard, D. J. T. Heatley, R. A. Lobbett, A. R. Beaumont, D. J. Hunkin, B. E. Daymond-John, R. C. Booth and G. R. Hill, 'Electro-optic frequency translators and their application in coherent optical fibre systems', *Br. Telecom Technol. J.*, **4**(4), pp. 16–22, 1986.

[67] K. K. Wong, R. De La Rue and S. Wright, 'Electro-optic waveguide frequency translator in $LiNbO_3$ fabricated by proton exchange', *Opt. Lett.*, **7**(11), pp. 546–548, 1982.

[68] F. Heismann and R. Ulrich, 'Integrated optical frequency translator with stripe waveguide', *Appl. Phys. Lett.*, **45**(5), pp. 490–492, 1984.

[69] F. Auracher and R. Keil, 'Method for measuring the RF modulating characteristics of Mach–Zehnder-type modulators', *Appl. Phys. Lett.*, **36**(8), pp. 626–629, 1980.

[70] C. M. Gee and G. D. Thurmond, 'High speed integrated optic travelling wave modulator', *Proc. 2nd European Conf. on Integrated Optics* (Italy), pp. 118–121, October 1983.

[71] B. E. Daymond-John, A. R. Beaumont, W. A. Stallard and R. C. Booth, 'Lithium niobate electro-optic frequency translators for coherent optical systems', *Proc. Integrated Optical Circuit Engineering II* (USA), pp. 214–219, September 1985.

[72] W.A. Stallard, A. R. Beaumont and R. C. Booth, 'Integrated optic devices for coherent transmission', *J. Lightwave Technol.*, **LT-4**(7), pp. 852–857, 1986.

[73] M. Nakamura and T. Ozeki 'Optoelectronic integration and its impact on system application', *IEEE J. on Selected Areas in Commun.*, **SAC-4**(9), 1509–1514, 1986.

[74] H. Matsueda, S. Sasaki and M. Nakamura, 'GaAs optoelectronic integrated light sources', *J. of Lightwave Technol.*, **LT-1**(1), pp. 261–269, 1983.

[75] P. J. T. Mellor, 'Gallium arsenide integrated circuits for telecommunication systems', *Br. Telecom Technol. J.*, **5**(4), pp. 5–18, 1987.

[76] H. Nobuhara, T. Sanada, M. Kuno, M. Makinchi, T. Funjii and O. Wada, 'OEIC transmitter fabricated by planar integration process', *18th Conf. Solid State Devices and Materials*, Tokyo, Japan, pp. 185–188, August 1986.

[77] H. Soda, M. Furutsu, K. Sato, M. Matsuda and H. Ishikawa, '5 Git/s modulation characteristics of optical intensity modulator monolithically integrated with DFB laser', *Electron. Lett.*, **25**(5), pp. 334–355, 1989.

[78] H. Matsueda, 'AlGaAs OEIC transmitters', *J. of Lightwave Technol.*, **LT-5**(10), pp. 1382–1390, 1987.

[79] K. Kasahara, T. Terakado, A. Suzuki and S. Murata, 'Monolithically integrated high-speed light source using 1.3 μm wavelength DFB-DC-PBH laser', *J. of Lightwave Technol.*, **LT-4**(7), pp. 908–912, 1986.

[80] A. Suzuki, K. Kasahara and M. Shikada, 'InGaAsP/InP long wavelength optoelectronic integrated circuits (OEIC's) for high-speed optical fibre communication systems', *J. of Lightwave Technol.*, **LT-5**(10), pp. 1479–1487, 1987.

[81] H. Verriele, J. L. Lorriaux, P. Legry, J. P. Gouy, J. P. Vilcot and D. Decoster, 'GaAs monolithic integrated photoreceiver for 0.8 μm wavelength: association of Schottky photodiode and FET', *IEE Proc., Pt. J*, **135**(2), 1988.

[82] K. Kasahara, A. Suzuki, S. Fujita, Y. Inomoto, T. Terakado and M. Shikada, 'InGaAsP/InP long wavelength transmitter and receiver OEIC's for high speed optical transmission systems', in *12th European Conf. Optical Fiber Commun.*, (Spain), pp. 119–122, 1986.

[83] O. Wada, H. Nobuhara, T. Sanada, M. Kuno, M. Makiuchi, T. Fujii and T. Sakurai, 'Optoelectronic integrated four-channel transmitter array incorporating AlGaAs/GaAs quantum well lasers', *J. of Lightwave Technol.*, **7**(1), pp. 186–197, 1989.

[84] S. R. Forrest, 'Optoelectronic integrated circuits', *Proc. IEEE*, **75**(11), pp. 1488–1497, 1987.

[85] O. Wada, H. Hamaguchi, M. Makiuchi, T. Kumai, M. Ito, K. Nakai, T. Horimatsu and T. Sakurai, 'Monolithic four-channel photodiode/amplifier receiver array integrated on a GaAs substrate', *J. of Lightwave Technol.*, **LT-4**, pp. 1694–1703, 1986.

[86] K. Kobayashi, 'Integrated optical and electronic devices', in S. E. Miller and I. P. Kaminow (Eds.), *Optical Fiber Telecommunications II*, Academic Press, pp. 601–630, 1988.

[87] T. Suhara, Y. Hunda, H. Nishihara and J. Koyama, 'Monolithic integrated micrograting and photodiodes for wavelength demultiplexing', *Appl. Phys. Lett.*, **40**(2), pp. 120–122, 1982.

[88] T. Baba, Y. Kokubun and H. Watanabe, 'Monolithic integration of an ARROW-type demultiplexer and photodetector in the shorter wavelength region', *J. of Lightwave Technol.*, **8**(1), pp. 99–104, 1990.

[89] N. Bar-Chain, K. Y. Lau, I. Ury and A. Yariv, 'Gallium aluminium arsenide integrated optical repeater', *Proc. SPIE Int. Soc. Eng. (USA)*, **466**, pp. 65–68, 1984.

[90] S. Hata, M. Ikeda, S. Kondo and Y. Noguchi, 'PIN-FET-LD, integrated device in long wavelength region', *Tech. Dig. Domestic Conf., IECE*, Japan, p. 58, 1985.

[91] R. I. MacDonald, 'Optolectronic switching', *IEEE Commun. Mag.*, **25**(5), pp. 33–36, 1987.

[92] T. Iwama, Y. Oikawa, K. Yamaguchi, T. Horimatsu, M. Makiuchi and H. Hamaguchi, 'A 4×4 GaAs OEIC switch module', *Optical Fiber Commun. Conf.* (USA), **3**, paper WG3, 1987.

[93] W. J. Tomlinson and C. A. Brackett, 'Telecommunications applications of integrated optics and optoelectronics', *Proc. IEEE*, **75**(11), pp. 1512–1523, 1987.

[94] R. Cush and M. Goodwin, 'Optical logic devices', *National Electronic Review*, UK, pp. 51–55, 1987.

[95] P. W. Smith, I. P. Kaminow, P. J. Maloney and L. W. Stulz, 'Integrated bistable optical devices', *Appl. Phys. Lett.*, **33**(1), pp. 24–26, 1978.

[96] D. A. B. Miller, 'Multiple quantum well optical non-linearities'; bistability from increasing absorption and the self-electro-optic effect' *Phil. Trans. R. Soc. Lond.*, **A313**, pp. 239–248, 1984.

[97] D. Jager, F. Forsman and H. C. Zhai, 'Hybrid optical bistability based on increasing absorption in depletion layer of an Si Schottky SEED device', *Electron. Lett.*, **23**(10), 490–491, 1987.

[98] A. C. Walker, F. A. P. Tooley, M. E. Prise, J. G. H. Mathew, A. K. Kar, M. R. Taghizadeh and S. D. Smith, 'InSb devices: transphasors with high gain, bistable switches and sequential logic gates', *Phil. Trans. R. Soc. Lond.*, **A313**, pp. 249–256, 1984.

[99] S. D. Smith, J. G. H. Mathew, M. R. Taghizadeh, A. C. Walker, B. S. Wherret and A. Henry, 'Room temperature, visible wavelength optical bistability in ZnSe interference filters', *Optics Communications*, **51**, pp. 357–362, 1984.

[100] S. D. Smith, 'Optical bistability, phononic logic and optical computation', *Appl. Opt.*, **25**, pp.1550–1564, 1986.

[101] N. Peyghambarian, 'Recent advances in optical bistability', *Fiber and Integ. Optics*, **6**(2), pp. 117–123, 1987.

[102] P. Li Kam Wa, J. W. Sitch, N. J. Mason, J. S. Roberts and P. N. Robson, 'All-optical multiple-quantum well waveguide switch', *Electron. Lett.*, **21**, pp. 26–27, 1985.

[103] J. G. McInerney and D. M. Heffernan, 'Optical bistability in semiconductor injection lasers', *IEE Proc., Pt. J.*, **134**(1), pp. 41–50, 1987.

[104] Y. Odagiri, K. Komastu and S. Suzuki, 'Bistable laser diode memory for optical time-division switching applications', *Internat. Conf. on Lasers and Electro-optics*, Anaheim, California, USA, paper ThJ3, 1984.

[105] Y. Silberberg, 'All-optical repeater', *Opt. Lett.*, **11**(6), pp. 392–394, 1986.

[106] J. E. Midwinter, 'Light electronics, myth or reality', *IEE Proc., Pt. J.*, **132**, pp. 371–383, 1985.

[107] J. E. Midwinter, 'Novel approach to the design of optically activated wide band switching matrices', *IEE Proc., Pt. J.*, **134**(5), pp. 261–268, 1987.

[108] 'Research on nonlinear optical materials: an assessment', *Appl. Opt.*, **26**(2), pp. 211–234, 1987.

[109] J. A. Neff, 'Major initiatives for optical computing', *Opt. Eng.*, **26**(1), pp. 2–9, 1987.

[110] W. D. Hillis, *The Connection Machine*. The MIT Press, Cambridge, USA, 1985.

[111] B. K. Jenkins, P. Chavel, R. Forchheimer, A. A. Sawchuk and T. C. Strand', Architectural implications of a digital optical processor', *Appl. Opt.*, **23**(19), pp. 3465–3474, 1984.

[112] 'Optical computer: is concept becoming reality', *OE Reports, SPIE Int. Soc. Opt. Eng. (USA)*, **75**, pp. 1–2, March 1990.

11

Optical fiber systems 1: intensity modulation/direct detection

11.1 Introduction

The transfer of information in the form of light propagating within an optical fiber requires the successful implementation of an optical fiber communication system. This system, in common with all systems, is composed of a number of discrete components which are connected together in a manner that enables them to perform a desired task. Hence, to achieve reliable and secure communication using optical fibers it is essential that all the components within the transmission system

are compatible so that their individual performances, as far as possible, enhance rather than degrade the overall system performance.

The principal components of a general optical fiber communication system for either digital or analog transmission are shown in the system block schematic of Figure 11.1. The transmit terminal equipment consists of an information encoder or signal shaping circuit preceding a modulation or electronic driver stage which operates the optical source. Light emitted from the source is launched into an optical fiber incorporated within a cable which constitutes the transmission medium. The light emerging from the far end of the transmission medium is converted back into an electrical signal by an optical detector positioned at the input of the receive terminal equipment. This electrical signal is then amplified prior to decoding or demodulation in order to obtain the information originally transmitted.

The operation and characteristics of the optical components of this general system have been discussed in some detail within the preceding chapters. However, to enable the successful incorporation of these components into an optical fiber communication system it is necessary to consider the interaction of one component with another, and then to evaluate the overall performance of the system. Furthermore, to optimize the system performance for a given application it is often helpful to offset a particular component characteristic by trading it off against the performance of another component, in order to provide a net gain within the overall system. The electronic components play an important role in this context, allowing the system designer further choices which, depending on the optical components utilized, can improve the system performance.

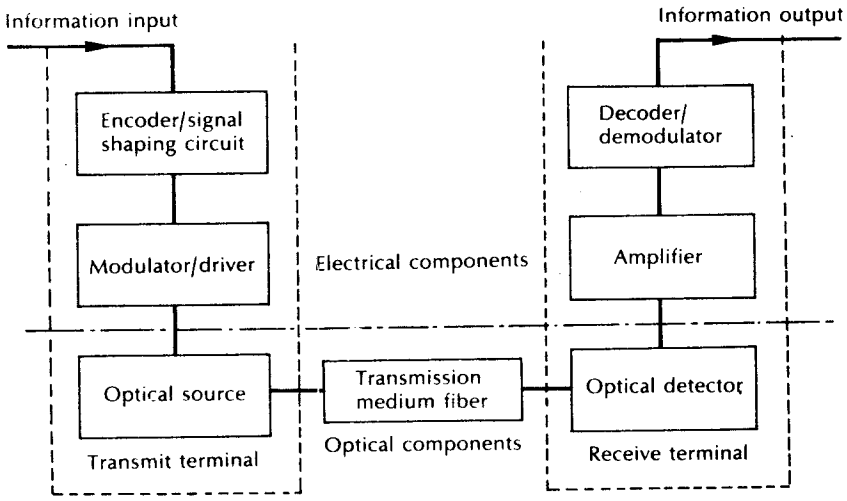

Figure 11.1 The principal components of an optical fiber communication system.

The purpose of this chapter is to bring together the important performance characteristics of the individual system elements, and to consider their interaction within optical fiber communication systems. In particular we concentrate on the major current implementations of optical fiber communication systems which employ some form of intensity modulation (IM) of the optical source, together with simple direct detection (DD) of the modulated optical signal at the receiver (see Chapter 9). Such IM/DD optical fiber systems are in widespread use within many application areas and do not employ the more sophisticated coherent detection techniques which are discussed in Chapter 12.

It is intended that this chapter provide guidance in relation to the various possible component configurations which may be utilized for different IM/DD system applications, whilst also giving an insight into system design and optimization. Hence, the optical components and the associated electronic circuits will be discussed prior to consideration of general system design procedures. Although the treatment is by no means exhaustive, it will indicate the various problems involved in system design and provide a description of the basic techniques and practices which may be adopted to enable successful system implementation.

We commence in Section 11.2 with a discussion of the optical transmitter circuit. This includes consideration of the source limitations prior to description of various LED and laser drive circuits for both digital and analog transmission. In Section 11.3 we present a similar discussion for the optical receiver including examples of preamplifier and main amplifier circuits. General IM/DD system design considerations are then dealt with in Section 11.4. This is followed by a detailed discussion of digital systems, commencing with an outline of the operating principles of pulse code modulated (PCM) systems in Section 11.5, before continuing to consider the various aspects of digital IM/DD optical fiber systems in Section 11.6.

Analog IM/DD optical fiber systems are dealt with in Section 11.7 where the various possible analog modulation techniques are described and analysed. Following, in Section 11.8, consideration is given to IM/DD optical fiber systems configured not simply as point-to-point links but as distribution systems. Then, in Section 11.9 the major multiplexing strategies (both digital and analog) which can be employed in IM/DD optical fiber systems are discussed in further detail to provide a greater understanding of the techniques which are being adopted to increase the information transmission capacity of both currently deployed and potential future systems. Finally, the deployment of optical amplifiers (see Chapter 10), particularly on long-haul IM/DD optical fiber links, is dealt with in Section 11.10 to complement the earlier consideration of multiplexing strategies and to enable the reader to appreciate the interaction of these advanced optical fiber communication techniques.

11.2 The optical transmitter circuit

The unique properties and characteristics of the injection laser and the light emitting diode (LED) which make them attractive sources for optical fiber communications were discussed in Chapters 6 and 7.

Although both device types exhibit a number of similarities in terms of their general performance and compatibility with optical fibers, striking differences exist between them in relation to both system application and transmitter design. It is useful to consider these differences, as well as the limitations of the two source types, prior to discussion of transmitter circuits for various applications.

11.2.1 Source limitations

11.2.1.1 Power

The electrical power required to operate both injection lasers and LEDs is generally similar, with typical current levels of between 20 and 300 mA (certain laser thresholds may be substantially higher than this – of the order of 1 to 2 A), and voltage drops across the terminals of 1.5 to 2.5 V. However, the optical output power against current characteristic for the two devices varies considerably, as indicated in Figure 11.2. The injection laser is a threshold device which must be operated in the region of stimulated emission (i.e. above the threshold) where continuous optical output power levels are typically in the range 1 to 10 mW.

Much of this light output may be coupled into an optical fiber because the isotropic distribution of the narrow linewidth, coherent radiation is relatively directional. In addition, the spatial coherence of the laser emission allows it to be readily focused by appropriate lenses within the numerical aperture of the fiber. Coupling efficiencies near 30% may be obtained by placing a fiber close to a laser mirror, and these can approach 80% with a suitable lens arrangement [Refs. 1 and

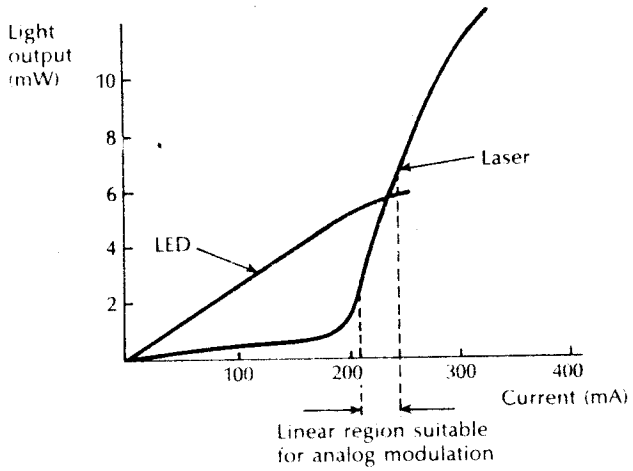

Figure 11.2 Light output (power) emitted into air as a function of d.c. drive current for a typical high radiance LED and for a typical injection laser. The curves exhibit nonlinearity at high currents due to junction heating.

2]. Therefore injection lasers are capable of launching between 0.5 and several milliwatts of optical power into a fiber.

LEDs are capable of similar optical output power levels to injection lasers depending on their structure and quantum efficiency, as indicated by the typical characteristic for a surface emitter shown in Figure 11.2. However, the spontaneous emission of radiation over a wide linewidth from the LED generally exhibits a Lambertian intensity distribution which gives poor coupling into optical fibers. Consequently only between 1% and perhaps 10% (using a good edge emitter) of the emitted optical power from an LED may be launched into a multimode fiber, even with appropriate lens coupling (see Section 7.3.6). These considerations translate into optical power levels from a few to several hundred microwatts launched into individual multimode fibers. Thus the optical power coupled into a fiber from an LED can be 10 to 20 dB below that obtained with a typical injection laser. The power advantage gained with the injection laser is a major factor in the choice of source, especially when considering a long-haul optical fiber link.

11.2.1.2 Linearity

Linearity of the optical output power against current characteristic is an important consideration with both the injection laser and LED. It is especially pertinent to the design of analog optical fiber communication systems where source nonlinearities may cause severe distortion of the transmitted signal. At first sight the LED may appear to be ideally suited to analog transmission as its output is approximately proportional to the drive current. However, most LEDs display some degree of nonlinearity in their optical output against current characteristic because of junction heating effects which may either prohibit their use or necessitate the incorporation of a linearizing circuit within the optical transmitter. Certain LEDs (e.g. etched-well surface emitters) do display good linearity, with distortion products (harmonic and intermodulation) between 35 and 45 dB below the signal level [Refs. 3 and 4].

An alternative approach to obtaining a linear source characteristic is to operate an injection laser in the light-generating region above its threshold, as indicated in Figure 11.2. This may prove more suitable for analog transmission than would the use of certain LEDs. However, gross nonlinearities due to mode instabilities may occur in this region. These are exhibited as kinks in the laser output characteristic (see Section 6.5.1). Therefore, many of the multimode injection lasers have a limited use for analog transmission without additional linearizing circuits within the transmitter, although some of the single-mode structures have demonstrated linearity suitable for most analog applications. Alternatively, digital transmission, especially that utilizing a binary (2 level) format, is far less sensitive to source nonlinearities and is therefore often preferred when using both injection lasers and LEDs.

11.2.1.3 Thermal

The thermal behaviour of both injection lasers and LEDs can limit their operation within the optical transmitter. However, as indicated in Section 6.7.1 the variation

of injection laser threshold current with the device junction temperature can cause a major operating problem. Threshold currents of typical AlGaAs devices increase by approximately 1% per degree centigrade increase in junction temperature. Hence any significant increase in the junction temperature may cause loss of lasing and a subsequent dramatic reduction in the optical output power. This limitation cannot usually be overcome by simply cooling the device on a heat sink, but must be taken into account within the transmitter design, through the incorporation of optical feedback, in order to obtain a constant optical output power level from the device.

The optical output from an LED is also dependent on the device junction temperature, as indicated in Section 7.4.2. Most LEDs exhibit a decrease in optical output power following an increase in junction temperature, which is typically around −1% per degree centigrade. This thermal behaviour, however, although significant is not critical to the operation of the device due to its lack of threshold. Nevertheless, this temperature dependence can result in a variation in optical output power of several decibels over the temperature range 0 to 70 °C. It is therefore a factor within system design considerations which, if not tolerated, may be overcome by providing a circuit within the transmitter which adjusts the LED drive current with temperature.

11.2.1.4 Response

The speed of response of the two types of optical source is largely dictated by their respective radiative emission mechanisms. Spontaneous emission from the LED is dependent on the effective minority carrier lifetime in the semiconductor material (see Section 7.4.3). In heavily doped (10^{18} to 10^{19} cm^{-3}) gallium arsenide this is typically between 1 and 10 ns. However, the response of an optical fiber source to a current step input is often specified in terms of the 10 to 90% rise time, a parameter which is reciprocally related to the device frequency response (see Section 11.6.5). The rise time of the LED is at least twice the effective minority carrier lifetime, and often much longer because of junction and stray capacitance. Hence, the rise times for many available LEDs lie between 2 and 50 ns and give 3 dB bandwidths of around 7 to at best 175 MHz. Therefore, LEDs have tended to be restricted to lower bandwidth applications, although suitable drive circuits can maximize their bandwidth capabilities (i.e. reduce rise times).

Stimulated emission from injection lasers occurs over a much shorter period giving rise times of the order of 0.1 to 1 ns, thus allowing 3 dB bandwidths above 1 GHz. However injection laser performance is limited by the device switch-on delay (see Section 6.7.2). To achieve the highest speeds it is therefore necessary to minimize the switch-on delay. Transmitter circuits, which prebias the laser to just below or just above threshold in conjunction with high speed drive currents which take the device well above threshold, prove useful in the reduction of this limitation.

11.2.1.5 Spectral width

The finite spectral width of the optical source causes pulse broadening due to material dispersion on an optical fiber communication link. This results in a

limitation on the bandwidth–length product which may be obtained using a particular source and fiber. The incoherent emission from an LED usually displays a spectral linewidth of between 20 and 50 nm (full width at half power (FWHP) points) when operating in the 0.8 to 0.9 μm wavelength range. This limits the bandwidth–length product with a silica fiber to around 100 and 160 MHz km at wavelengths of 0.8 and 0.9 μm respectively. Hence the overall system bandwidth for an optical fiber link over several kilometres may be restricted by material dispersion rather than the response time of the source.

The problem may be alleviated by working at a longer wavelength where the material dispersion in high silica fibers approaches zero (i.e. near 1.3 μm, see Section 3.9.1). In this region the source spectral width is far less critical and bandwidth–length products approaching 1 GHz km are feasible using LEDs.

Alternatively, an optical source with a narrow spectral linewidth may be utilized in place of the LED. The coherent emission from an injection laser generally has a linewidth of 1 nm or less (FWHP). Use of the injection laser greatly reduces the effect of material dispersion within the fiber, giving bandwidth–length products of 1 GHz km at 0.8 μm, and far higher at longer wavelengths. Hence, the requirement for a system operating at a particular bandwidth over a specific distance will influence both the choice of source and operating wavelength.

11.2.1.6 Nonzero extinction ratio

When the optical source is either intentionally prebiased-on during a 0 bit period, as indicated in Section 11.2.1.4, or simply not turned fully off, then some optical power will be emitted during the 0 pulse. This is particularly important with injection lasers when they are biased just below threshold and hence they launch spontaneous emissions into the fiber. In the case when optical power is incident on the photodetector during the 0 bit period, then the system is said to exhibit a nonzero extinction ratio.

The extinction ratio ε is usually defined as the ratio of the optical energy emitted in the 0 bit period to that emitted during the 1 bit period. For an ideal system $\varepsilon = 0$, and the extinction ratio therefore varies between this value and unity. It should be noted, however, that in some cases the extinction ratio is defined as the reciprocal of the above, which implies that it takes up values between 1 and ∞.

Typical values for the extinction ratio are between 0.05 and 0.10 and such nonzero ratios give rise to a noise penalty (often called an extinction ratio penalty) within the optical fiber communication system. The extinction ratio penalty can be evaluated and in practice it is often found to be in the range 1 to 2 dB. Any dark current present in the photodetector will also appear to increase the extinction ratio as it adds to the signal current in both the 0 and 1 bit periods. The greatest penalty occurs, however, in the case of quantum noise limited detection.

11.2.2 LED drive circuits

Although the LED is somewhat restricted in its range of possible applications in comparison with the more powerful, higher speed injection laser, it is generally

far easier to operate. Therefore in this section we consider some of the circuit configurations that may be used to convert the information voltage signal at the transmitter into a modulation current suitable for an LED source. In this context it is useful to discuss circuits for digital and analog transmission independently.

11.2.2.1 Digital transmission

The operation of the LED for binary digital transmission requires the switching on and off of a current in the range of several tens to several hundreds of milliamperes. This must be performed at high speed in response to logic voltage levels at the driving circuit input. A common method of achieving this current switching operation for an LED is shown in Figure 11.3. The circuit illustrated uses a bipolar transistor switch operated in the common emitter mode. This single stage circuit provides current gain as well as giving only a small voltage drop across the switch when the transmitter is in saturation (i.e. when the collector–base junction is forward biased, the emitter to collector voltage V_{CE} (sat) is around 0.3 V).

The maximum current flow through the LED is limited by the resistor R_2 whilst independent bias to the device may be provided by the incorporation of resistor R_3. However, the switching speed of the common emitter configuration is limited by space charge and diffusion capacitance; thus bandwidth is traded for current gain. This may, to a certain extent, be compensated by overdriving (pre-emphasizing) the base current during the switch-on period. In the circuit shown in Figure 11.3 pre-emphasis is accomplished by use of the speed-up capacitor C.

Increased switching speed may be obtained from an LED without a pulse shaping or speed-up element by use of a low impedance driving circuit, whereby charging of the space charge and diffusion capacitance occurs as rapidly as possible. This may be achieved with the emitter follower drive circuit shown in Figure 11.4 [Ref.

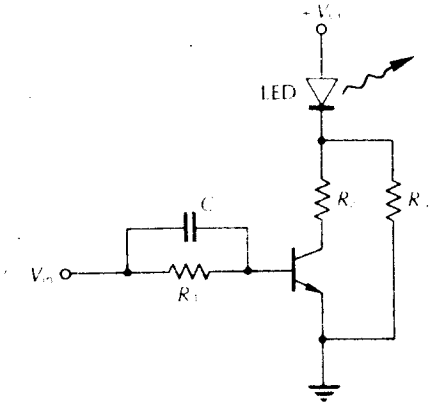

Figure 11.3 A simple drive circuit for binary digital transmission consisting of a common emitter saturating switch.

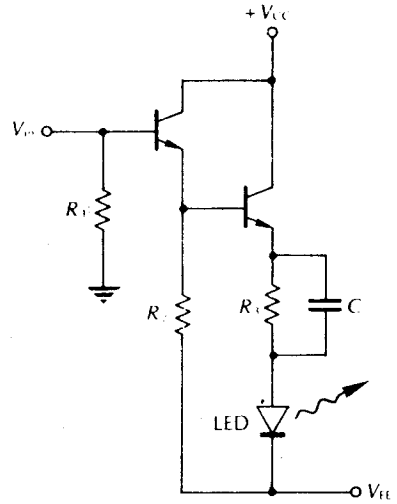

Figure 11.4 Low impedance drive circuit consisting of an emitter follower with compensating matching network [Ref. 5].

5]. The use of this configuration with a compensating matching network (R_3C) provides fast direct modulation of LEDs with relatively low drive power. A circuit, with optimum values for the matching network, is capable of giving optical rise times of 2.5 ns for LEDs with capacitance of 180 pF, thus allowing 100 Mbit s^{-1} operation [Ref. 6].

Another type of low impedance driver is the shunt configuration shown in Figure 11.5. The switching transistor in this circuit is placed in parallel with the LED, providing a low impedance path for switching off the LED by shunting current around it. The switch-on performance of the circuit is determined by the combination of resistor R and the LED capacitance. Stored space charge may be removed by slightly reverse biasing the LED when the device is switched off. This may be achieved by placing the transistor emitter potential V_{EE} below ground. In this case a Schottky clamp (shown dotted) may be incorporated to limit the extent of the reverse bias without introducing any extra minority carrier stored charge into the circuit.

A frequent requirement for digital transmission is the interfacing of the LED by drive circuit with a common logic family, as illustrated in the block schematic of Figure 11.6(a). In this case the logic interface must be considered along with possible drive circuits. Compatibility with TTL may be achieved by use of commercial integrated circuits, as shown in Figure 11.6(b) and (c). The configuration shown in Figure 11.6(b) uses a Texas Instruments' 74S140 line driver which provides a drive current of around 60 mA to the LED when R_1 is 50 Ω. Moreover, the package contains two sections which may be connected in parallel

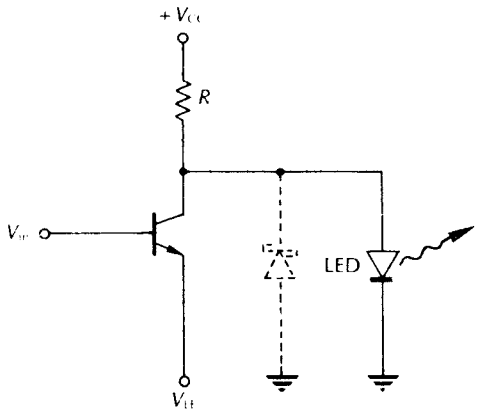

Figure 11.5 Low impedance drive circuit consisting of a simple shunt configuration.

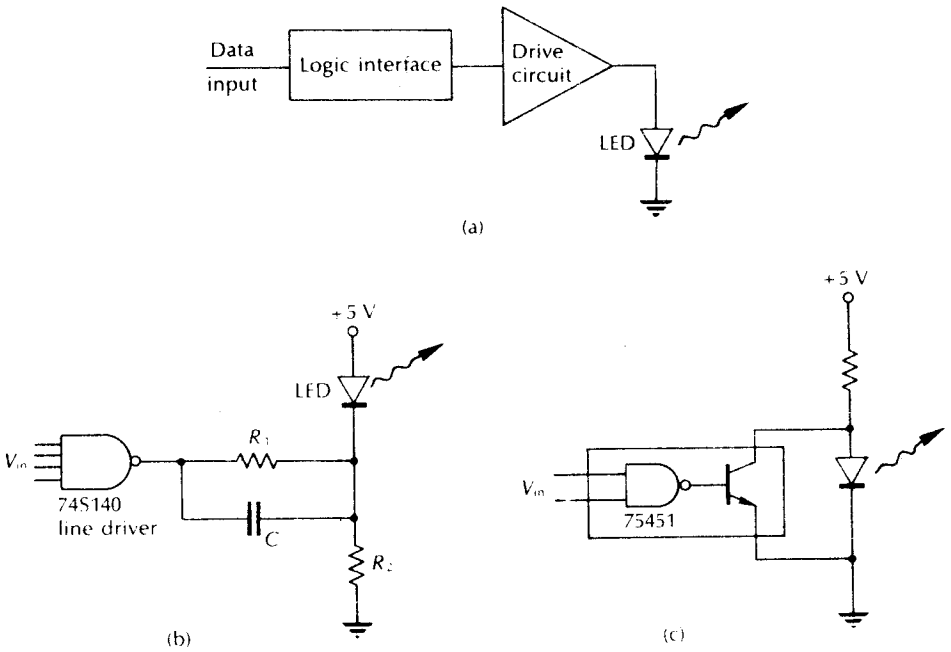

Figure 11.6 Logic interfacing for digital transmission: (a) block schematic showing the interfacing of the LED drive circuit with logic input levels; (b) a simple TTL compatible LED drive circuit employing a Texas Instruments' 74S140 line driver [Ref. 7]; (c) a TTL shunt drive circuit using a commercially available integrated circuit [Ref. 7].

in order to obtain a drive current of 120 mA. The incorporation of a suitable speed-up capacitor (e.g. $C = 47$ pF) gives optical rise times of around 5 ns when using LEDs with between 150 and 200 pF capacitance [Ref. 7]. Figure 11.6(c) illustrates the shunt configuration using a standard TTL 75451 integrated circuit. The rise time of this shunt circuit may be improved through maintenance of charge on the LED capacitance by placing a resistor between the shunt switch collector and the LED [Ref. 7].

An alternative important drive circuit configuration is the emitter coupled circuit shown in Figure 11.7 [Ref. 7]. The LED acts as a load in one collector so that the circuit provides current gain and hence a drive current for the device. Thus the circuit resembles a linear differential amplifier, but it is operated outside the linear range and in the switching mode. Fast switching speeds may be obtained due to the configuration's nonsaturating characteristic which avoids switch-off time degradations caused by stored charge accumulation on the transistor base region. The lack of saturation also minimizes the base drive requirements for the transistors, thus preserving their small signal current gain. The emitter coupled driver configuration shown in Figure 11.7 is compatible with commercial emitter coupled logic (ECL). However, to achieve this compatibility the circuit includes two level shifting transistors which give ECL levels (high -0.8 V, low -1.8 V) when the positive terminal of the LED is at earth potential. The response of this circuit is specified [Ref. 7] at up to 50 Mbit s^{-1}, with a possible extension to 300 Mbit s^{-1} when using a faster ECL logic family and high speed transistors. The emitter coupled drive circuit configuration may also be interfaced with other logic families, and a TTL compatible design is discussed in Ref. 8.

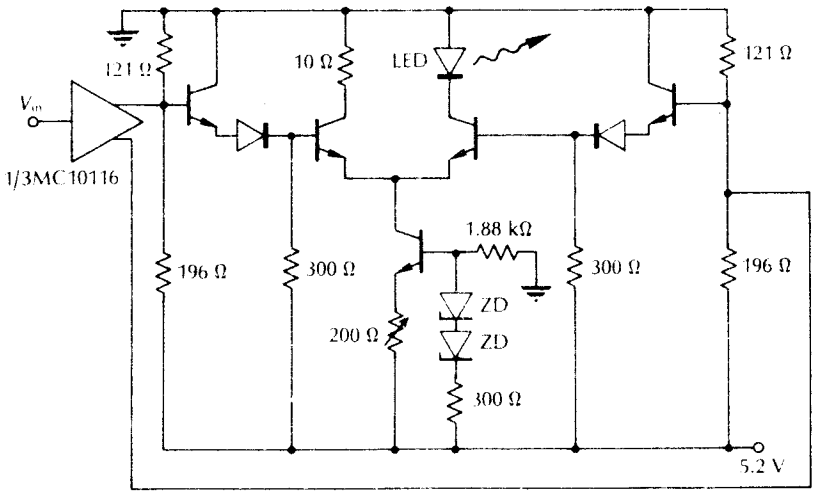

Figure 11.7 An emitter coupled drive circuit which is compatible with ECL [Ref. 7].

11.2.2.2 Analog transmission

For analog transmission the drive circuit must cause the light output from an LED source to follow accurately a time-varying input voltage waveform in both amplitude and phase. Therefore, as indicated previously, it is important that the LED output power responds linearly to the input voltage or current. Unfortunately, this is not always the case because of inherent nonlinearities within LEDs which create distortion products on the signal. Thus the LED itself tends to limit the performance of analog transmission systems unless suitable compensation is incorporated into the drive circuit. However, unless extremely low distortion levels are required, simple transistor drive circuits may be utilized.

Two possible high speed drive circuit configurations are illustrated in Figure 11.8. Figure 11.8(a) shows a driver consisting of a common emitter transconductance amplifier which converts an input base voltage into a collector current. The circuit is biased for a class A mode of operation with the quiescent collector current about half the peak value. A similar transconductance configuration which utilizes a Darlington transistor pair in order to reduce the impedance of the source is shown in Figure 11.8(b). A circuit of this type has been used to drive high radiance LEDs at frequencies of 70 MHz [Ref. 9].

Another simple drive circuit configuration is shown in Figure 11.9. It consists of a differential amplifier operated over its linear region which directly modulates the LED. The LED operating point is controlled by a reference voltage V_{ref} whilst the current generator provided by the transistor T_3 feeding the differential stage (T_1 and T_2) limits the maximum current through the device. The transimpedance of the driver is reduced through current series feedback provided by the two resistors R_1 and R_2 which are normally assigned equal values. Furthermore, variation between these feedback resistors can be used to compensate for the transfer function of both the drive circuit and the LED.

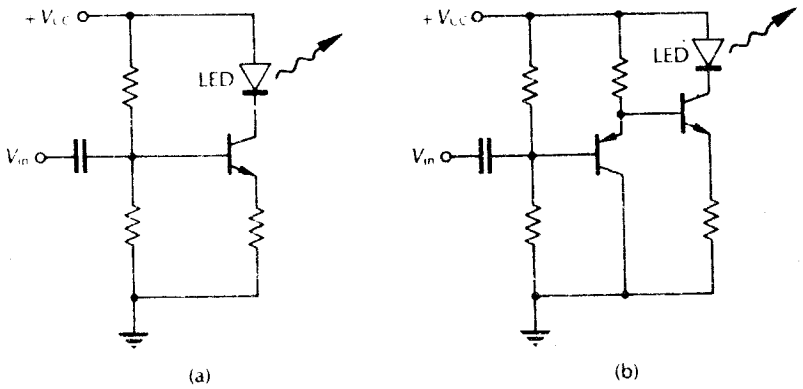

Figure 11.8 Transconductance drive circuits for analog transmission: (a) common emitter configuration; (b) Darlington transistor pair.

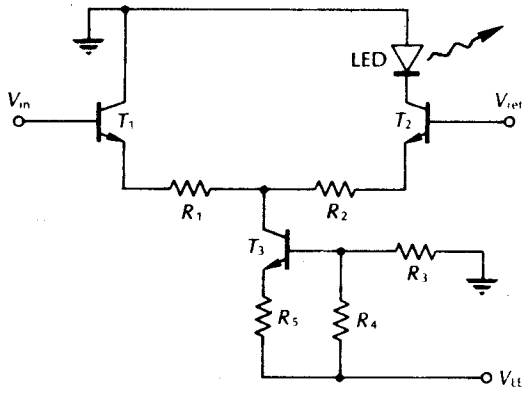

Figure 11.9 A differential amplifier drive circuit.

Although in many communication applications where a single analog signal is transmitted certain levels of amplitude and phase distortion can be tolerated, this is not the case in frequency multiplexed systems (see Section 11.4.2) where a high degree of linearity is required in order to minimize interference between individual channels caused by the generation of intermodulation products. Also, baseband video transmission of TV signals requires the maintenance of extremely low levels of amplitude and phase distortion. For such applications the simple drive circuits described previously are inadequate without some form of linearization to compensate for both LED and drive circuit nonlinearities. A number of techniques have been reported [Ref. 10], some of which are illustrated in Figure 11.10. Figure 11.10(a) shows the complementary distortion technique [Ref. 11] where additional nonlinear devices are included in the system. It may take the form of predistortion compensation (before the source drive circuit) or postdistortion compensation (after the receiver). This approach has been shown [Ref. 12] to reduce harmonic distortion by up to 20 dB over a limited range of modulation amplitudes.

In the negative feedback compensation technique shown in Figure 11.10(b), the LED is included in the linearization scheme. The optical output is detected and compared with the input waveform, the amount of compensation being dependent on the gain of the feedback loop. Although the technique is straightforward, large bandwidth requirements (i.e. video) can cause problems at high frequencies [Ref. 13].

The technique shown in Figure 11.10(c) employs phase shift modulation for selective harmonic compensation using a pair of LEDs with similar characteristics [Ref. 14]. The input signal is divided into equal parts which are phase shifted with respect to each other. These signals then modulate the two LEDs giving a cancellation of the second and third harmonic with a 90° and 60° phase shift respectively. However, although there is a high degree of distortion cancellation, both harmonics cannot be reduced simultaneously.

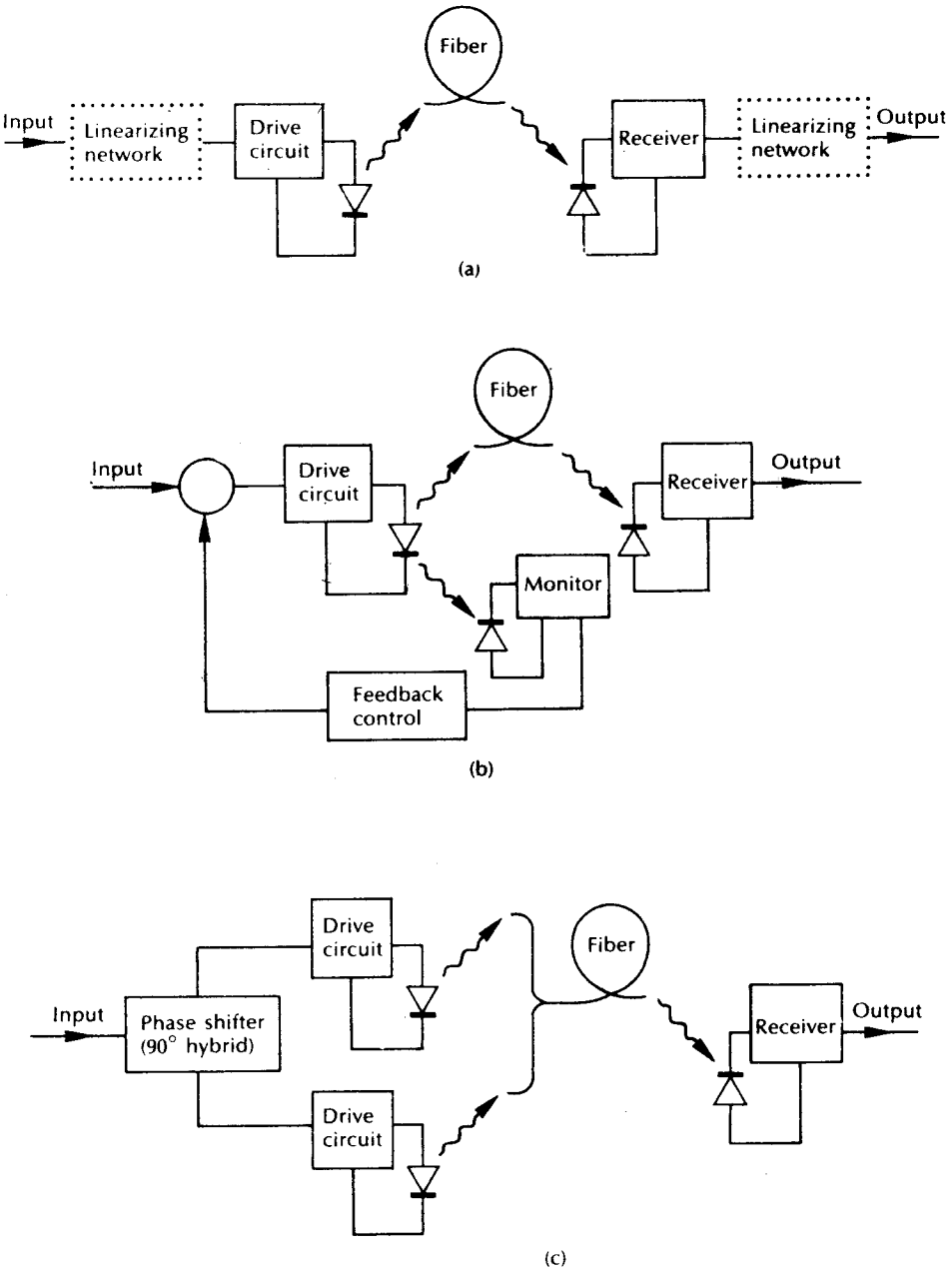

Figure 11.10 Block schematics of some linearization methods for LED drive circuits: (a) complementary distortion technique; (b) negative feedback compensation technique; (c) selective harmonic compensation technique.

Other linearization techniques include cascade compensation [Ref. 15], feedforward compensation [Ref. 16] and quasi-feedforward compensation [Refs. 17 and 18].

11.2.3 Laser drive circuits

A number of configurations described for use as LED drive circuits for both digital and analog transmission may be adapted for injection laser applications with only minor changes. The laser, being a threshold device, has somewhat different drive current requirements from the LED. For instance, when digital transmission is considered, the laser is usually given a substantial applied bias, often referred to as prebias, in the off state. Reasons for biasing the laser near but below threshold in the off state are as follows:

1. It reduces the switch-on delay and minimizes any relaxation oscillations.
2. It allows easy compensation for changes in ambient temperature and device ageing.
3. It reduces the junction heating caused by the digital drive current since the on and off currents are not widely different for most lasers.

Although biasing near threshold causes spontaneous emission of light in the off state, this is not normally a problem for digital transmission because the stimulated emission in the on state is generally greater by, at least, a factor of 10.

A simple laser drive circuit for digital transmission is shown in Figure 11.11. This circuit is a shunt driver utilizing a field effect transistor (FET) to provide high speed laser operation. Sufficient voltage is maintained in series with the laser using the resistor R_2 and the compensating capacitor C such that the FET is biased into its

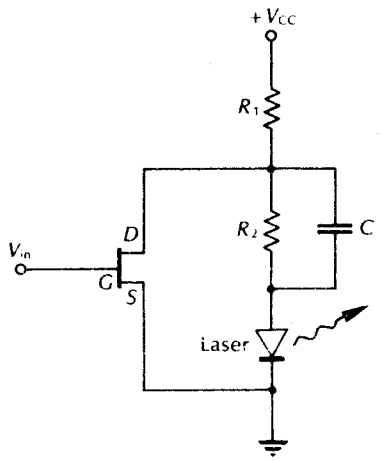

Figure 11.11 A shunt drive circuit for use with an injection laser.

active or pinch-off region. Hence for a particular input voltage V_{in} (i.e. V_{GS}) a specific amount of the total current flowing through R_1 is diverted around the laser leaving the balance of the current to flow through R_2 and provide the off state for the device. Using stable gallium arsenide MESFETs (see Section 9.5.1) the circuit shown in Figure 11.11 has modulated lasers at rates in excess of 1 Gbit s^{-1} [Ref. 19].

An alternative high speed laser drive circuit employing bipolar transistors is shown in Figure 11.12 [Ref. 20]. This circuit configuration, again for digital transmission, consists of two differential amplifiers connected in parallel. The input stage, which is ECL compatible, exhibits a 50 Ω input impedance by use of an emitter follower T_1 and a 50 Ω resistor in parallel with the input. The transistor T_2 acts as a current source with the zener diode ZD adjusting the signal level for ECL operation. The two differential amplifiers provide sufficient modulation current amplitude for the laser under the control of a d.c. control current I_E through the two emitter resistors R_{E1} and R_{E2}; I_E is provided by an optical feedback control circuit, to be discussed shortly. Finally, a prebias current is applied to the laser from a separate current source. This circuit when utilizing microwave transistors was operated with a return to zero digital format (see Section 3.8) at 1 Gbit s^{-1} [Ref. 20].

A major difference between the drive circuits of Figures 11.11 and 11.12 is the absence and use, respectively, of feedback control for adjustment of the laser output level. For this reason it is unlikely that the shunt drive circuit of Figure 11.11 would be used for a system application. Some form of feedback control is generally

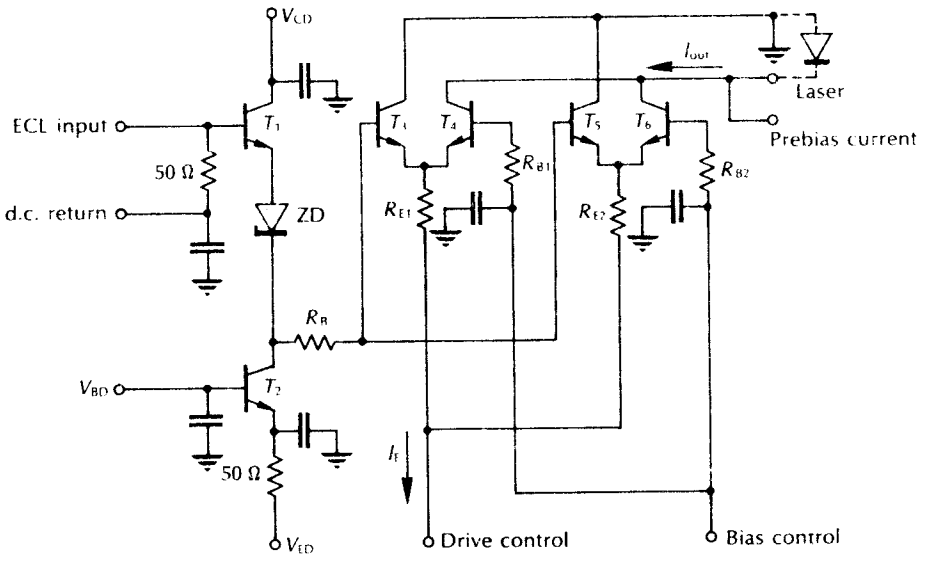

Figure 11.12 An ECL compatible high speed laser drive circuit [Ref. 20].

required to ensure continuous laser operation because the device lasing threshold is a sensitive function of temperature. Also, the threshold level tends to increase as the laser ages following an increase in internal device losses. Although lasers may be cooled to compensate for temperature variations, ageing is not so easily accommodated by the same process. However, both problems may be overcome through control of the laser bias using a feedback technique. This may be achieved using low speed feedback circuits which adjust the generally static bias current when necessary. For this purpose it is usually found necessary to monitor the light output from the laser in order to keep some aspect constant.

Several strategies of varying complexity are available to provide automatic output level control for the laser. The simplest and perhaps most common form of laser drive circuit incorporating optical feedback is the mean power control circuit shown in Figure 11.13. Often the monitor detector consists of a cheap, slow photodiode positioned next to the rear face of the laser package, as indicated in Figure 11.13. Alternatively, an optical coupler at the fiber input can be used to direct some of the radiation emitted from the laser into the monitor photodiode. The detected signal is integrated and compared with a reference by an operational amplifier which is used to servo-control the d.c. bias applied to the laser. Thus the mean optical power is maintained constant by varying the threshold current level. This technique is suitable for both digital and analog transmission.

An alternative control method for digital systems which offers accurate threshold tracking and very little device dependence is the switch-on delay technique illustrated in Figure 11.14 [Ref. 24]. This circuit monitors the switch-on delay of an optical pulse in order to control the laser bias current. The switch-on delay is measured for a zero level set below threshold and the feedback is set to a constant fixed delay to control it. Hence, the circuit provides a reference signal proportional to the delay period. This signal is used to control the bias level. The technique

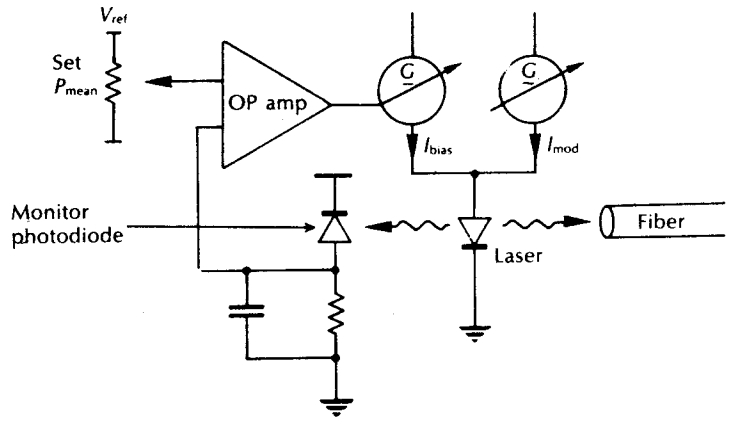

Figure 11.13 Mean power feedback circuit for control of the laser bias current.

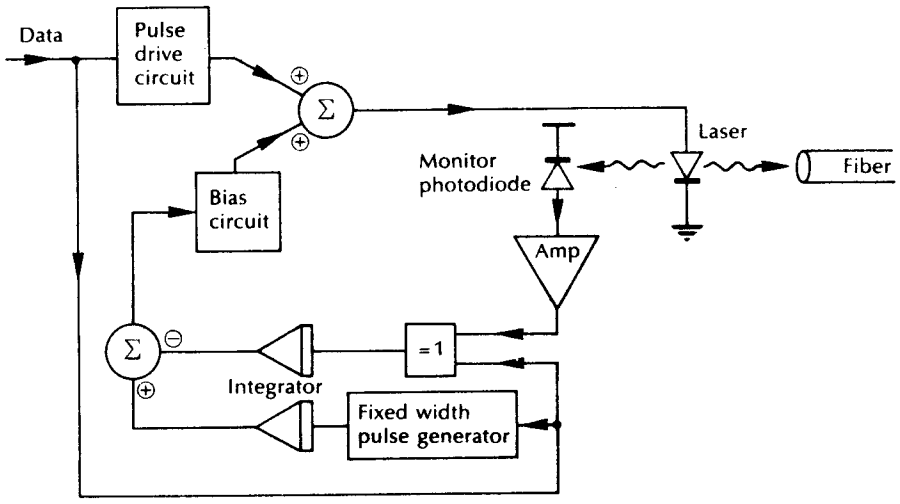

Figure 11.14 Switch-on delay feedback laser control circuit [Ref. 24].

requires a fast monitor photodiode as well as a wideband amplifier to allow measurement of the small delay periods. It is also essential that the zero level is set below the lasing threshold because the feedback loop will only stabilize for a finite delay (i.e. the delay falls to zero at the threshold).

A major disadvantage, however, with just controlling the laser bias current is that it does not compensate for variations in the laser slope efficiency. The modulation current for the device is preset and does not take into account any slope changes with temperature and ageing. In order to compensate for such changes, the a.c. and d.c. components of the monitored light output must be processed independently. This is especially important in the case of high bit rate digital systems where control of the on and off levels as well as the light level is required. A circuit which utilizes both a.c. and d.c. information in the laser output control the device drive current and bias independently is shown in Figure 11.15 [Ref. 20]. The electrical output from the monitor photodiode is fed into a low drift d.c. amplifier $A1$ and into a wideband amplifier $A2$. Therefore the mean value of the laser output power $P_e(\text{ave})$ is proportional to the output from $A1$ whilst the a.c. content of the monitoring signal is peak detected after the amplifier $A2$. The peak signals correspond to the maximum $P_e(\text{max})$ and the minimum $P_e(\text{min})$ laser output powers within a certain time interval. The difference signal proportional to $(P_e(\text{max}) - P_e(\text{min}))$ is acquired in $A3$ and compared with a drive reference voltage in order to control the current output from $A4$ and, consequently, the laser drive current. In this way the modulation amplitude of the laser is controlled. Control of the laser bias current is achieved from the difference between the output signal of $A1$ ($P_e(\text{ave})$) and $P_e(\text{min})$ which is acquired in $A5$. The output voltage of $A5$, which is proportional to $P_e(\text{min})$, is compared with a bias reference voltage in $A6$

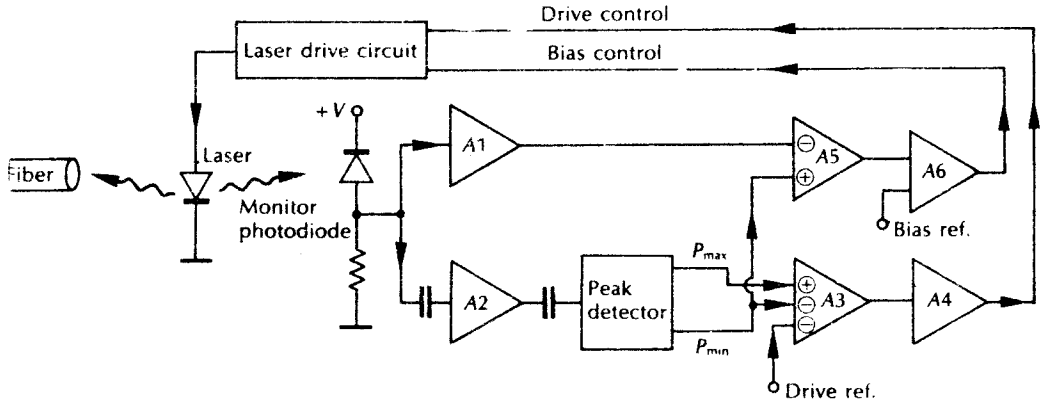

Figure 11.15 A laser feedback control circuit which uses a.c. and d.c. information in the monitored light output to control the laser drive and bias currents independently [Ref. 20].

which supplies a current output to control the laser d.c. bias. This feedback control circuit was designed for use with the laser drive circuit shown in Figure 11.12 to give digital operation at bit rates in the gigahertz range.

11.3 The optical receiver circuit

The noise performance for optical fiber receivers incorporating both major detector types (the *p–i–n* and avalanche photodiode) was discussed in Chapter 9. Receiver noise is of great importance within optical fiber communications as it is the factor which limits receiver sensitivity and therefore can dictate the overall system design. It was necessary within the analysis given in Chapter 9 to consider noise generated by electronic amplification (i.e. within the preamplifier) of the low level signal as well as the noise sources associated with the optical detector. Also, the possible strategies for the configuration of the preamplifier were considered (see Section 9.4) as a guide to optimization of the receiver noise performance for a particular application. In this section we extend the discussion to consider different possible circuit arrangements which may be implemented to achieve low noise preamplification, as well as further amplification (main amplification) and processing of the detected optical signal.

A block schematic of an optical fiber receiver is shown in Figure 11.16. Following the linear conversion of the received optical signal into an electrical current at the detector, it is amplified to obtain a suitable signal level. Initial amplification is performed in the preamplifier circuit where it is essential that additional noise is kept to a minimum in order to avoid corruption of the received signal. As noise sources within the preamplifier may be dominant, its configuration and design are

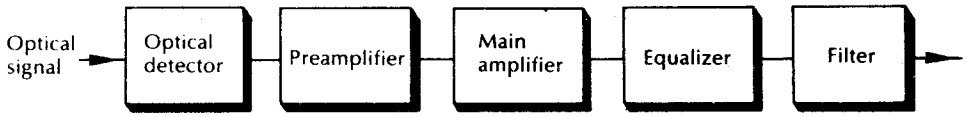

Figure 11.16 Block schematic showing the major elements of an optical fiber receiver.

major factors in determining the receiver sensitivity. The main amplifier provides additional low noise amplification of the signal to give an increased signal level for the following circuits.

Although optical detectors are very linear devices and do not themselves introduce significant distortion on to the signal, other components within the optical fiber communication system may exhibit nonlinear behaviour. For instance, the received optical signal may be distorted due to the dispersive mechanisms, within the optical fiber. Alternatively, the transfer function of the preamplifier–main amplifier combination may be such that the input signal becomes distorted (especially the case with the high impedance front end preamplifier). Hence, to compensate for this distortion and to provide a suitable signal shape for the filter, an equalizer is often included in the receiver. It may precede or follow the main amplifier, or may be incorporated in the functions of the amplifier and filter. In Figure 11.16 the equalizer is shown as a separate element following the amplifier and preceding the filter.

The function of the final element in the receiver, the filter, is to maximize the received signal to noise ratio whilst preserving the essential features of the signal. In digital systems the function of the filter is primarily to reduce intersymbol interference, whereas in analog systems it is generally required to hold the amplitude and phase response of the received signal within certain limits. The filter is also designed to reduce the noise bandwidth as well as inband noise levels.

Finally, the general receiver consisting of the elements depicted in Figure 11.16 is often referred to as a linear channel because all operations on the received optical signal may be considered to be mathematically linear.

11.3.1 The preamplifier

The choice of circuit configuration for the preamplifier is largely dependent upon the system application. Bipolar or field effect transistors (FETs) can be operated in three useful connections. These are the common emitter or source, the common base or gate, and the emitter or source follower for the bipolar and field effect transistors respectively. Each connection has characteristics which will contribute to a particular preamplifier configuration. It is therefore useful to discuss the three basic preamplifier structures (low impedance, high impedance and transimpedance front end) and indicate possible choices of transistor connection. In this context the discussion is independent of the type of optical detector utilized. However, it must be noted that there are a number of significant differences in the performance

characteristics between the *p–i–n* and avalanche photodiode (see Chapter 8) which must be considered within the overall design of the receiver.

The simplest preamplifier structure is the low input impedance voltage amplifier. This design is usually implemented using a bipolar transistor configuration because of the high input impedance of FETs. The common emitter and the grounded emitter (without an emitter resistor) amplifier shown in Figure 11.17 are favoured connections, as they may be designed with reasonably low input impedance and therefore give operation over a moderate bandwidth without the need for equalization. However, this is achieved at the expense of increased thermal noise due to the low effective load resistance presented to the detector. Nevertheless, it is possible to reduce the thermal noise contribution of this preamplifier by choosing a transistor with characteristics which give a high current gain at a low emitter current in order to maintain the bandwidth of the stage. Also, an inductance may be inserted at the collector to provide partial equalization for any integration performed by the stage. The alternative connection giving very low input impedance is the common base circuit. Unfortunately, this configuration has an input impedance which gives insufficient power gain when connected to the high impedance of the optical detector.

The preferred preamplifier configurations for low noise operation use either a high impedance integrating front end or a transimpedance amplifier (see Sections 9.4.2 and 9.4.3). Careful design employing these circuit structures can facilitate high gain coupled with low noise performance and therefore enhanced receiver sensitivity. Although the bipolar transistor incorporated in the emitter follower circuit may be used to realize a high impedance front end amplifier, the FET is generally employed for this purpose because of its low noise operation. It was indicated in Section 9.5 that the grounded source FET connection was a useful circuit to provide a high impedance front end amplifier. The same configuration with a source resistor (common source connection) shown in Figure 11.18 provides

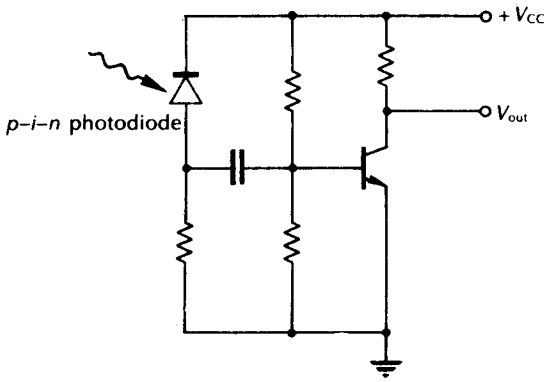

Figure 11.17 A *p–i–n* photodiode with a grounded emitter, low input impedance voltage preamplifier.

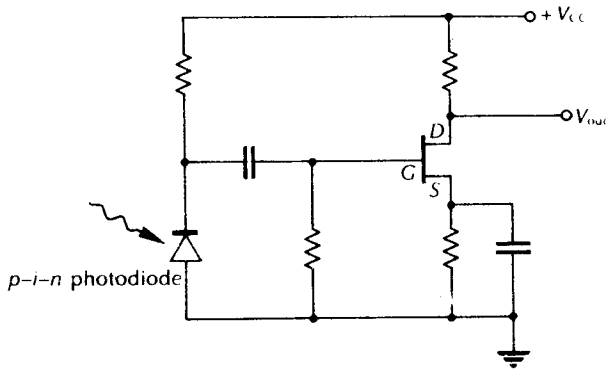

Figure 11.18 An FET common source preamplifier configuration which provides high input impedance for the *p–i–n* photodiode.

a similar high input impedance and may also be used (often both configurations are referred to as the common source connection). When operating in this mode the FET power gain and output impedance are both high, which tends to minimize any noise contributions from the following stages. It is especially the case when the voltage gain of the common source stage is minimized in order to reduce the Miller capacitance [Ref. 27] associated with the gate to drain capacitance of the FET. This may be achieved by following the common source stage with a stage having a low input impedance.

Two configurations which provide a low input impedance stage are shown in Figure 11.19. Figure 11.19(a) shows the grounded source FET followed by a bipolar transistor in the common emitter connection with shunt feedback over the stage. Another favoured configuration to reduce Miller capacitance in the first stage FET is shown in Figure 11.19(b). In this case the second stage consists of a bipolar transistor in the common base configuration which, with the initial grounded source FET, forms the cascode configuration.

The high impedance front end structure provides a very low noise preamplifier design but suffers from two major drawbacks. The first is with regard to equalization, which must generally be tailored to the amplifier in order to compensate for distortion introduced on to the signal. Secondly, the high input–impedance approach suffers from a lack of dynamic range which occurs because the charge on the input capacitance from the low frequency components in the signal builds up over a period of time, causing premature saturation of the amplifier at high input signal levels. Therefore, although the circuits shown in Figure 11.19 are examples of possible high impedance integrating front end amplifier configurations, similar connections may be employed with overall feedback (to the first stage) to obtain a transimpedance preamplifier.

The transimpedance or shunt feedback amplifier finds wide application in preamplifier design for optical fiber communications. This front end structure

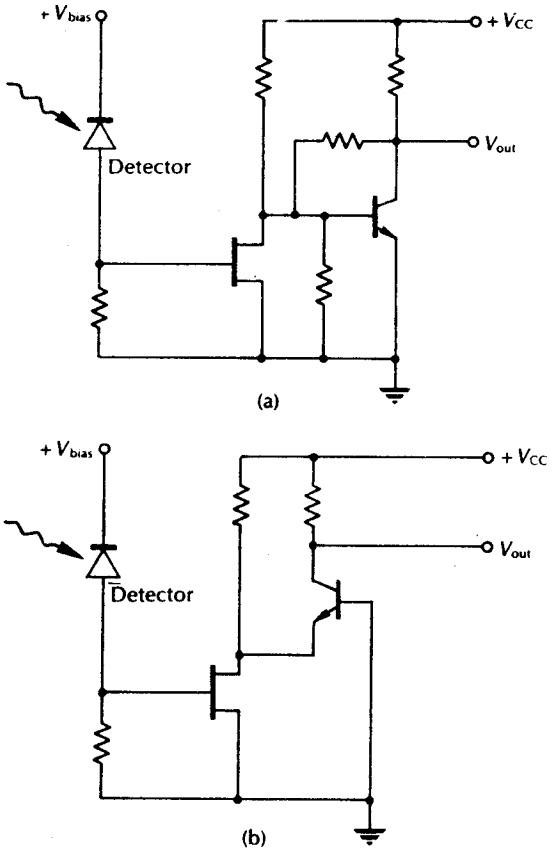

Figure 11.19 High input impedance preamplifier configurations: (a) grounded source FET followed by common emitter connection with shunt feedback; (b) cascode connection. The separate bias voltage indicates the use of either *p–i–n* or avalanche photodiode.

which acts as a current–voltage converter gives low noise performance without the severe limitations on bandwidth imposed by the high input impedance front end design. It also provides greater dynamic range than the high input impedance structure. However, in practice the noise performance of the transimpedance amplifier is not quite as good as that achieved with the high impedance structure due to the noise contribution from the feedback resistor (see Section 9.4.3). Nevertheless, the transimpedance design incorporating a large value of feedback resistor can achieve a noise performance which approaches that of the high impedance front end.

Two examples of transimpedance front end configurations are shown in Figure 11.20. Figure 11.20(a) illustrates a bipolar transistor structure consisting of a

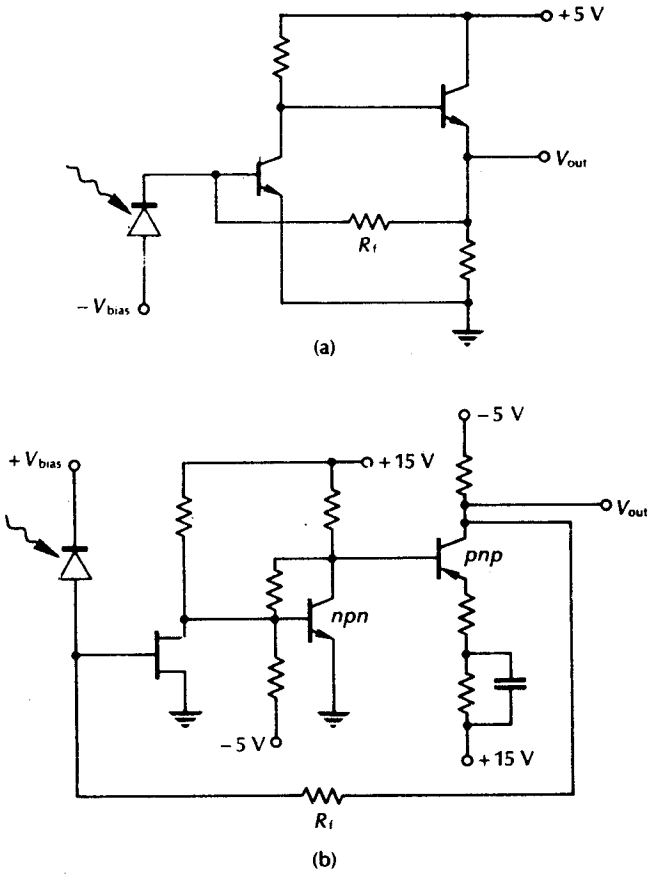

Figure 11.20 Transimpedance front end configuration: (a) bipolar transistor design [Refs. 28 and 29]; (b) FET front end and bipolar transistor cascade structure [Ref. 32].

common emitter stage followed by an emitter follower [Refs. 28 and 29] with overall feedback through resistor R_f. The output signal level from this transimpedance pair may be increased by the addition of a second common emitter stage [Ref. 30] after the emitter follower. This stage is not usually included in the feedback loop. An FET front end transimpedance design is shown in Figure 11.20(b) [Ref. 32].

The circuit consists of a grounded source configuration followed by a bipolar transistor cascade with feedback over the three stages. In this configuration the bias currents for the bipolar stages and the feedback resistance may be chosen to give good open loop bandwidth whilst making the noise contribution from these stages negligible.

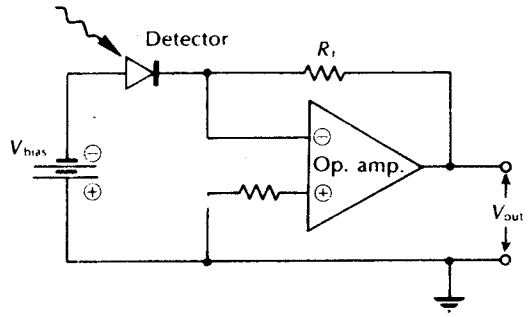

Figure 11.21 A typical circuit for an operational amplifier transimpedance fron end [Ref. 33].

Finally, for lower bandwidth, shorter-haul applications an FET operational amplifier front end is often adequate [Ref. 33]. Such a transimpedance preamplifier circuit, which is generally used with a *p–i–n* photodiode, is shown in Figure 11.21. The choice of the operational amplifier is dependent on the gain versus bandwidth product for the device. In a simple digital receiver design all that may be required in addition to the circuit shown in Figure 11.21 is a logic (e.g. TTL) interface stage following the amplifier.

11.3.2 Automatic gain control (AGC)

It may be noted from the preceding section that the receiver circuit must provide a steady reverse bias voltage for the optical detector. With a *p–i–n* photodiode this is not critical and a voltage of between 5 and 80 V supplying an extremely low current is sufficient. The avalanche photodiode requires a much larger bias voltage of between 100 and 400 V which defines the multiplication factor for the device. An optimum multiplication factor is usually chosen so that the receiver signal to noise ratio is maximized (see Section 9.3.3). The multiplication factor for the APD varies with the device temperature (see Section 8.9.5) making provision of fine control for the bias voltage necessary in order to maintain the optimum multiplication factor. However, the multiplication factor can be held constant by some form of automatic gain control (AGC). An additional advantage in the use of AGC is that it reduces the dynamic range of the signals applied to the preamplifier giving increased optical dynamic range at the receiver input.

One method of providing AGC is simply to bias the APD with a constant d.c. current source I_{bias}, as illustrated in Figure 11.22. The constant current source is decoupled by a capacitor C at all signal frequencies to prevent gain modulation. When the mean optical input power is known, the mean current to the APD is defined by the bias which gives a constant multiplication factor (gain) at all temperatures. Any variation in the multiplication factor will produce a variation in the charge on C, thus adjusting the biasing of the APD back to the required

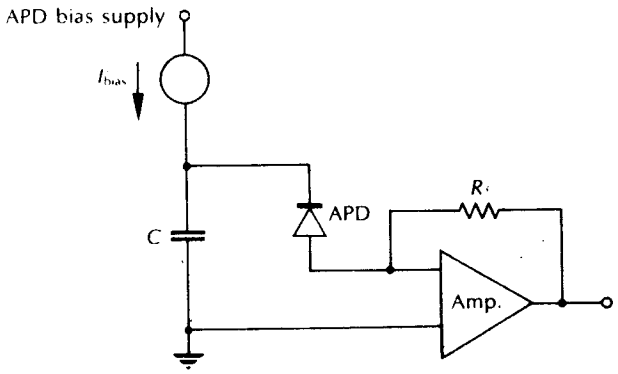

Figure 11.22 Bias of an APD with a constant current source to provide simple AGC.

multiplication factor. Therefore, the output current from the photodetector is only defined by the input current from the constant current source, giving full automatic gain control. However, this simple AGC technique is dependent on a constant, mean optical input power level, and takes no account of dark current generated within the detector.

A more widely used method which allows for the effect of variations in the detector dark current whilst providing critical AGC is to peak detect the a.c. coupled signal after suitable low noise amplification, as shown in Figure 11.23. The signal from the final stage of the main amplifier is compared with a preset reference level and fed back to adjust the high voltage bias supply in order to maintain a constant signal level. This effectively creates a constant current source with the dark current subtracted.

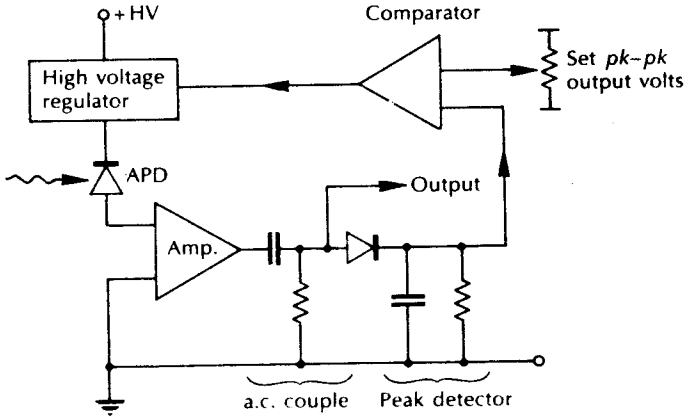

Figure 11.23 Bias of an APD by peak detection and feedback to provide AGC.

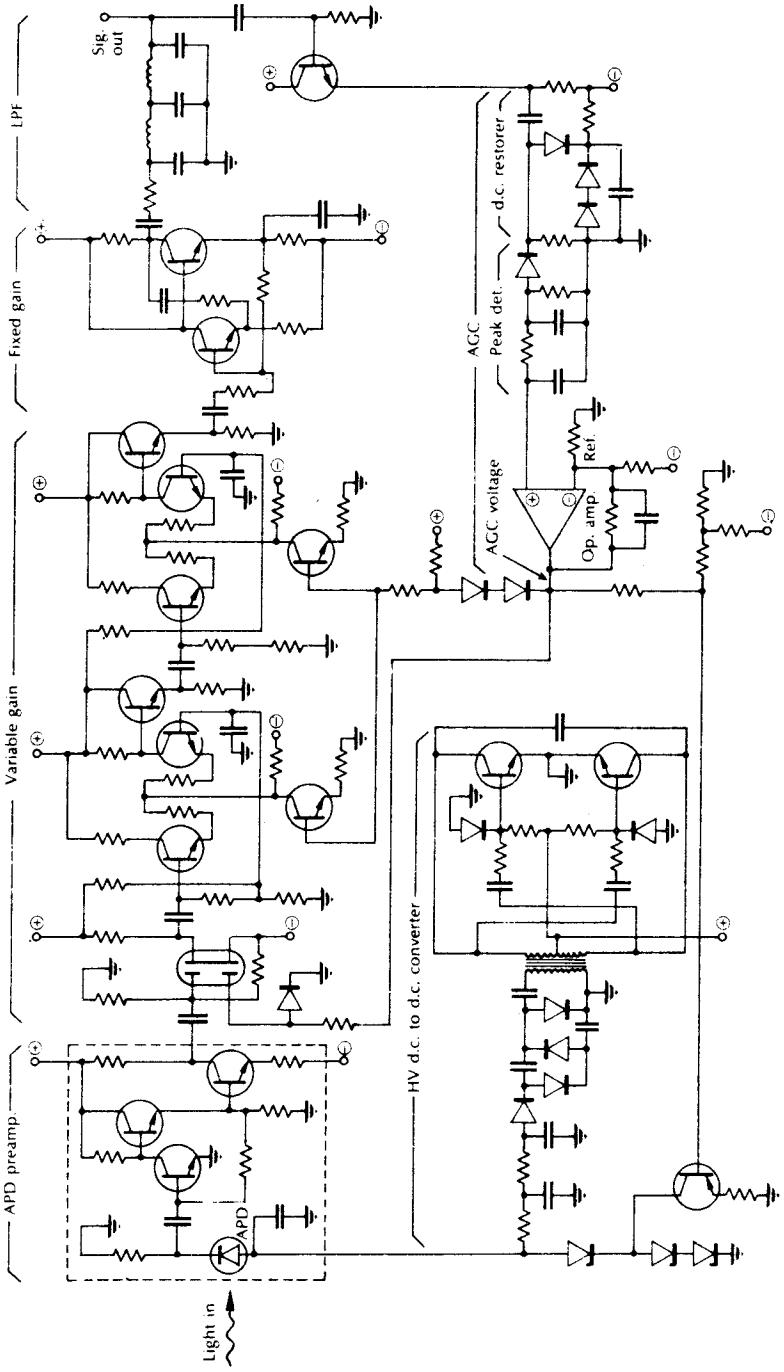

Figure 11.24 An optical fiber receiver circuit for digital transmission with AGC provided by both control of the APD bias and the main amplifier gain [Ref. 34].

A further advantage of this technique is that it may also be used to provide AGC for the main amplifier giving full control of the receiver gain.

A digital receiver circuit for an APD employing full AGC is shown in Figure 11.24 [Ref. 34]. The APD is followed by a transimpedance preamplifier employing bipolar transistors, the output of which is connected into a main amplifier consisting of a variable gain amplifier followed by a fixed gain amplifier. The first stage of the main amplifier is provided by a dual gate FET which gives a variable gain over a range of 20 dB. This variable gain amplifier also incorporates two stages, each of which consists of an emitter coupled pair with a gain variation of 14 dB. The following fixed gain amplifier gives a 2 V peak to peak signal to the low pass filter, the output of which is maintained at 1 V peak to peak by the AGC. Peak detection is provided in the AGC where the signal level is compared with a preset reference prior to control of the gain for both the APD and the main amplifier. The gain of the APD is controlled via a simple d.c. to d.c. converter which supplies the bias from a low voltage input, whereas the gain of the main amplifier is controlled by an input on the dual gate FET front end. This circuit allows a gain variation of 26 and 47 dB for the APD and the main amplifier respectively. The APD bias circuit is designed to protect the device against possible excess power dissipation at very high optical input power levels, as well as excess power dissipation when there is no optical input.

11.3.3 Equalization

The linear channel provided by the optical fiber receiver is often required to perform equalization as well as amplification of the detected optical signal. In order to discuss the function of the equalizer it is useful to assume the light falling on the detector to consist of a series of pulses given by:

$$P_o(t) = \sum_{k=-\infty}^{+\infty} a_k h_p(t - k\tau) \tag{11.1}$$

where $h_p(t)$ is the received pulse shape, $a_k = 0$ or 1 corresponding to the binary information transmitted and τ is the pulse repetition time or pulse spacing. In digital transmission τ corresponds to the bit period, although the pulse length does not necessarily fill the entire time period τ. For a typical optical fiber link, the received pulse shape is dictated by the transmitted pulse shape $h_t(t)$ and the fiber impulse response $h_f(t)$ following:

$$h_p(t) = h_t(t) * h_f(t) \tag{11.2}$$

where * denotes convolution. Hence determination of the received pulse shape requires knowledge of the fiber impulse response which is generally difficult to characterize. However, it can be shown [Ref. 37] for fiber which exhibits mode coupling that the impulse response is close to a Gaussian shape in both the time and frequency domain.

It is likely that the pulses given by Eq. (11.1) will overlap due to pulse broadening caused by dispersion on the link giving intersymbol interference (ISI). Following detection and amplification Eq. (11.1) may be written in terms of a voltage $v_A(t)$ as:

$$v_A(t) = \sum_{k=-\infty}^{+\infty} a_k h_A(t - k\tau) \tag{11.3}$$

where the response $h_A(t)$ includes any equalization required to compensate for distortion (e.g. integration) introduced by the amplifier. Therefore, although there is equalization for degradations caused by the amplifier, distortion caused by the channel and the resulting intersymbol interference is still included in $h_A(t - k\tau)$. The pulse overlap causing this intersymbol interference, may be reduced through the incorporation of a suitable equalizer with a frequency response $H_{eq}(\omega)$ such that:

$$H_{eq}(\omega) = \frac{\mathcal{F}\{h_{out}(t)\}}{\{h_A(t)\}} = \frac{H_{out}(\omega)}{H_A(\omega)} \tag{11.4}$$

where $h_{out}(t)$ is the desired output pulse shape and $\mathcal{F}$ indicates Fourier transformation. A block diagram indicating the pulse shapes in the time and frequency domains at the various points in an optical fiber system is shown in Figure 11.25.

An equalizer characterized by Eq. (11.4) will provide high frequency enhancement in the linear channel to compensate for high frequency roll off in the received pulses, thus giving the desired pulse shape. However, in order to construct such an equalizer we require knowledge of $h_A(t)$ and therefore $h_p(t)$. In turn, this

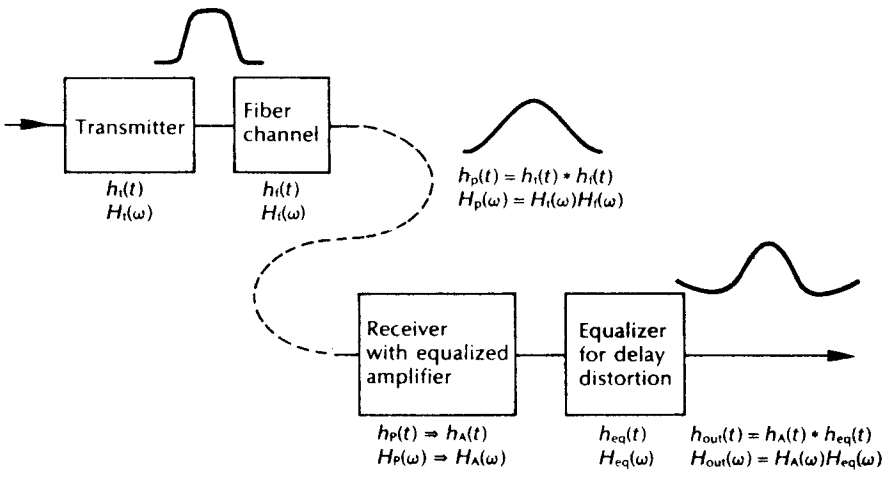

Figure 11.25 Block schematic of an optical fiber system illustrating the transmitted and received optical pulse shapes, together with electrical pulse shape, at the linear channel output.

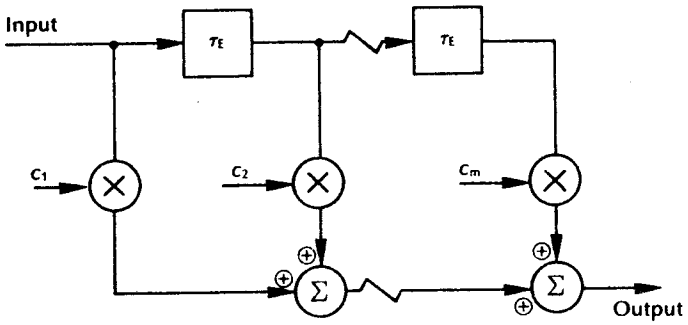

Figure 11.26 The transversal equalizer employing a tapped delay line.

necessitates information on the fiber impulse response $h_f(t)$ which may not be easily obtained.

Nevertheless, the conventional transversal equalizer shown in Figure 11.26 may be incorporated into the linear channel to keep ISI at tolerable levels, even if it is difficult to design a circuit which gives the optimum system response indicated in Eq. (11.4).

The transversal equalizer consists of a delay line tapped at τ_E second intervals. Each tap is connected through a variable gain device with tap coefficients c_i to a summing amplifier. Intersymbol interference is reduced by filtering the input signal and by the computing values for the tap coefficients which minimize the peak ISI. It is likely that further reduction in ISI will be accomplished using adaptive equalization which has yet to be rigorously applied to optical fiber communications. This is discussed further in Ref. 40.

11.4 System design considerations

Many of the problems associated with the design of optical fiber communication systems occur as a result of the unique properties of the glass fiber as a transmission medium. However, in common with metallic line transmission systems, the dominant design criteria for a specific application using either digital or analog transmission techniques are the required transmission distance and the rate of information transfer.

Within optical fiber communications these criteria are directly related to the major transmission characteristics of the fiber, namely optical attenuation and dispersion. Unlike metallic conductors where the attenuation (which tends to be the dominant mechanism) can be adjusted by simply changing the conductor size, entirely different factors limit the information transfer capability of optical fibers (see Chapter 3). Nevertheless, it is mainly these factors, together with the associated constraints within the terminal equipment, which finally limit the maximum

distance that may be tolerated between the optical fiber transmitter and receiver. Where the terminal equipment is more widely spaced than this maximum distance, as in long-haul telecommunication applications, it is necessary to insert repeaters at regular intervals, as shown in Figure 11.27. The repeater incorporates a line receiver in order to convert the optical signal back into the electrical regime where, in the case of analog transmission, it is amplified and equalized (see Section 11.3.3) before it is retransmitted as an optical signal via a line transmitter. When digital transmission techniques are used the repeater also regenerates the original digital signal in the electrical regime (a regenerative repeater which is often simply called a regenerator) before it is retransmitted as a digital optical signal. In this case the repeater may additionally provide alarm, supervision and engineering order wire facilities.

The installation of repeaters substantially increases the cost and complexity of any line communication system. Hence a major design consideration for long-haul telecommunication systems is the maximum distance of unrepeatered transmission so that the number of intermediate repeaters may be reduced to a minimum. In this respect optical fiber systems display a marked improvement over alternative line transmission systems using metallic conductors. However, this major advantage of optical fiber communications is somewhat reduced due to the present requirement for electrical signal processing at the repeater. This necessitates the supply of electrical power to the intermediate repeaters via metallic conductors, as may be observed in Figure 11.27.

Before any system design procedures can be initiated it is essential that certain basic system requirements are specified. These specifications include:

(a) transmission type: digital or analog;
(b) acceptable system fidelity, generally specified in terms of the received BER for digital systems or the received SNR and signal distortion for analog systems;
(c) required transmission bandwidth;
(d) acceptable spacing between the terminal equipment or intermediate repeaters;
(e) cost;
(f) reliability.

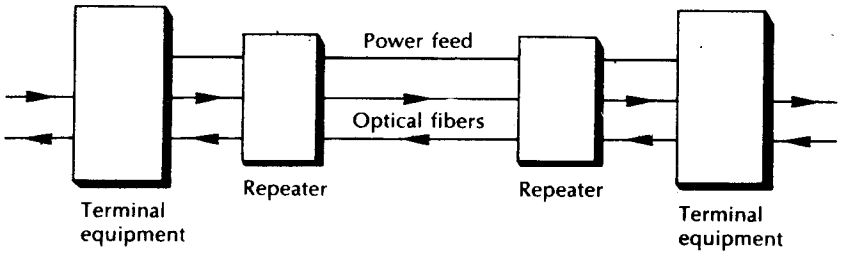

Figure 11.27 The use of repeaters in a long-haul optical fiber communication system.

However, the exclusive use of the above specifications inherently assumes that system components are available which will allow any system, once specified, to be designed and implemented. Unfortunately, this is not always the case, especially when the desired result is a wideband, long-haul system. In this instance it may be necessary to make choices by considering factors such as availability, reliability, cost and ease of installation and operation, before specifications (a) to (d) can be fully determined. A similar approach must be adopted in lower bandwidth, shorter-haul applications where there is a requirement for the use of specific components which may restrict the system performance. Hence it is likely that the system designer will find it necessary to consider the possible component choices in conjunction with the basic system requirements.

11.4.1 Component choice

The system designer has many choices when selecting components for an optical fiber communication system. In order to exclude certain components at the outset it is useful if the operating wavelength of the system is established (i.e. shorter wavelength region 0.8 to 0.9 μm or longer wavelength region 1.1 to 1.6 μm). This decision will largely be dictated by the overall requirements for the system performance, the ready availability of suitable reliable components, and cost. Hence the major component choices are:

1. Optical fiber type and parameters. Multimode or single-mode; size, refractive index profile, attenuation, dispersion, mode coupling, strength, cabling, jointing, etc.
2. Source type and characteristics. Laser or LED; optical power launched into the fiber, rise and fall time, stability, etc.
3. Transmitter configuration. Design for digital or analog transmission; input impedance, supply voltage, dynamic range, optical feedback, etc.
4. Detector type and characteristics, p–n, p–i–n, or avalanche photodiode; responsivity, response time, active diameter, bias voltage, dark current, etc.
6. Receiver configuration. Preamplifier design (low impedance, high impedance or transimpedance front end), BER or SNR, dynamic range, etc.
7. Modulation and coding. Source intensity modulation; using pulse modulation techniques for either digital (e.g. pulse code modulation, adaptive delta modulation) or analog (pulse amplitude modulation, pulse frequency modulation, pulse width modulation, pulse position modulation) transmission. Also, encoding schemes for digital transmission such as biphase (Manchester) and delay modulation (Miller) codes [Ref. 7]. Alternatively analog transmission using direct intensity modulation or frequency modulation of the electrical subcarrier (subcarrier FM). In the latter technique the frequency of an electrical subcarrier is modulated rather than the frequency of the optical source, as would be the case with direct frequency modulation. The electrical subcarrier, in turn, intensity modulates the optical source (see Section 11.7.5).

Digital and analog modulation techniques which require coherent detection are under investigation but system components which will permit these modulation methods to be utilized are not yet widely available (see Chapter 12).

Decisions in the above areas are interdependent and may be directly related to the basic system requirements. The potential choices provide a wide variety of economic optical fiber communication systems. However, it is necessary that the choices are made in order to optimize the system performance for a particular application.

11.4.2 Multiplexing

In order to maximize the information transfer over an optical fiber communication link it is usual to multiplex several signals on to a single fiber. It is possible to convey these multichannel signals by multiplexing in the electrical time or frequency domain, as with conventional electrical line or radio communication, prior to intensity modulation of the optical source. Hence, digital pulse modulation schemes may be extended to multichannel operation by time division multiplexing (TDM) narrow pulses from multiple modulators under the control of a common clock. Pulses from the individual channels are interleaved and transmitted sequentially, thus enhancing the bandwidth utilization of a single fiber link.

Alternatively, a number of baseband channels may be combined by frequency division multiplexing (FDM). In FDM the optical channel bandwidth is divided into a number of nonoverlapping frequency bands and each signal is assigned one of these bands of frequencies. The individual signals can be extracted from the combined FDM signal by appropriate electrical filtering at the receive terminal. Hence, frequency division multiplexing in an IM/DD system is generally performed electrically at the transmit terminal prior to intensity modulation of a single optical source. However, it is possible to utilize a number of optical sources, each operating at a different wavelength on the single fiber link. In this technique, often referred to as wavelength division multiplexing (WDM), the separation and extraction of the multiplexed signals (i.e. wavelength separation) is performed with optical filters (e.g. interference filters, diffraction grating filters, or prism filters) [Ref. 41].

Finally, a multiplexing technique which does not involve the application of several message signals on to a single fiber is known as space division multiplexing (SDM). In SDM, each signal channel is carried on a separate fiber within a fiber bundle or multifiber cable form. The good optical isolation offered by fibers means that cross coupling between channels can be made negligible. However, this technique necessitates an increase in the number of optical components required (e.g. fiber, connectors, sources, detectors) within a particular system and therefore has not been widely used to date.

11.5 Digital systems

Most of the future expansion of the telecommunication network is being planned around digital telephone exchanges linked by digital transmission systems. The shift towards digitizing the network followed the introduction of digital circuit techniques and, especially, integrated circuit technology which made the transmission of discrete time signals both advantageous and economic. Digital transmission systems generally give superior performance over their analog counterparts, as well as providing an ideal channel for data communications and compatibility with digital computing techniques.

Optical fiber communication is well suited to baseband digital transmission in several important ways. For instance, it offers a tremendous advantage with regard to the acceptable signal to noise ratio (SNR) at the optical fiber receiver over analog transmission by some 20 to 30 dB (for practical systems), as indicated in the noise considerations of Section 9.2. Also, the use of baseband digital signalling reduces problems involved with optical source (and sometimes detector) nonlinearities and temperature dependence which may severely affect analog transmission. Therefore, most high capacity optical fiber communication systems convey digital information in the baseband using intensity modulation of the optical source.

In common with electrical transmission systems, analog signals (e.g. speech) may be digitized for transmission utilizing pulse code modulation (PCM). Encoding the analog signal into a digital bit pattern is performed by initially sampling the analog signal at a frequency in excess of the Nyquist rate (i.e. greater than twice the maximum signal frequency). Within the European telecommunication network where the 3 dB telephone bandwidth is defined as 3.4 kHz, the sampling rate is 8 kHz. Hence, the amplitude of the constant width sampling pulses varies in proportion to the sample values of the analog signal giving a discrete signal known as pulse amplitude modulation (PAM), as indicated in Figure 11.28. The sampled analog signal is then quantized into a number of discrete levels, each of which is designated by a binary code which provides the PCM signal. This process is also illustrated in Figure 11.28 using a linear quantizer with eight levels (or seven steps) so that each PAM sample is encoded into three binary bits. The analog signal is thus digitized and may be transmitted as a baseband signal or, alternatively, be modulated by amplitude, frequency or phase shift keying [Ref. 43]. However, in practical PCM systems for speech transmission, nonlinear encoding (A law in Europe and μ law in North America) is generally employed over 256 levels (2^8), giving eight binary bits per sample (seven bits for code levels plus one polarity bit). Hence, the bandwidth requirement for PCM transmission is substantially greater (in this case by a factor of approximately 16) than the corresponding baseband analog transmission. This is not generally a problem with optical fiber communications because of the wideband nature of the optical channel.

Nonlinear encoding may be implemented via a mechanism known as companding where the input signal is compressed before transmission to give a nonlinear

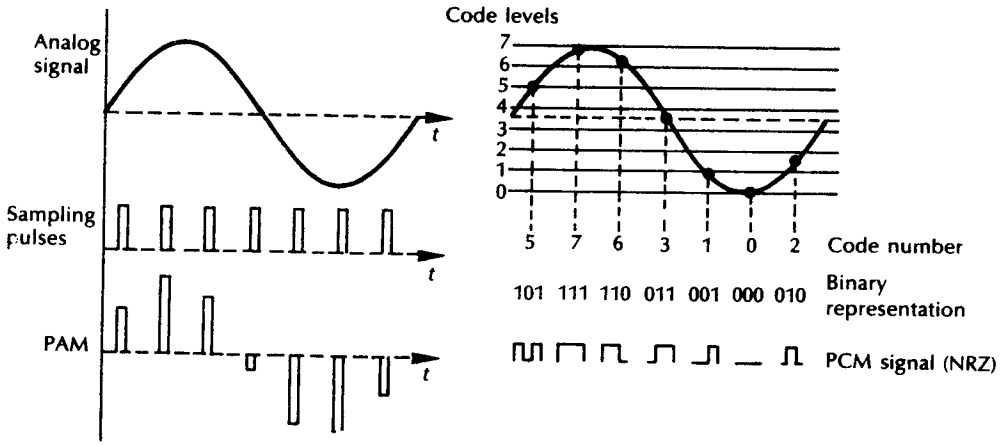

Figure 11.28 The quantization and encoding of an analog signal into PCM using a linear quantizer with eight levels.

encoding characteristic and expanded again at the receive terminal after decoding. A typical nonlinear input–output characteristic giving compression is shown in Figure 11.29. Companding is used to reduce the quantization error on small amplitude analog signal levels when they are encoded from PAM to PCM. The quantization error (i.e. the rounding off to the nearest discrete level) is exhibited as distortion or noise on the signal (often called quantization noise). Companding tapers the step size, thus reducing the distance between levels for small amplitude signals whilst increasing the distance between levels for higher amplitude signals. This substantially reduces the quantization noise on small amplitude signals at the expense of slightly increased quantization noise, in terms of signal amplitude, for

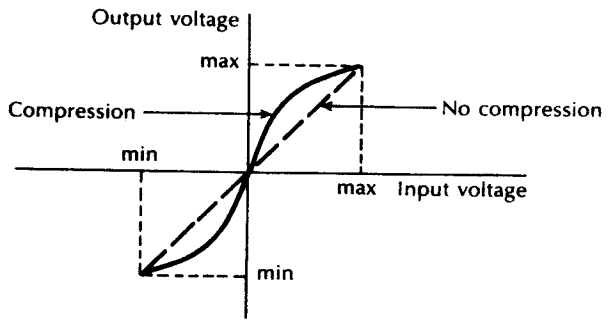

Figure 11.29 A typical nonlinear input–output characteristic which provides compression.

the larger signal levels. The corresponding SNR improvement for small amplitude signals significantly reduces the overall signal degradation of the system due to the quantization process.

A block schematic of a simplex (one direction only) baseband PCM system is shown in Figure 11.30(a). The optical interface is not shown but reference may be made to Figure 11.1 which illustrates the general optical fiber communication system. It may be noted from Figure 11.30(a) that the received PCM waveform is decoded back to PAM via the reverse process to encoding, and then simply passed through a low pass filter to recover the original analog signal.

The conversion of a continuous analog waveform into a discrete PCM signal allows a number of analog channels to be time division multiplexed (TDM) for simultaneous transmission down one optical fiber link, as illustrated in Figure 11.30(b). The encoded samples from the different channels are interleaved within the multiplexer to give a single composite signal consisting of all the interleaved pulses. This signal is then transmitted over the optical channel. At the receive terminal the interleaved samples are separated by a synchronous switch or demultiplexer before each analog signal is reconstructed from the appropriate set of samples. Time division multiplexing a number of channels on to a single link can be used with any form of digital transmission and is frequently employed in the transmission of data as well as with the transmission of digitised analog signals. However, the telecommunication network is primarily designed for the transmission of analog speech signals, although the compatibility of PCM with data signals has encouraged the adoption of digital transmission systems.

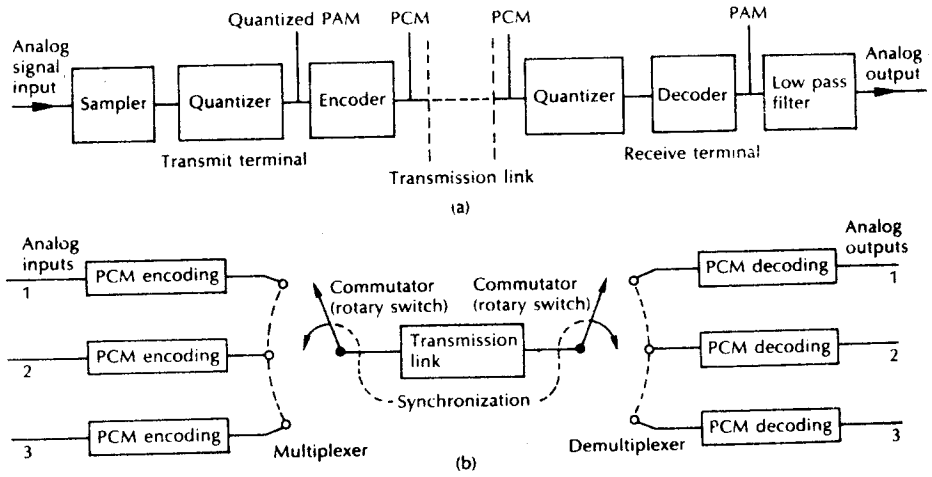

Figure 11.30 PCM transmission: (a) block schematic of a baseband PCM transmission system for single channel transmission; (b) time division multiplexing of three PCM channels on to a single transmission link and subsequent demultiplexing at the link output.

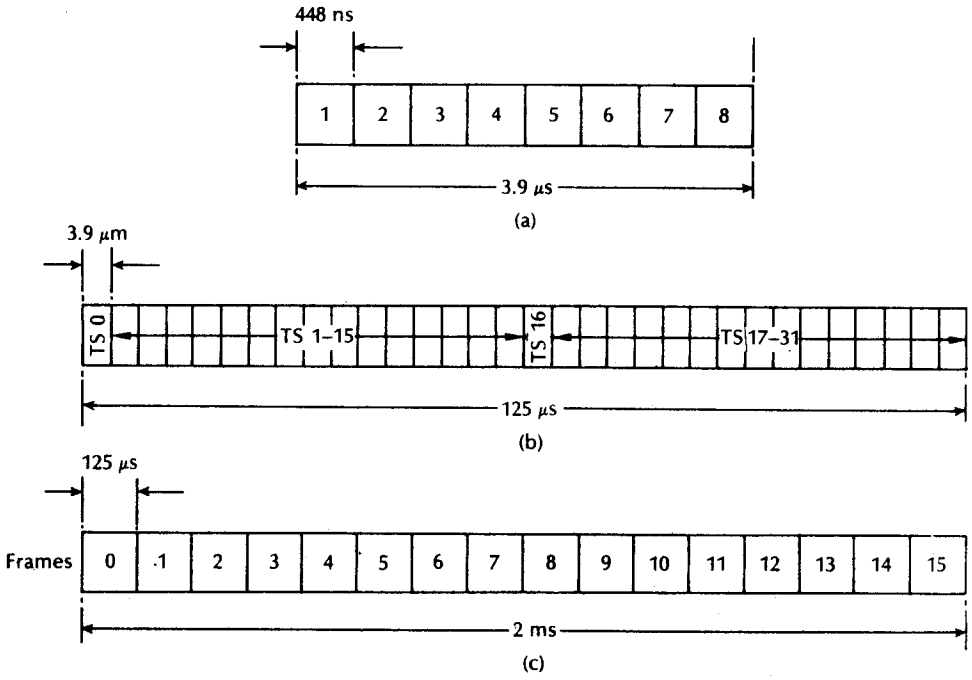

Figure 11.31 The timing for the line signalling structure of the European standard thirty channel PCM system: (a) bits per time slot; (b) time slots per frame; (c) frames per multiframe.

A current European standard for speech transmisson using PCM on metallic conductors (i.e. coaxial line) is the thirty channel system. In this system the PAM samples from each channel are encoded into eight binary bits which are incorporated into a single time slot. Time slots from respective channels are interleaved (multiplexed) into a frame consisting of thirty-two time slots. The two additional time slots do not carry encoded speech but signalling and synchronization information. Finally, sixteen frames are incorporated into a multiframe which is a self contained timing unit. The timing for this line signalling structure is shown in Figure 11.31 and calculated in Example 11.1.

Example 11.1

The sampling rate for each speech channel on the 30 channel PCM system is 8 kHz and each sample is encoded into eight bits. Determine:

(a) the transmission or bit rate for the system:
(b) the duration of a time slot;
(c) the duration of a frame and multiframe.

Solution: (a) The 30 channel PCM system has 32 time slots each eight bits wide which make up a frame. Therefore,

$$\textit{Number of bits in a frame} = 32 \times 8 = 256 \text{ bits}$$

This frame must be transmitted within the sampling period and thus 8×10^3 frames are transmitted per second. Hence, the transmission rate for the system is:

$$8 \times 10^3 \times 256 = 2.048 \text{ Mbit s}^{-1}$$

(b) The bit duration is simply:

$$\frac{1}{2.048 \times 10^6} = 488 \text{ ns}$$

Therefore, the duration of a time slot is:

$$8 \times 488 \text{ ns} = 3.9 \ \mu\text{s}$$

(c) The duration of a frame is thus:

$$32 \times 3.9 \ \mu\text{s} = 125 \ \mu\text{s}$$

and the duration of a multiframe is:

$$16 \times 125 \ \mu\text{s} = 2 \text{ ms}$$

The signalling structure shown in Figure 11.31 applies to thirty channel PCM systems which were originally designed to transmit over metallic conductors using a high density bipolar line code (HDB 3). The increased bandwidth with optical fiber communications allows transmission rates far in excess of 2.048 Mbit s^{-1}. Therefore an increased number of telephone channels may be sampled, encoded, multiplexed and transmitted on an optical fiber link. In Europe the increased bit rates were chosen as multiples of the thirty channel system, whereas in North America they tend to be multiples of a twenty-four channel system. These bit rates and the corresponding number of transmitted telephone channels are specified in Table 11.1.

It must be noted that a bipolar code with a zero mean level (i.e. with positive and negative going pulses in the electrical regime) such as HDB 3 cannot be transmitted directly over an optical fiber link unless the mean level is raised to allow both positive and negative going pulses to be transmitted by the intensity modulated optical source. The resultant ternary (three level) optical transmission is not always suitable for telecommunication applications and therefore binary coding after appropriate scrambling, biphase (Manchester encoding), delay modulation (Miller encoding), etc., is often employed. This involves additional complexity at the transmit and receive terminals as well as necessitating extra redundancy (i.e. bits which do not contain the transmitted information, thus giving a reduction in the information per transmitted symbol) in the line code. This topic is considered in greater detail in Section 11.6.7.

Table 11.1 Digital bit rates for multichannel PCM transmission in Europe and North America

Europe		North America	
Telephone channels	Bit rates Mbit s^{-1}	Telephone channels	Bit rates Mbit s^{-1}
30	2.048	24	1.544
120	8.448	48	3.152
480	34.368	96	6.312
1920	139.264	672	44.736
7680	565.148	4032	274.176

11.6 Digital system planning considerations

The majority of digital optical fiber communication systems for the telecommunication network or local data applications utilize binary intensity modulation of the optical source. Therefore, we choose to illustrate the planning considerations for digital transmission based on this modulation technique. Baseband PCM transmission using source intensity modulation is usually designated as PCM–IM.

11.6.1 The regenerative repeater

In the case of the long-haul, high capacity digital systems, the most important overall system performance parameter is the spacing of the regenerative repeaters. It is therefore useful to consider the performance of the digital repeater, especially as it is usually designed with the same optical components as the terminal equipment. Figure 11.32 shows the functional parts of a typical regenerative repeater for optical fiber communications. The attenuated and dispersed optical pulse train is detected and amplified in the receiver unit. This consists of a photodiode followed by a low noise preamplifier. The electrical signal thus acquired is given a further increase in power level in a main amplifier prior to reshaping in order to compensate for the transfer characteristic of the optical fiber (and the amplifier) using an equalizer. Depending on the photodiode utilized, automatic gain control may be provided at this stage for both the photodiode bias current and the main amplifier (see Section 11.3.2).

Accurate timing (clock) information is then obtained from the amplified and equalized waveform using a timing extraction circuit such as a ringing circuit or phase locked loop. This enables precise operation of the following regenerator circuit within the bit intervals of the original pulse train. The function of the regenerator circuit is to reconstitute the originally transmitted pulse train, ideally without error. This can be achieved by setting a threshold above which a binary one is registered, and below which a binary zero is recorded, as indicated in Figure

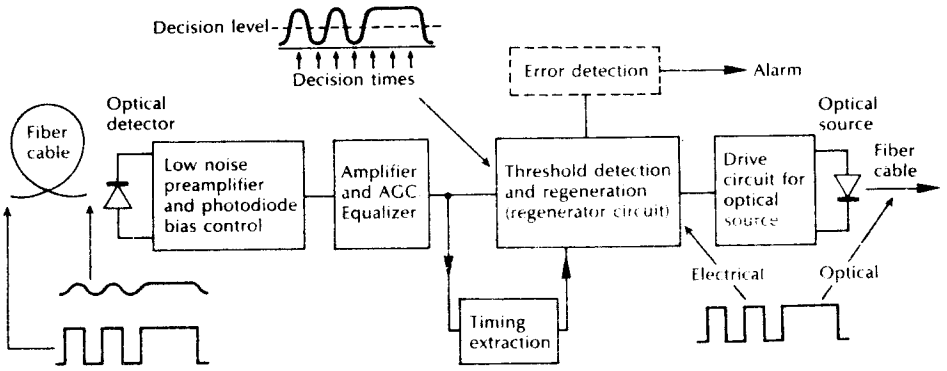

Figure 11.32 Block schematic showing a typical regenerative repeater for digital optical fiber communications.

11.32. The regenerator circuit makes these decisions at times corresponding to the centre of the bit intervals based on the clock information provided by the timing circuit.

Hence the decision times are usually set at the mid-points between the decision level crossings of the pulse train. The pulse train is sampled at a regular frequency equal to the bit rate, and at each sample instant a decision is made of the most probable symbol being transmitted. The symbols are then regenerated in their original form (either a binary one or zero) before retransmission as an optical signal using a source operated by an electronic drive circuit. Hence the possible regeneration of an exact replica of the originally transmitted waveform is a major advantage of digital transmission over corresponding analog systems. Repeaters in analog systems filter, equalize and amplify the received waveform, but are unable to reconstitute the originally transmitted waveform entirely free from distortion and noise. Signal degradation in long-haul analog systems is therefore accumulative, being a direct function of the number of repeater stages. In contrast the signal degradation encountered in PCM systems is purely a function of the quantization process and the system bit error rate.

Errors may occur in the regeneration process in the following situations:

1. The signal to noise ratio at the decision instant is insufficient for an accurate decision to be made. For instance, with high noise levels, the binary zero may occur above the threshold and hence be registered as a binary one.
2. There is intersymbol interference due to dispersion on the optical fiber link. This may be reduced by equalization which forces the transmitted binary one to pass through zero at all neighbouring decision times.
3. There is a variation in the clock rate and phase degradations (jitter) such as distortion of the zero crossings and static decision time misalignment.

A method which is often used to obtain a qualitative indication of the

performance of a regenerative repeater or a PCM system is the examination of the received waveform on an oscilloscope using a sweep rate which is a fraction of the bit rate. The display obtained over two bit intervals' duration, which is the result of superimposing all possible pulse sequences, is called an eye pattern or diagram. An illustration of an eye pattern for a binary system with little distortion and no additive noise is shown in Figure 11.33(a).It may be observed that the pattern has the shape of a human eye which is open and that the decision time corresponds to the centre of the opening. To regenerate the pulse sequence without error the eye must be open thereby indicating that a decision area exists, and the decision crosshair (provided by the decision time and the decision threshold) must be within this open area. The effect of practical degradations on the pulses (i.e. intersymbol interference and noise) is to reduce the size of, or close, the eye, as shown in Figure 11.33(b). Hence for reliable transmission it is essential that the eye is kept open, the margin against an error occurring being the minimum distance between the decision crosshair and the edge of the eye.

In practice, a low bit error rate (BER) in the region 10^{-7} to 10^{-10} may be tolerated with PCM transmission. However, with data transmission (e.g. computer communications) any error can cause severe problems, and it is necessary to incorporate error detecting and possibly correcting circuits into the regenerator. This invariably requires the insertion of a small amount of redundancy into the transmitted pulse train (see Section 11.6.7).

Calculation of the possible repeater spacing must take account of the following system component performances:

(a) the average optical power launched into the fiber based on the end of life transmitter performance;
(b) the receiver input power required to achieve an acceptably low BER (e.g. 10^{-9}), taking into account component deterioration during the system's lifetime;

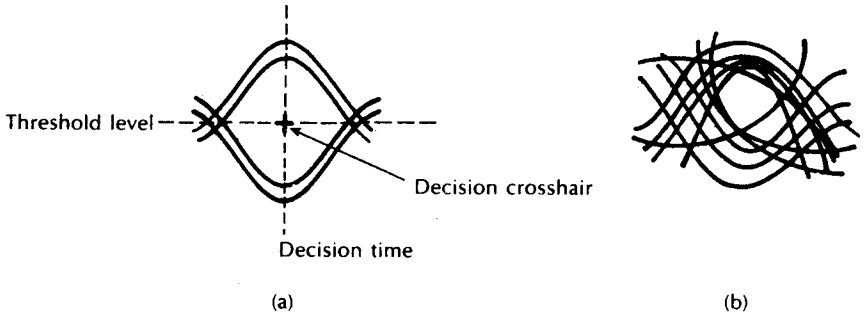

Figure 11.33 Eye patterns in binary digital transmission: (a) the pattern obtained with a bandwidth limitation but no additive noise (open eye); (b) the pattern obtained with a bandwidth limitation and additive noise (partially closed eye).

(c) the installed fiber cable loss including jointing and coupling (to source and detector) losses as well as the effects of ageing and from anticipated environmental changes;
(d) the temporal response of the system including the effects of pulse dispersion on the channel; this becomes an important consideration with high bit rate multimode fiber systems which may be dispersion limited.

These considerations are discussed in detail in the following sections.

11.6.2 The optical transmitter

The average optical power launched into the fiber from the transmitter depends upon the type of source used and the required system bit rate, as indicated in Section 11.2.1. These factors may be observed in Figure 11.34 [Ref. 45] which compares the optical power available from an injection laser and an LED for transmission over a multimode fiber with a core diameter of 50 μm and a numerical aperture of 0.2. Typically, the laser launches around 1 mW, whereas usually the LED is limited to about 100 μW. It may also be noted that both device types emit less optical power at higher bit rates. However, the LED gives reduced output at modulation bandwidths in excess of 50 MHz, whereas laser output is unaffected below 200 MHz. Also, the fact that generally the optical power which may be

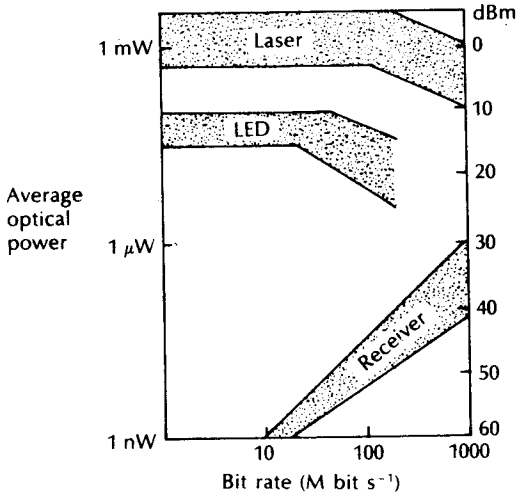

Figure 11.34 The average power launched into multimode optical fiber from typical injection lasers and LEDs as a function of digital bit rate (upper bands). Also included in the lower band is the received optical power required for binary NRZ pulses transmitted with a BER of 10^{-9}. Reproduced with permission from D. C. Gloge and T. Li, 'Multimode-fiber technology for digital transmission', *Proc. IEEE*, **68**, p. 1269, 1980. Copyright © 1980 IEEE.

launched into a fiber from an LED even at low bit rates is 10 to 15 dB down on that available from a laser is an important consideration, especially when receiver noise is a limiting factor within the system.

11.6.3 The optical receiver

The input optical power required at the receiver is a function of the detector combined with the electrical components within the receiver structure. It is strongly dependent upon the noise (i.e. quantum, dark current and thermal) associated with the optical fiber receiver. The theoretical minimum pulse energy or quantum limit required to maintain a given BER was discussed in Section 9.2.4.

It was predicted that approximately twenty-one incident photons were necessary at an ideal photodetector in order to register a binary one with a BER of 10^{-9}. However, this is a fundamental limit which cannot be achieved in practice and therefore it is essential that estimates of the minimum required optical input power are made in relation to practical devices and components.

Although the statistics of quantum noise follow a Poisson distribution, other important sources of noise within practical receivers (e.g. thermal) are characterized by a Gaussian probability distribution. Hence estimates of the required SNR to maintain particular bit error rates may be obtained using the procedure adopted for error performance of electrical digital systems where the noise distribution is considered to be white Gaussian. This Gaussian approximation [Ref. 46] is

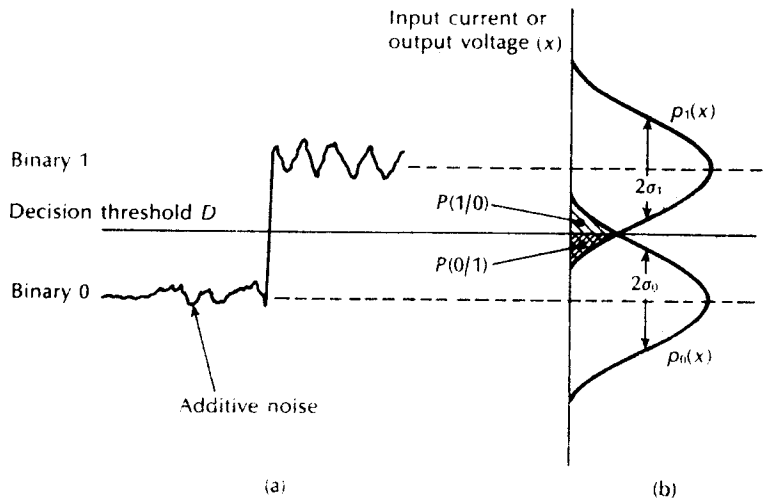

Figure 11.35 Binary transmission: (a) the binary signal with additive noise; (b) probability density functions for the binary signal showing the decision case. P(0/1) is the probability of falsely identifying a binary one and P(1/0) is the probability of falsely identifying a binary zero.

sufficiently accurate for design purposes and is far easier to evaluate than the more exact probability distribution within the receiver [Ref. 47]. The receiver sensitivities calculated by using the Gaussian approximation are generally within 1 dB of those calculated by other methods [Ref. 29].

Although the transmitted signal consists of two well defined light levels, in the presence of noise the signal at the receiver is not as well defined. This situation is shown in Figure 11.35(a) which illustrates a binary signal in the presence of noise. The signal plus the additive noise at the detector may be defined in terms of the probability density functions (PDFs) shown in Figure 11.35(b). These PDFs describe the probability that the input current (or output voltage) has a value i (or v) within the incremental range di (or dv). The expected values of the signal in the two transmitted states, namely 0 and 1, are indicated by $p_0(x)$ and $p_1(x)$ respectively. When the additive noise is assumed to have a Gaussian distribution, the PDFs of the two states will also be Gaussian. The Gaussian PDF which is continuous is defined by:

$$p(x) = \frac{1}{\sigma\sqrt{(2\pi)}} \exp - [(x-m)^2/2\sigma^2] \tag{11.5}$$

where m is the mean value and σ the standard deviation of the distribution. When $p(x)$ describes the probability of detecting a noise current or voltage, σ corresponds to the rms value of that current or voltage.

If a decision threshold D is set between the two signal states, as indicated in Figure 11.35, signals greater than D are registered as a one and those less than D as a zero. However when the noise current (or voltage) is sufficiently large it can either decrease a binary one to a zero or increase a binary zero to a one. These error probabilities are given by the integral of the signal probabilities outside the decision region. Hence the probability that a signal transmitted as a 1 is received as a 0, $P(0/1)$, is proportional to the shaded area indicated in Figure 11.35(b). The probability that a signal transmitted as a 0 is received as a 1, $P(1/0)$, is similarly proportional to the other shaded area shown in the diagram. If $P(1)$ and $P(0)$ are the probabilities of transmission for binary ones and zeros, respectively, then the total probability of error $P(\mathrm{e})$ may be defined as

$$P(\mathrm{e}) = P(1)P(0/1) + P(0)P(1/0) \tag{11.6}$$

Now let us consider a signal current i_{sig} together with an additive noise current i_N and a decision threshold set at $D = i_D$. If at any time when a binary 1 is transmitted the noise current is negative such that:

$$i_N < -(i_{sig} - i_D) \tag{11.7}$$

then the resulting current $i_{sig} + i_N$ will be less than i_D and an error will occur. The corresponding probability of the transmitted 1 being received as a 0 may be written as:

$$P(0/1) = \int_{-\infty}^{i_D} p(i, i_{sig})\, \mathrm{d}i \tag{11.8}$$

and following Eq. (11.5)

$$p_1(x) = p(i, i_{sig}) = \frac{1}{(\overline{i_N^2})^{\frac{1}{2}}\sqrt{(2\pi)}} \exp - \left[\frac{(i - i_{sig})^2}{2(\overline{i_N^2})}\right] \tag{11.9}$$

$$= \text{Gsn}\,[i, i_{sig}, (\overline{i_N^2})^{\frac{1}{2}}] \tag{11.10}$$

where i is the actual current, i_{sig} is the peak signal current during a binary 1 (this corresponds to the peak photocurrent I_p when only a signal component is present), and $\overline{i_N^2}$ is the mean square noise current. Substituting Eq. (11.10) into Eq. (11.8) gives:

$$P(0/1) = \int_{-\infty}^{i_D} \text{Gsn}\,[i, i_{sig}, (\overline{i_N^2})^{\frac{1}{2}}]\ \text{d}i \tag{11.11}$$

Similarly, the probability that a binary 1 will be received when a 0 is transmitted is the probability that the received current will be greater than i_D at some time during the zero bit interval. It is given by:

$$P(1/0) = \int_{i_D}^{\infty} p(i, 0) \tag{11.12}$$

Assuming the mean square noise current in the zero state is equal to the mean square noise current in the one state ($\overline{i_N^2}$) (this is an approximation if shot noise is dominant), and that for a zero bit $i_{sig} = 0$, then following Eq. (11.5):

$$p_0(x) = p(i, 0) = \frac{1}{(\overline{i_N^2})^{\frac{1}{2}}\sqrt{(2\pi)}} \exp - \left[\frac{(i - 0)^2}{2(\overline{i_N^2})}\right] \tag{11.13}$$

$$= \text{Gsn}\,[i, 0, (\overline{i_N^2})^{\frac{1}{2}}] \tag{11.14}$$

Hence substituting Eq. (11.14) into Eq. (11.12) gives:

$$P(1/0) = \int_{i_D}^{\infty} \text{Gsn}\,[i, 0, (\overline{i_N^2})^{\frac{1}{2}}]\ \text{d}i \tag{11.15}$$

The integrals of Eqs. (11.11) and (11.15) are not readily evaluated but may be written in terms of the error function (erf)* where:

$$\text{erf}(u) = \frac{2}{\sqrt{\pi}} \int_0^u \exp\,(-z^2)\ \text{d}z \tag{11.16}$$

and the complementary error function is:

$$\text{erfc}(u) = 1 - \text{erf}(u) = \frac{2}{\sqrt{\pi}} \int_u^{\infty} \exp\,(-z^2)\ \text{d}z \tag{11.17}$$

* Another form of the error function denoted by erf is defined in Problem 11.10.

Hence

$$P(0/1) = \frac{1}{2}\left[1 - \text{erf}\left(\frac{|\, i_{sig} - i_D \,|}{(\overline{i_N^2})^{\frac{1}{2}}\sqrt{2}}\right)\right]$$

$$= \tfrac{1}{2}\,\text{erfc}\left(\frac{|\, i_{sig} - i_D \,|}{(\overline{i_N^2})^{\frac{1}{2}}\sqrt{2}}\right) \tag{11.18}$$

and

$$P(1/0) = \tfrac{1}{2}\,\text{erfc}\left(\frac{|\, 0 - i_D \,|}{(\overline{i_N^2})^{\frac{1}{2}}\sqrt{2}}\right) = \tfrac{1}{2}\,\text{erfc}\left(\frac{|\, -i_D \,|}{(\overline{i_N^2})^{\frac{1}{2}}\sqrt{2}}\right) \tag{11.19}$$

If we assume that a binary code is chosen such that the number of transmitted ones and zeros are equal, then $P(0) = P(1) = \frac{1}{2}$, and the net probability of error is one half the sum of the shaded areas in Figure 11.35(b). Therefore Eq. (11.6) becomes:

$$P(e) = \tfrac{1}{2}[\,P(0/1) + P(1/0)] \tag{11.20}$$

and substituting for $P(0/1)$ and $P(1/0)$ from Eqs. (11.18) and (11.19) gives:

$$P(e) = \frac{1}{2}\left[\tfrac{1}{2}\,\text{erfc}\left(\frac{|\, i_{sig} - i_D \,|}{(\overline{i_N^2})^{\frac{1}{2}}\sqrt{2}}\right) + \tfrac{1}{2}\,\text{erfc}\left(\frac{|\, -i_D \,|}{(\overline{i_N^2})^{\frac{1}{2}}\sqrt{2}}\right)\right] \tag{11.21}$$

Equation (11.21) may be simplified by setting the threshold decision level at the mid-point between zero current and the peak signal current such that $i_D = i_{sig}/2$. In electrical systems this situation corresponds to an equal minimum probability of error in both states due to the symmetrical nature of the PDFs. It must be noted that for optical fiber systems this is not generally the case since the noise in each signal state contains shot noise contributions proportional to the signal level. Nevertheless, assuming a Gaussian distribution for the noise and substituting $i_D = i_{sig}/2$ into Eq. (11.21) we obtain:

$$P(e) = \frac{1}{2}\left[\tfrac{1}{2}\,\text{erfc}\left(\frac{|\, i_{sig}/2 \,|}{(\overline{i_N^2})^{\frac{1}{2}}\sqrt{2}}\right) + \tfrac{1}{2}\,\text{erfc}\left(\frac{|\, -i_{sig}/2 \,|}{(\overline{i_N^2})^{\frac{1}{2}}\sqrt{2}}\right)\right]$$

$$= \tfrac{1}{2}\,\text{erfc}\left(\frac{i_{sig}}{2(\overline{i_N^2})^{\frac{1}{2}}\sqrt{2}}\right) \tag{11.22}$$

The electrical SNR at the detector may be written in terms of the peak signal power to rms noise power (mean square noise current) as:

$$\frac{S}{N} = \frac{i_{sig}^2}{\overline{i_N^2}} \tag{11.23}$$

Comparison of Eq. (11.23) with Eq. (11.22) allows the probability of error to be expressed in terms of the analog SNR as:

$$P(e) = \tfrac{1}{2}\,\text{erfc}\left(\frac{(S/N)^{\frac{1}{2}}}{2\sqrt{2}}\right) \tag{11.24}$$

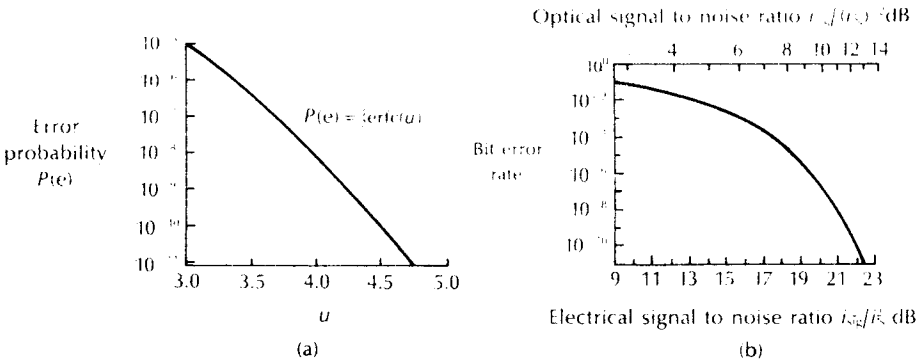

Figure 11.36 (a) A plot of the probability of error $\frac{1}{2}\,\mathrm{erfc}(u)$ against the argument of the error function u. (b) The bit error rate as a function of both the ratio of peak signal power to rms noise power (electrical SNR) and the ratio of peak signal current to rms noise current (optical SNR) for binary transmission.

Estimates of the required SNR to maintain a given error rate may be obtained using the standard table for the complementary error function. A plot of $P(\mathrm{e})$ against $\frac{1}{2}\,\mathrm{erfc}(u)$ is shown in Figure 11.36(a). This may be transposed into the characteristic illustrated in Figure 11.36(b) where the bit error rate which is equivalent to the error probability $P(\mathrm{e})$ is shown as a function of the SNR following Eq. (11.24).

Example 11.2

Using the Gaussian approximation determine the required signal to noise ratios (optical and electrical) to maintain a BER of 10^{-9} on a baseband binary digital optical fiber link. It may be assumed that the decision threshold is set midway between the one and the zero level and that $2 \times 10^{-9} = \mathrm{erfc}\ 4.24$.

Solution: Under the above conditions, the probability of error is given by Eq. (11.24) where,

$$P(\mathrm{e}) = \tfrac{1}{2}\,\mathrm{erfc}\left(\frac{(S/N)^{\frac{1}{2}}}{2\sqrt{2}}\right) = 10^{-9}$$

Hence

$$\mathrm{erfc}\left(\frac{(S/N)^{\frac{1}{2}}}{2\sqrt{2}}\right) = 2 \times 10^{-9}$$

and

$$\frac{(S/N)^{\frac{1}{2}}}{2\sqrt{2}} = 4.24$$

giving

$$(S/N)^{\frac{1}{2}} = 4.24 \times 2\sqrt{2} = 12$$

The optical SNR may be defined in terms of the peak signal current and rms noise current as $i_{sig}/(\overline{i_N^2})^{\frac{1}{2}}$. Therefore using Eq. (11.23):

$$\frac{i_{sig}}{(\overline{i_N^2})^{\frac{1}{2}}} = \left(\frac{S}{N}\right)^{\frac{1}{2}} = 12 \text{ or } 10.8 \text{ dB}$$

The electrical SNR is defined by Eq. (11.23) as:

$$\frac{\overline{i_{sig}^2}}{\overline{i_N^2}} = \frac{S}{N} = 144 \text{ or } 21.6 \text{ dB}$$

These results for the SNRs may be seen to correspond to a bit error rate of 10^{-9} on the curve shown in Figu e 11.36(b).

However, the plot shown in Figure 11.36(b) does not reflect the best possible results, or those which may be obtained with an optimized receiver design. In this case, if the system is to be designed with a particular BER, the appropriate value of the error function is established prior to adjustment of the parameter values (signal levels, decision threshold level, avalanche gain, component values, etc.) in order to obtain this BER [Ref. 48]. It is therefore necessary to use the generalized forms of Eqs. (11.18) and (11.19) where:

$$P(0/1) = \tfrac{1}{2}\,\text{erfc}\left(\frac{|i_{sig\,1} - i_D|}{(\overline{i_{N1}^2})^{\frac{1}{2}}\sqrt{2}}\right) \tag{11.25}$$

$$P(0/1) = \tfrac{1}{2}\,\text{erfc}\left(\frac{|i_D - i_{sig\,0}|}{(\overline{i_{N0}^2})^{\frac{1}{2}}\sqrt{2}}\right) \tag{11.26}$$

where $i_{sig\,1}$ and $i_{sig\,0}$ are the signal currents, in the 1 and 0 states, respectively, and $\overline{i_{N1}^2}$ and $\overline{i_{N0}^2}$ are the corresponding mean square noise currents which may include both shot and thermal noise terms. Equations (11.25) and (11.26) allow a more exact evaluation of the error performance of the digital optical fiber system under the Gaussian approximation [Refs. 48 and 49]. Unfortunately, this approach does not give as simple a direct relationship between the BER and the analog SNR as the one shown in Eq. (11.24). Thus for estimates of SNR within this text we will make use of the slightly poorer approximation given by Eq. (11.24). Although this approximation does not give the correct decision threshold level or optimum avalanche gain it is reasonably successful at predicting bit error rate as a function of signal power and hence provides realistic estimates of the number of photons required at a practical detector in order to maintain given bit error rates.

For instance, let us consider a good avalanche photodiode receiver which we assume to be quantum noise limited. Hence we ignore the shot noise contribution from the dark current within the APD, as well as the thermal noise generated by

the electronic amplifier. In practice, this assumption holds when the multiplication factor M is chosen to be sufficiently high to ensure that the SNR is determined by photon noise rather than by electronic amplifier noise, and the APD used has a low dark current. To determine the SNR for this ideal APD receiver it is useful to define the quantum noise on the primary photocurrent I_p within the device in terms of shot noise following Eq. (9.8). Therefore, the mean square shot noise current is given by:

$$\overline{i_s^2} = 2eBI_pM^2 \tag{11.27}$$

where e is the electronic charge and B is the post detection or effective noise bandwidth. It may be observed that the mean square shot noise current $\overline{i_s^2}$ given in Eq. (11.27) is increased by a factor M^2 due to avalanche gain in the APD. However, Eq. (11.27) does not give the total noise current at the output of the APD as there is an additional noise contribution from the random gain mechanism. The excess avalanche noise factor $F(M)$ incurred was discussed in Section 9.3.4 and defined by Eqs. (9.27) and (9.28). Equation (9.27) may be simplified [Ref. 50] to give an expression for electron injection in the low frequency limit of:

$$F(M) = kM + \left(2 - \frac{1}{M}\right)(1 - k) \tag{11.28}$$

where k is the ratio of the carrier ionization rates. Hence, the excess avalanche noise factor may be combined into Eq. (11.27) to give a total mean square shot noise current $\overline{i_n^2}$ as:

$$\overline{i_n^2} = 2eBI_pM^2F(M) \tag{11.29}$$

Furthermore, the avalanche multiplication mechanism raises the signal current to MI_p and therefore the SNR in terms of the peak signal power to rms noise power may be written as:

$$\frac{S}{N} = \frac{(MI_p)^2}{2eBI_pM^2F(M)} = \frac{I_p}{2eBF(M)} \tag{11.30}$$

Now, if we let z_{md} correspond to the average number of photons detected in a time period of duration τ, then

$$I_p = \frac{z_{md}e}{\tau} = \frac{z_m e\eta}{\tau} \tag{11.31}$$

where z_m is the average number of photons incident on the APD and η is the quantum efficiency of the device. Substituting for I_p in Eq. (11.30) we have:

$$\frac{S}{N} = \frac{z_m\eta}{2B\tau F(M)} \tag{11.32}$$

Rearranging Eq. (11.32) gives an expression for the average number of photons required within the signalling interval τ to detect a binary one in terms of the

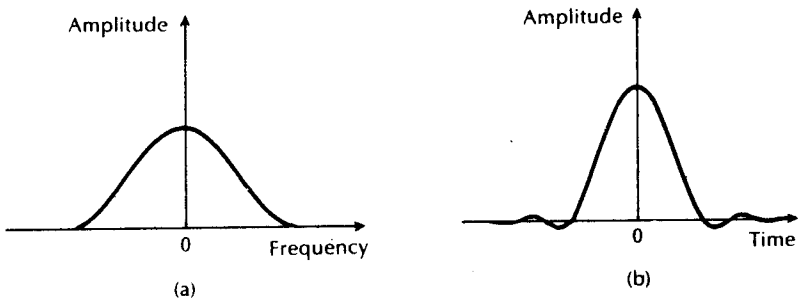

Figure 11.37 (a) Raised cosine spectrum. (b) Output of a system with a raised cosine output spectrum for a single input pulse.

received SNR for the good APD receiver as:

$$z_m = \frac{2B\tau F(M)}{\eta}\left(\frac{S}{N}\right) \tag{11.33}$$

A reasonable pulse shape obtained at the receiver in order to reduce intersymbol interference has the raised cosine spectrum shown in Figure 11.37. The raised cosine spectrum for the received pulse gives a pulse response resulting in a binary pulse train passing through either full or zero amplitude at the centres of the pulse intervals and with transitions passing through half amplitude at points which are midway in time between pulse centres. For raised cosine pulse shaping and full τ signalling $B\tau$ is around 0.6. Hence the average number of photons required to detect a binary one using a good APD receiver at a specified BER may be estimated using Eq. (11.33) in conjunction with Eq. (11.24).

Example 11.3

A good APD is used as a detector in an optical fiber PCM receiver designed for baseband binary transmission with a decision threshold set midway between the zero and one signal levels. The APD has a quantum efficiency of 80%, a ratio of carrier ionization rates of 0.02 and is operated with a multiplication factor of 100. Assuming a raised cosine signal spectrum at the receiver, estimate the average number of photons which must be incident on the APD to register a binary one with a BER of 10^{-9}.

Solution: The electrical SNR required to obtain a BER of 10^{-9} at the receiver is given by the curve shown in Figure 11.36(b), or the solution to example 11.2 as 21.6 dB or 144. Also, the excess avalanche noise factor $F(M)$ may be determined

using Eq. (11.28) where:

$$F(M) = kM + \left(2 - \frac{1}{M}\right)(1 - k)$$
$$= 2 + (2 - 0.01)(1 - 0.02)$$
$$= 3.95 \simeq 4$$

The average number of photons which must be incident at the receiver in order to maintain the BER can be estimated using Eq. (11.33) (assuming $B\tau = 0.6$ for the raised cosine pulse spectrum) as:

$$z_m = \frac{2B\tau F(M)}{\eta}\left(\frac{S}{N}\right)$$
$$= \frac{2 \times 0.6 \times 4 \times 144}{0.8}$$
$$= 864 \text{ photons}$$

The estimate in Example 10.3 gives a more realistic value for the average number of incident photons required at a good APD receiver in order to register a binary one with a BER of 10^{-9} than the quantum limit of twenty-one photons determined for an ideal photodetector in Example 9.1. However, it must be emphasized that the estimate in Example 11.3 applies to a good silicon APD receiver (with high sensitivity and low dark current) which is quantum noise limited, and that no account has been taken of the effects of either dark current within the APD or thermal noise generated within the preamplifier. It is therefore likely that at least 1000 incident photons are required at a good APD receiver to register a binary one and provide a BER of 10^{-9} [Ref, 51]. Nevertheless somewhat lower values may be achieved by setting the decision threshold below the half amplitude level because the shot noise on the zero level is lower than the shot noise on the one level.

The optical power required at the receiver P_o is simply the optical energy divided by the time interval over which it is incident. The optical energy E_o may be obtained directly from the average number of photons required at the receiver in order to maintain a particular BER following:

$$E_o = z_m hf \tag{11.34}$$

where hf is the energy associated with a single photon which is given by Eq. (6.1). In order that a binary one is registered at the receiver, the optical energy E_o must be incident over the bit interval τ. For system calculations we can assume a zero disparity code which has an equal density of ones and zeros. In this case the optical power required to register a binary one may be considered to be incident over two

bit intervals giving:

$$P_o = \frac{E_o}{2\tau} \tag{11.35}$$

Substituting for E_o from Eq. (10.34) we obtain:

$$P_o = \frac{z_m hf}{2\tau} \tag{11.36}$$

Also as the bit rate B_T for the channel is the reciprocal of the bit interval τ, Eq. (11.36) may be written as:

$$P_o = \frac{z_m hf B_T}{2} \tag{11.37}$$

Equation (11.37) allows estimates of the incident optical power required at a good APD receiver in order to maintain a particular BER, based on the average number of incident photons. In system calculations these optical power levels are usually expressed in dBm. It may also be observed that the required incident optical power is directly proportional to the bit rate B_T which typifies a shot noise limited receiver.

Example 11.4

The receiver of example 11.3 operates at a wavelength of 1 μm. Assuming a zero disparity binary code, estimate the incident optical power required at the receiver to register a binary one with a BER of 10^{-9} at bit rates of 10 Mbit s^{-1} and 140 Mbit s^{-1}.

Solution: Under the above conditions, the required incident optical power may be obtained using Eq. (11.37) where,

$$P_o = \frac{z_m hf B_T}{2} = \frac{z_m hc B_T}{2\lambda}$$

At 10 Mbit s^{-1}:

$$P_o = \frac{864 \times 6.626 \times 10^{-34} \times 2.998 \times 10^8 \times 10^7}{2 \times 1 \times 10^{-6}}$$

$$= 858.2 \text{ pW}$$

$$= -60.7 \text{ dBm}$$

At 140 Mbit s^{-1}:

$$P_o = \frac{864 \times 6.626 \times 10^{-34} \times 2.998 \times 10^8 \times 14 \times 10^7}{2 \times 1 \times 10^{-14}}$$

$$= 12.015 \text{ nW}$$

$$= -49.2 \text{ dBm}$$

Example 11.4 illustrates the effect of direct proportionality between the optical power required at the receiver and the system bit rate. In the case considered, the required incident optical power at the receiver to give a BER of 10^{-9} must be increased by around 11.5 dB (factor of 14) when the bit rate is increased from 10 to 140 Mbit s^{-1} Also, comparison with Example 9.1 where a similar calculation was performed for an ideal photodetector operating at 10 Mbit s^{-1} emphasizes the necessity of performing the estimate for a practical photodiode. The good APD receiver considered in Example 11.4 exhibits around 16 dB less sensitivity than the ideal photodetector (i.e. quantum limit).

The assumptions made in the evaluation of Examples 11.3 and 11.4 are not generally valid when considering *p–i–n* photodiode receivers because these devices are seldom quantum noise limited due to the absence of internal gain within the photodetector. In this case thermal noise generated within the electronic amplifier is usually the dominating noise contribution and is typically 1×10^3 to 3×10^3 times larger than the peak response produced by the displacement current of a single electron–hole pair liberated in the detector. Hence, for reliable performance with a BER of 10^{-9}, between 1 and 3×10^4 photons must be detected when a binary one is incident on the receiver [Ref. 53].

This translates into sensitivities which are about 30 dB or more, less than the quantum limit. Finally, for a thermal noise limited receiver the input optical power is proportional to the square root of both the post detection or effective noise bandwidth and the SNR (i.e. $P_0 \propto |(S/N)B|^{\frac{1}{2}}$). However, this result is best obtained from purely analog SNR considerations and therefore is dealt with in Section 11.7.1.

11.6.4 Channel losses

Another important factor when estimating the permissible separation between regenerative repeaters or the overall link length is the total loss encountered between the transmitter(s) and receiver(s) within the system. Assuming there are no dispersion penalties on the link, the total channel loss may be obtained by simply summing in decibels the installed fiber cable loss, the fiber–fiber jointing losses and the coupling losses of the optical source and detector. The fiber cable loss in decibels per kilometre α_{fc} is normally specified by the manufacturer, or alternatively it may be obtained by measurement (see Sections 13.2 and 13.10). It must be noted that the cabled fiber loss is likely to be greater than the uncabled fiber loss usually measured in the laboratory due to possible microbending of the fiber within the cabling process (see Section 4.8.1).

Loss due to joints (generally splices) on the link may also, for simplicity, be specified in terms of an equivalent loss in decibels per kilometre α_j. In fact, it is more realistic to regard α_j as a distributed loss since the optical attenuation resulting from the disturbed mode distribution at a joint does not only occur in the vicinity of the joint. Finally, the loss contribution attributed to the connectors α_{cr} (in decibels) used for coupling the optical source and detector to the fiber must be

included in the overall channel loss. Hence the total channel loss C_L (in decibels) may be written as:

$$C_L = (\alpha_{fc} + \alpha_j)L + \alpha_{cr} \tag{11.38}$$

where L is the length in kilometres of the fiber cable either between regenerative repeaters or between the transmit and receive terminals for a link without repeaters.

Example 11.5

An optical fiber link of length 4 km comprises a fiber cable with an attenuation of 5 dB km^{-1}. The splice losses for the link are estimated at 2 dB km^{-1}, and the connector losses at the source and detector are 3.5 and 2.5 dB respectively. Ignoring the effects of dispersion on the link determine the total channel loss.

Solution: The total channel loss may be simply obtained using Eq. (11.38) where:

$$\begin{aligned} C_L &= (\alpha_{fc} + \alpha_j)L + \alpha_{cr} \\ &= (5 + 2)4 + 3.5 + 2.5 \\ &= 34 \text{ dB} \end{aligned}$$

11.6.5 Temporal response

The system design considerations must also take into account the temporal response of the system components. This is especially the case with regard to pulse dispersion on the optical fiber channel. The formula given in Eq. (11.38) allows determination of the overall channel loss in the absence of any pulse broadening due to the dispersion mechanisms within the transmission medium. However, the finite bandwidth of the optical system may result in overlapping of the received pulses or intersymbol interference, giving a reduction in sensitivity at the optical receiver. Therefore, either a worse BER must be tolerated, or the ISI must be compensated by equalization within the receiver (see Section 11.3.3). The latter necessitates an increase in optical power at the receiver which may be considered as an additional loss penalty. This additional loss contribution is usually called the dispersion–equalization or ISI penalty. The dispersion–equalization penalty D_L becomes especially significant in high bit rate multimode fiber systems and has been determined analytically for Gaussian shaped pulses [Ref. 48]. In this case it is given by:

$$D_L = \left(\frac{\tau_e}{\tau}\right)^4 \text{ dB} \tag{11.39}$$

where τ_e is the $1/e$ full width pulse broadening due to dispersion on the link and τ is the bit interval or period. For Gaussian shaped pulses, τ_e may be written in

terms of the rms pulse width σ as (see Appendix B):

$$\tau_e = 2\sigma\sqrt{2} \tag{11.40}$$

Hence, substituting into Eq. (11.39) for τ_e and writing the bit rate B_T as the reciprocal of the bit interval τ gives:

$$D_L = 2(2\sigma B_T\sqrt{2})^4 \text{ dB} \tag{11.41}$$

Since the dispersion–equalization penalty as defined by Eq. (11.41) is measured in decibels, is may be included in the formula for the overall channel loss given by Eq. (11.38). Therefore, the total channel loss including the dispersion–equalization penalty C_{LD} is given by:

$$C_{LD} = (\alpha_{fc} + \alpha_j)L + \alpha_{cr} + D_L \text{ dB} \tag{11.42}$$

The dispersion–equalization penalty is usually only significant in wideband multimode fiber systems which exhibit intermodal as well as intramodal dispersion. Single-mode fiber systems which are increasingly being utilized for wideband long-haul applications are not generally limited by pulse broadening on the channel because of the absence of intermodal dispersion. However, it is often the case that intermodal dispersion is the dominant mechanism within multimode fibers. In Section 3.10.1 intermodal pulse broadening was considered to be a linear function of the fiber length L. Furthermore, it was indicated that the presence of mode coupling within the fiber made the pulse broadening increase at a slower rate proportional to L. Hence it is useful to consider the dispersion–equalization penalty in relation to fibers without and with mode coupling operating at various bit rates.

Example 11.6

The rms pulse broadening resulting from intermodal dispersion within a multimode optical fiber is 0.6 ns km^{-1}. Assuming this to be the dominant dispersion mechanism, estimate the dispersion–equalization penalty over an unrepeatered fiber link of length 8 km at bit rates of (a) 25 Mbit s^{-1} and (b) 150 Mbit s^{-1}. In both cases evaluate the penalty without and with mode coupling. The pulses may be assumed to have a Gaussian shape.

Solution: (a) *Without mode coupling.* The total rms pulse broadening over 8 km is given by:

$$\sigma_T = \sigma \times L = 0.6 \times 8 = 4.8 \text{ ns}$$

The dispersion–equalization penalty is given by Eq. (11.41) where:

$$D_L = 2(2\sigma_T B_T\sqrt{2})^4 = 2(2 \times 4.8 \times 10^{-9} \times 25 \times 10^6\sqrt{2})^4$$
$$= 0.03 \text{ dB}$$

With mode coupling. The total rms pulse broadening is:

$$\sigma_T \simeq \sigma\sqrt{L} = 0.6 \times \sqrt{8} = 1.7 \text{ ns}$$

Hence the dispersion–equalization penalty is:

$$D_L = 2(2 \times 1.7 \times 10^{-9} \times 25 \times 10^6\sqrt{2})^4$$
$$= 4.2 \times 10^{-4} \text{ dB (i.e. negligible)}$$

(b) *Without mode coupling.*

$$\sigma_T = 4.8 \text{ ns}$$
$$D_L = 2(2 \times 4.8 \times 10^{-9} \times 150 \times 10^6\sqrt{2})^4 = 34.38 \text{ dB}$$

With mode coupling.

$$\sigma_T = 1.7 \text{ ns}$$
$$D_L = 2(2 \times 1.7 = 10^{-9} \times 150 \times 10^6\sqrt{2})^4 = 0.54 \text{ dB}$$

Example 11.6(a) demonstrates that at low bit rates the dispersion–equalization penalty is very small if not negligible. In this case the slight advantage of the effect of mode coupling on the penalty is generally outweighed by increased attenuation on the link because of the mode coupling, which may be of the order of 1 dB km^{-1} Example 11.6(b) indicates that at higher bit rates with no mode coupling the dispersion–equalization penalty dominates to the extent that it would be necessary to reduce the repeater spacing to between 4 and 5 km. However, it may be observed that encouragement of mode coupling on the link greatly reduces this penalty and outweighs any additional attenuation incurred through mode coupling within the fiber. In summary, it is clear that the dispersion equalization penalty need only be applied when considering wideband systems. Moreover, it is frequently the case that lower bit rate systems may be up-graded at a later date to a higher capacity without incurring a penalty which might necessitate a reduction in repeater spacing.

An alternative approach involving the calculation of the system rise time can be employed to determine the possible limitation on the system bandwidth resulting from the temporal response of the system components. Therefore, if there is not a pressing need to obtain the maximum possible bit rate over the maximum possible distance, it is sufficient within the system design to establish that the total temporal response of the system is adequate for the desired system bandwidth. Nevertheless this approach does allow for a certain amount of optimization of the system components, but at the exclusion of considerations regarding equalization and the associated penalty.

The total system rise time may be determined from the rise times of the individual system components which include the source (or transmitter), the fiber cable, and the detector (receiver). These times are defined in terms of a Gaussian response as the 10–90% rise (or fall) times of the individual components. The fiber cable 10–90% rise time may be separated into rise times arising from intermodal T_n

and intramodal or chromatic dispersion T_c. The total system rise time is given by [Ref. 56]:

$$T_{syst} = 1.1(T_S^2 + T_n^2 + T_c^2 + T_D^2)^{\frac{1}{2}} \tag{11.43}$$

where T_S and T_D are the source and detector 10 to 90% rise times, respectively, and all the rise times are measured in nanoseconds. Comparison of the rise time edge with the overall pulse dispersion results in the weighting factor of 1.1.

The maximum system bit rate $B_T(\text{max})$ is usually defined in terms of T_{syst} by consideration of the rise time of the simple RC filter circuit shown in Figure 11.38(a). For a voltage step input of amplitude V, the output voltage waveform $v_{out}(t)$ as a function of time t is:

$$v_{out}(t) = V[1 - \exp(-t/RC)] \tag{11.44}$$

Hence the 10 to 90% rise time t_r for the circuit is given by:

$$t_r = 2.2\ RC \tag{11.45}$$

The transfer function for this circuit is shown in Figure 11.38 (b) and is given by:

$$|H(\omega)| = \frac{1}{(1 + \omega^2 C^2 R^2)^{\frac{1}{2}}} \tag{11.46}$$

Therefore the 3 dB bandwidth for the circuit is

$$B = \frac{1}{2\pi RC} \tag{11.47}$$

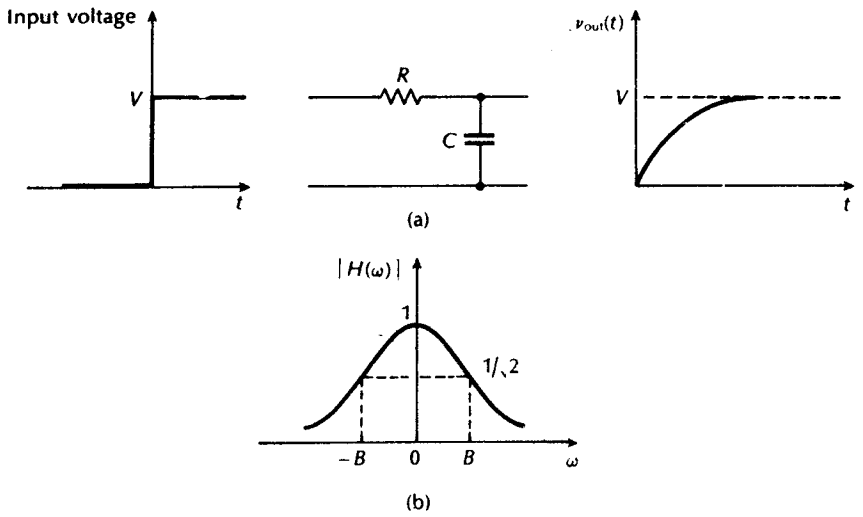

Figure 11.38 (a) The response of a low pass RC filter circuit to a voltage step input. (b) The transfer function $H(\omega)$ for the circuit in (a).

Combining Eqs. (11.45) and (11.47) gives,

$$t_r = \frac{2.2}{2\pi B} = \frac{0.35}{B} \tag{11.48}$$

The result for the 10 to 90% rise time indicated in Eq. (11.48) is of general validity, but a different constant term may be obtained with different filter circuits. However, for rise time calculations involving optical fiber systems the constant 0.35 is often utilized and hence in Eq. (11.48), $t_r = T_{syst}$. Alternatively, if an ideal (unrealizable) filter with an arbitrarily sharp cutoff is considered, the constant in Eq. (11.48) becomes 0.44. However, although this value for the constant is frequently employed when calculating the bandwidth of fiber from pulse dispersion measurements (see Section 13.3.1), the more conservative estimate obtained using a constant term of 0.35 is generally favoured for use in system rise time calculations [Refs. 56 and 57]. Also, in both cases it is usually accepted [Ref. 43] that to conserve the shape of a pulse with a reasonable fidelity through the RC circuit then the 3 dB bandwidth must be at least large enough to satisfy the condition $B\tau = 1$, where τ is the pulse duration. Combining this relation with Eq. (11.48) gives:

$$T_{syst} = t_r = 0.35\tau \tag{11.49}$$

For an RZ pulse format, the bit rate $B_T = B = 1/\tau$ (see Section 3.8) and hence substituting into Eq. (11.49) gives:

$$B_T(\text{max}) = \frac{0.35}{T_{syst}} \tag{11.50}$$

Alternatively for an NRZ pulse format $B_T = B/2 = 1/2\tau$ and therefore the maximum bit rate is given by:

$$B_T(\text{max}) = \frac{0.7}{T_{syst}} \tag{11.51}$$

Thus the upper limit on T_{syst} should be less than 35% of the bit interval for an RZ pulse format and less than 70% of the bit interval for an NRZ pulse format.

The effects of mode coupling are usually neglected in calculations involving system rise time, and hence the pulse dispersion is assumed to be a linear function of the fiber length. This results in a pessimistic estimate for the system rise time and therefore provides a conservative value for the maximum possible bit rate.

Example 11.7

An optical fiber system is to be designed to operate over an 8 km length without repeaters. The rise times of the chosen components are:

Source (LED)	8 ns
Fiber: intermodal	5 ns km^{-1}
(pulse broadening) intramodal	1 ns km^{-1}
Detector (p–i–n photodiode)	6 ns

From system rise time considerations, estimate the maximum bit rate that may be achieved on the link when using an NRZ format.

Solution: The total system rise time is given by Eq. (11.43) as:

$$\begin{aligned} T_{syst} &= 1.1(T_S^2 + T_n^2 + T_c^2 + T_D^2)^{\frac{1}{2}} \\ &= 1.1(8^2 + (8 \times 5)^2 + (8 \times 1)^2 + 6^2)^{\frac{1}{2}} \\ &= 46.2 \text{ ns} \end{aligned}$$

Hence the maximum bit rate for the link using an NRZ format is given by Eq. (11.51) where:

$$B_T(\max) = \frac{0.7}{T_{syst}} = \frac{0.7}{46.2 \times 10^{-9}} \simeq 15.2 \text{ Mbit s}^{-1}$$

The rise time calculations indicate that this will support a maximum bit rate of 15.2 Mbit s^{-1} which for an NRZ format is equivalent to a 3 dB optical bandwidth of 7.6 MHz (i.e. the NRZ format has two bit intervals per wavelength).

Once it is established that pulse dispersion is not a limiting factor, the major design exercise is the optical power budget for the system.

11.6.6 Optical power budgeting

Power budgeting for a digital optical fiber communication system is performed in a similar way to power budgeting within any communication system. When the transmitter characteristics, fiber cable losses and receiver sensitivity are known, the relatively simple process of power budgeting allows the repeater spacing or the maximum transmission distance for the system to be evaluated. However, it is necessary to incorporate a system margin into the optical power budget so that small variations in the system operating parameters do not lead to an unacceptable decrease in system performance. The operating margin is often included in a safety margin M_a which also takes into account possible source and modal noise, together witn receiver impairments such as equalization error, noise degradations and eye opening impairments. The safety margin depends to a large extent on the system components as well as the system design procedure and is typically in the range 5 to 10 dB. Systems using an injection laser transmitter generally require a larger safety margin (e.g. 8 dB) than those using an LED source (e.g. 6 dB) because the temperature variation and ageing of the LED are less pronounced.

The optical power budget for a system is given by the following expression:

$$P_i = P_o + C_L + M_a \text{ dB} \tag{11.52}$$

where P_i is the mean input optional power launched into the fiber, P_o is the mean incident optical power required at the receiver and C_L (or C_{LD} when there is a dispersion–equalization penalty) is the total channel loss given by Eq. (11.38) (or

Eq. (11.42)). Therefore the expression given in Eq. (11.52) may be written as:

$$P_i = P_o + (\alpha_{fc} + \alpha_j)L + \alpha_{cr} + M_a \text{ dB} \tag{11.53}$$

Alternatively, when a dispersion–equalization penalty is included Eq. (11.52) becomes:

$$P_i = P_o + (\alpha_{fc} + \alpha_j)L + \alpha_{cr} + D_L + M_a \text{ dB} \tag{11.54}$$

Equations (11.53) and (11.54) allow the maximum link length without repeaters to be determined, as demonstrated in Example 11.8.

Example 11.8

The following parameters are established for a long-haul single-mode optical fiber system operating at a wavelength of 1.3 μm.

Mean power launched from the laser transmitter	−3 dBm
Cabled fiber loss	0.4 dB km^{-1}
Splice loss	0.1 dB km^{-1}
Connector losses at the transmitter and receiver	1 dB each
Mean power required at the APD receiver:	
when operating at 35 Mbit s^{-1} (BER 10^{-9})	−55 dBm
when operating at 400 Mbit s^{-1} (BER 10^{-9})	−44 dBm
Required safety margin	7 dB

Estimate:

(a) the maximum possible link length without repeaters when operating at 35 Mbit s^{-1} (BER 10^{-9}). It may be assumed that there is no dispersion–equalization penalty at this bit rate.

(b) the maximum possible link length without repeaters when operating at 400 Mbit s^{-9} (BER 10^{-9}) and assuming no dispersion–equalization penalty.

(c) the reduction in the maximum possible link length without repeaters of (b) when there is a dispersion–equalization penalty of 1.5 dB. It may be assumed for the purposes of this estimate that the reduced link length has the 1.5 dB penalty.

Solution: (a) When the system is operating at 35 Mbit s^{-1} an optical power budget may be performed using Eq. (11.53), where

$$P_i - P_o = (\alpha_{fc} + \alpha_j)L + \alpha_{cr} + M_a \text{ dB}$$
$$-3 \text{ dBm} - (-55 \text{ dBm}) = (\alpha_{fc} + \alpha_j)L + \alpha_{cr} + M_a$$

Hence,

$$(\alpha_{fc} + \alpha_j)L = 52 - \alpha_{cr} - M_a$$
$$0.5L = 52 - 2 - 7$$
$$L = \frac{43}{0.5} = 86 \text{ km}$$

(b) Again using Eq. (11.53) when the system is operating at 400 Mbit s^{-1}.

$$-3 \text{ dBm} - (-44 \text{ dBm}) = (\alpha_{fc} + \alpha_j)L + \alpha_{cr} + M_a$$

$$(a_{fc} + \alpha_j)L = 41 - 2 - 7$$

$$L = \frac{32}{0.5} = 64 \text{ km}$$

(c) Performing the optical power budget using Eq. (11.54) gives:

$$P_i - P_o = (\alpha_{fc} + \alpha_j)L + \alpha_{cr} + D_L + M_a$$

Hence,

$$0.5L = 41 - 2 - 1.5 - 7$$

and

$$L = \frac{30.5}{0.5} = 61 \text{ km}$$

Thus there is a reduction of 3 km in the maximum possible link length without repeaters.

Although in Example 11.8 we have demonstrated the use of the optical power budget to determine the maximum link length without repeaters, it is also frequently used to aid decisions in relation to the combination of components required for a particular optical fiber communication system. In this case the maximum transmission distance and the required bandwidth may already be known. Therefore, the optical power budget is used to provide a basis for optimization in the choice of the system components, whilst also establishing that a particular component configuration meets the system requirements.

Example 11.9

Components are chosen for a digital optical fiber link of overall length 7 km and operating at a 20 Mbit s^{-1} using an RZ code. It is decided that an LED emitting at 0.85 μm with graded index fiber to a *p–i–n* photodiode is a suitable choice for the system components, giving no dispersion–equalization penalty. An LED which is capable of launching an average of 100 μW of optical power (including the connector loss into a 50 μm core diameter graded index fiber is chosen. The proposed fiber cable has an attenuation of 2.6 dB km^{-1} and requires splicing every kilometre with a loss of 0.5 dB per splice. There is also a connector loss at the receiver of 1.5 dB. The receiver requires mean incident optical power of -41 dBm in order to give the necessary BER of 10^{-10}, and it is predicted that a safety margin of 6 dB will be required.

Write down the optical power budget for the system and hence determine its viability.

Solution:

Mean optical power launched into the fiber from the transmitter (100 μm)	−10 dBm
Receiver sensitivity at 20 Mbit s^{-1} (BER 10^{-10})	−41 dBm
Total system margin	31 dB
Cabled fiber loss (7×2.6 dB km^{-1})	18.2 dB
Splice losses (6×0.5 dB)	3.0 dB
Connector loss (1×1.5 dB)	1.5 dB
Safety margin	6.0 dB
Total system loss	28.7 dB
Excess power margin	2.3 dB

Based on the figures given the system is viable and provides a 2.3 dB excess power margin. This could give an extra safety margin to allow for possible future splices if these were not taken into account within the original safety margin.

11.6.7 Line coding

The preceding discussions of digital system design have assumed that only information bits are transmitted, and that the 0 and 1 symbols are equally likely. However, within digital line transmission there is a requirement for redundancy in the line coding to provide efficient timing recovery and synchronization (frame alignment) as well as possible error detection and correction at the receiver. Line coding also provides suitable shaping of the transmitted signal power spectral density. Hence the choice of line code is an important consideration within digital optical fiber system design.

Binary line codes are generally preferred because of the large bandwidth available in optical fiber communications. In addition, these codes are less susceptible to any temperature dependence of optical sources and detectors. Under these conditions two level codes are more suitable than codes which utilize an increased number of levels (multilevel codes). Nevertheless, these factors do not entirely exclude the use of multilevel codes, and it is likely that ternary codes (three levels 0, $\frac{1}{2}$, 1) which give increased information transmission per symbol over binary codes will be considered for some system applications. The corresponding symbol transmission rate (i.e. bit rate) for a ternary code may be reduced by a factor of 1.58 ($\log_2 3$), whilst still providing the same information transmission rate as a similar system using a binary code. It must be noted that this gain in information capacity for a particular bit rate

is obtained at the expense of the dynamic range between adjacent levels as there are three levels inserted in place of two. This is exhibited as a 3 dB SNR penalty at the receiver when compared with a binary system at a given BER. Therefore ternary codes (and higher multilevel codes) are not attractive for long-haul systems.

For the reasons described above most digital optical fiber communication systems currently in use employ binary codes. In practice, binary codes are designed which insert extra symbols into the information data stream on a regular and logical basis to minimize the number of consecutive identical received symbols, and to facilitate efficient timing extraction at the receiver by producing a high density of decision level crossings. The reduction in consecutive identical symbols also helps to minimize the variation in the mean signal level which provides a reduction in the low frequency response requirement of the receiver. This shapes the transmitted signal spectrum by reducing the d.c. component. However, this factor is less important for optical fiber systems where a.c. coupling is performed with capacitors, unlike metallic cable systems where transformers are often used, and the avoidance of d.c. components is critical. A further advantage is apparent within the optical receiver with a line code which is free from long identical symbol sequences, and where the continuous presence of 0 and 1 levels aids decision level control and avoids gain instability effects.

Two level block codes of the *nBmB* type fulfil the above requirements through the addition of a limited amount of redundancy. These codes convert blocks of n bits into blocks of m bits where $m > n$ so that the difference between the number of transmitted ones and zeros is on average zero. A simple code of this type is the *1B2B* code in which a 0 may be transmitted as 01, and a 1 as 10. This encoding format is shown in Figure 11.39(b) and is commonly referred to as biphase or Manchester encoding. It may be observed that with this code there are never more than two consecutive identical symbols, and that two symbols must be transmitted

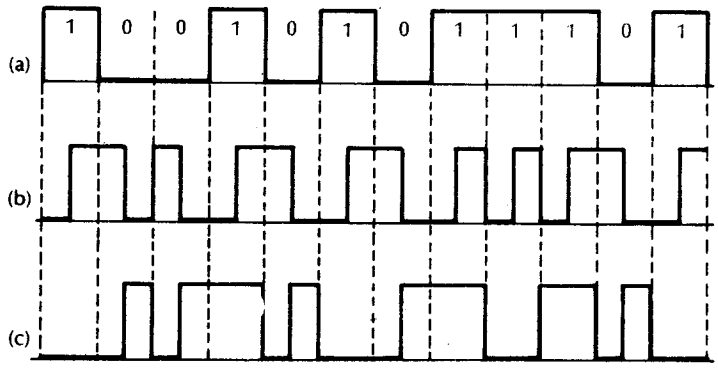

Figure 11.39 Examples of binary 1B2B codes used in optical fiber communications: (a) unencoded NRZ data; (b) biphase or Manchester encoding; (c) coded mark inversion (CMI) encoding.